Fire weather climatology dataset for Victoria

Final Report to the Victoria Department of Environment, Water, Land and Planning
August 2015

Timothy Brown[a,b], Graham Mills[b], Sarah Harris[b], Domagoj Podnar[a], Hauss Reinbold[a] and Matt Fearon[a]

[a]*Desert Research Institute, Reno Nevada USA, tim.brown@dri.edu*
[b]Monash University, Clayton Victoria Australia, sarah.harris@monash.edu

EXECUTIVE SUMMARY

Climatology data of fire weather across the landscape can provide science-based evidence to inform strategic decisions to ameliorate the impacts (at times extreme) of bushfires on community socio-economic wellbeing and to sustain ecosystem health and functions. A long-term climatology requires spatial and temporal data that are consistent to represent the landscape in sufficient detail to be useful for fire weather studies and management purposes. In Victoria there are some considerable barriers in creating a long-term homogeneous climatology strictly from meteorological observations, given the relatively low number of reliable, long-term observation records available for analyses. These barriers exist in both space and time. Spatially, the majority of the observations are based near population centres, and so do not necessarily reflect the conditions in the forests where the bulk of major bushfires primarily occur concentrated in the slopes and valleys of the ranges through central and eastern Victoria. Temporal inhomogeneities include changes with time in both observation network density and in reporting frequency. The latter is particularly evident during the period of transition from mostly manual synoptic (3-hourly at best) observations to hourly or half-hourly Automatic Weather Station observations that occurred during the 1990's.

To address this inhomogeneity problem for analyses of a variety of fire weather interests and to provide a dataset for management decision-support, a homogeneous 41-year (1972-2012), hourly interval, 4-km gridded climate dataset for Victoria has been generated using a combination of mesoscale modelling, global reanalysis data, surface observations, and historic observed rainfall analyses.

The project objectives were:

- Provide a high-resolution temporally and spatially complete record of temperature, humidity, wind, precipitation, drought and fire danger;
- Provide decision-support information for fire management - Phoenix (Tolhurst et al 2008), planned burning, fire behaviour, vegetation management, fire danger and fire weather studies;
- Provide background information for climate change analyses (trends, variability);
- Fills in gaps between observation points; and
- To help determine if assumptions that go into policy and operations are supported by what is known about the climate record.

The Weather and Research Forecasting (WRF) mesoscale numerical meteorology model was used to generate the dataset. The model was initialised from 6-hourly global reanalysis atmospheric fields, with three domain nests down to 4-km. Hourly near-surface forecast fields were combined with Drought Factor (DF) fields calculated from the Australian Water Availability Project (AWAP) rainfall analyses to generate fields of hourly fire danger indices for each hour of the 41-year period. A quantile mapping (QM) bias correction technique utilizing available observations during the years 2003-2012 were used to ameliorate any model biases in wind speed, temperature and relative humidity. Quantiles were matched climatologically by month and hour (e.g., January had 24 quantile distributions developed consisting of up to 310 observations for each hour over the 10-year period). This approach yielded 288 quantile distributions total for the bias correction process.

The final dataset includes surface hourly temperature, relative humidity, wind speed, wind direction, Forest Fire Danger Index (FFDI), and daily DF and Keetch-Byram Drought Index (KBDI) at a 4-km spatial resolution for the period 1972-2012. However, WRF also generated a 32-level full 3-D volume atmosphere. Hence, data for upper-air analyses are also available such as might be used for smoke and air quality studies or for investigating atmospheric stability and fire behaviour relationships. Because of quality issues with precipitation, AWAP data were used instead to calculate daily DF and KBDI, and then these were used (in combination with bias corrected hourly temperature, relative humidity, and wind speed) to calculate hourly FFDI.

Extensive evaluation in three phases was undertaken including both quantitative and case study qualitative assessments. The first phase was during the initial and quite exhaustive configuration refinement, or tuning phase, when the model (mostly physics) parameters were tuned to produce stable both meteorologically and climatologically realistic fields, and this focused on relatively short (two-week to 1 season) periods. The second phase comprised assessments of the first 10 years (2003-2012) of the data set when a stable configuration for the WRF model had been determined. The third phase comprised the evaluation of the 1972-2002 period.

Overall, the evaluation demonstrated very satisfactory results. This is supported by quantitative bias and root mean square error statistics, along with numerous case study assessments. The evaluation showed that the meteorology produced by the WRF model in this project is quite realistic, though there are cases of model random error that will not exactly correspond to observations. However, these errors are generally averaged out when creating a long-term climatology dataset from a numerical meteorology model using initial boundary conditions with nudging. Thus, weekly to monthly to seasonal and longer time scales derived statistics from the model can match closely with the observations. It was the primary purpose of this project to produce a long-term climatology.

The results from the observation-fitting statistics, case studies and climatological assessments show that the quality of the data set is such that there are a great number of applications and analyses to which this data set might be usefully applied. However, there are a number of characteristics of the dataset that must be born in mind when it is being applied to any particular need. These are described in detail in the report, but briefly summarised here: 1) because the model generated a 4-km horizontal grid, there will not be an exact match to point observations, and therefore the model values should not be treated as observed values; 2) the modelled meteorology will represent a smoothed topography rather than the actual topography, highlighting caution in using the grid cells as exact points; 3) the meteorology represented by the WRF data set, while extra-ordinarily impressive in many cases (see Case Studies Appendix B), does contain a random error component and will affect, for example, simulations of the spread of actual historic fires; thus, in such applications careful assessment of the meteorology of the event should be a first step; 4) running a fire behaviour model with inputs spanning 15-day integration periods could be affected by the discontinuity; 5) because the global observing system has evolved dramatically over the 41 years of this data set, the dataset quality does include a certain degree of deterioration as going backwards in time, especially the 1972-1979 period; 6) the

QM bias correction method did at times slightly overcorrect the original output values for temperature, relative humidity and wind speed; however, for the median values this tended to be a very small amount not likely to affect many analyses; 7) when analysing extreme values in the WRF data set or from observations, care must be taken in their interpretation; and 8) a consequence of tuning the WRF model for accurate temperature, relative humidity and wind parameters (the direct meteorological inputs to fire danger equations) led to an inadvertent negative bias in the modeled rainfall.

At the time of writing this report, the complete dataset is stored at Monash University with a backup at DRI. Two file groups are available, the original uncorrected fields for all levels, and bias corrected surface fields based on the quantile mapping method described in this report. The file format is netCDF, which contains relevant metadata as part of the data structure. The data format can be directly used with Phoenix.

Outputs from this dataset provide an almost limitless opportunity for hitherto unavailable analyses – including fields of percentiles of the Forest Fire Danger Index, analysis of periods exceeding thresholds at any location, inter-annual and regional variations of fire season characteristics, analysis of prescribed burning windows, of atmospheric dispersion climates, of various atmospheric stability measures that might affect fire behavior. It also provides a data set with which to assess climatologies of more esoteric mesoscale weather events, such as mountain waves, that may affect fire behaviour. The hourly mesoscale data also provides a previously unavailable long-period homogeneous data set with which to drive fire spread models such as Phoenix. While this dataset was primarily created for fire weather planning purposes, the opportunities for other applications, such as climate change studies, are immense.

1 TABLE OF CONTENTS

1 INTRODUCTION

1.1 THE PROBLEM

Climatology data of fire weather across the landscape can provide science-based evidence to inform strategic decisions to ameliorate the impacts (at times extreme) of bushfires on community socio-economic wellbeing and to sustain ecosystem health and functions. However, there are some considerable barriers in creating a long-term homogeneous climatology strictly from meteorological observations, as shown by the relatively low number of reliable, long-term observation records available for analyses such as that of Lucas et al. (2007). These issues can perhaps be broadly categorized into inhomogeneities in time and inhomogeneities in space of the Bureau of Meteorology observing sites.

In time there have been steady changes in observing networks, observing practice, and instrumentation. Figure 1 shows the Bureau's observing network over Victoria in 1972 and in 2008. There are clearly many more stations in recent than in earlier years. Further, in the early years the reporting frequency was at best 3-hourly, and a significant number of station's reports were only at 9 am and 3 pm. In addition, stations opened, closed, or were moved during this period. A significant change in reporting frequency and in observing practice occurred from the early 1990's, when Automatic Weather Stations (AWS) gradually replaced the manual observations. This had several benefits, including much more frequent reporting, the benefit of not having to site the instrumentation at a place where personnel needed to be available at each observation time, and, enormously important from a fire weather perspective, anemometers were universal with these AWS. This provided for quantitative rather than estimated wind speeds. The implication of these inhomogeneities in wind speed estimation/measurement for fire weather calculations is shown in Lucas (2010).

Inhomogeneities in space of the observing network also have significant implications for fire weather applications. The bulk of the observations are based near population centres, and so do not necessarily reflect the conditions in the forests where the bulk of major bushfires occur, and which are concentrated in the slopes and valleys of the ranges through central and eastern Victoria.

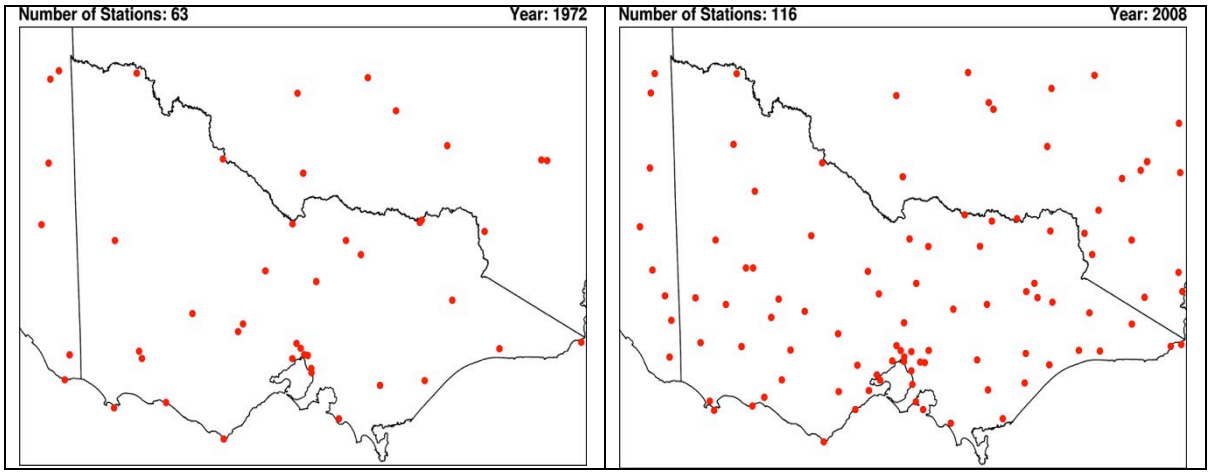

Figure 1. Observing network in and near Victoria in 1972 (left) and 2008 (right).

It is logistically possible to spatially interpolate between observing stations to obtain a regular grid of data using distance-weighted averages, or more complex schemes, and this has long been used in Numerical Weather Prediction (NWP) systems. However, ensuring physical consistency when interpolating across regions of varying elevation or land surface type requires additional statistical assumptions that rapidly lead to excessive complication and error. Further, the fact that observations are not available at hourly intervals throughout the period desired also makes some form of interpolation in time necessary if hourly fields are desired, and this also adds complication as any assumptions regarding diurnal cycles of variables would generally ignore differences through the synoptic weather cycle.

An alternative approach is to generate mesoscale NWP model outputs, as these outputs are physically constrained by the model's equations of motion and thermodynamics, include realistic topography for the resolution of the model's grid, and provide output at regular time and space intervals.

Operational NWP outputs, while archived by most national weather services, suffer from the fact that these models are upgraded every few years, and so can produce major inhomogeneities if they are to be used for climatological studies. These model changes are desired for improved forecasting, but a gridded dataset for climatological purposes requires a homogeneous dataset produced by a consistent model. For global climate studies "reanalyses" have been prepared – these data sets use a consistent and contemporary data assimilation scheme that includes a numerical prediction model to re-analyse the historical data record. While these data sets have a grid-spacing that is too coarse for the needs of this project, they can be used as initial and boundary conditions for mesoscale NWP model integrations, with multiple nests if desired, to achieve high spatial detail in the inner nests. This option was chosen for the current project.

This report describes the methodology and output of a 1972-2012 high temporal- and spatial-resolution climatology of Victoria's fire weather using a NWP approach. The climatology combines hourly values of meteorological variables on a regular, high spatial resolution, grid over Victoria with Drought Factors based on the Australian Water Availability Project (AWAP) rainfall and temperature analyses (Jones et al. 2009) to generate hourly gridded fields of the Forest Fire Danger Index (FFDI). Included in this report are the model configuration, running strategy, and quality control/assessment procedures that were used in developing the data set.

The dataset provides baseline climatology information for risk management assessments and climate change adaptation planning. The benefits of the dataset to the Victoria Department of Environment, Water, Land and Planning and others include:

- Provides a high-resolution temporally and spatially complete record of temperature, humidity, wind, precipitation, drought and fire danger.
- Allows for analyses at local through regional through state scales.
- Shows interannual and decadal variability for the elements produced, as well as climate trend.

- Quantitatively links climate variability and trend to impacts from fire, heat waves, drought, etc.
- Provides a historical baseline that can be used in comparison studies with downscaled regional or place-based future climate data.
- Serves as input data for decision-support tools to obtain historic baselines.
- Provides quantitative climate values to help test agency strategies and predict ecological outcomes.
- Helps determine if assumptions that go into policy and operations are supported by what is known about the climate record.
- Helps determine the extent that fire management responses have been “driven” by climate versus other forcing factors (e.g., political, economic, public perceptions).

Specific fire management relevance and uses include, but are not limited to:

- Estimating climate related bushfire risk
- Estimating number of days suitable for planned burning
- Input into the allocation of fire management resources - including planned burning
- Bushfire case study analysis, refinement and improvement of burning prescriptions
- Development of climate envelopes for vegetation communities
- Development of weather predictions for "fire use" decision making, and future bushfire climate predictions for strategic planning
- Providing hourly high-resolution weather input for fire spread models

The Project Objectives:

- Provide a high-resolution temporally and spatially complete record of temperature, humidity, wind, precipitation, drought and fire danger
- Provide decision-support information for fire management (Phoenix, planned burning, fire behaviour, vegetation management, fire danger and fire weather studies)
- Provide background information for climate change analyses (trends, variability)
- Fills in gaps between observation points
- To help determine if assumptions that go into policy and operations are supported by what is known about the climate record

1.2 Comparison with other studies

A model that has become increasingly popular for producing high spatial and temporal gridded outputs is the Weather Research and Forecasting (WRF) model (Skamarock et al. 2008). This model has been well established in simulations conducted over various regions globally, as explained in Andrys et al. (2015), and is used operationally such as by the U.S. National Weather Service. There has been increasing use of the WRF model for purposes of forestry, fire and agricultural applications, however with varying results. For example, a recent study by Andrys et al. (2015) evaluated a gridded dataset of rainfall, minimum temperature and maximum temperature covering southwestern Western Australia over a 30-year period. Andrys et al. (2015) used two nested domains at 10- and 5-km resolution

with an aim of comparing how well differing resolutions resolves complexity. They found the model was able to simulate daily, seasonal and annual variations in temperature and precipitation well, including extreme events. They also found significant performance gains in modeling precipitation with higher grid resolution. A study by Simpson et al. (2013) used WRF to simulate fire weather conditions for a fire season (09-10) in New Zealand. This study simulated 12-hourly temperature, relative humidity, wind speed and direction along with daily rainfall, a New Zealand fire weather index and the Continuous Haines index. They found an under-prediction of temperature and relative humidity and an over-prediction of wind speeds and rainfall. Unfortunately, they also found issues around under-predicting the extremes, which limits the operational use of the dataset. Clarke et al. (2013) simulated fire weather for southeast Australia from 1985 to 2009. They compared their results to station based observations of FFDI and found WRF simulated the main features of the FFDI distribution and its spatial variation with an overall positive bias. They concluded that the errors in average FFDI were mostly caused by relative humidity whereas the errors in extreme FFDI were mostly driven by wind speed. Finally, in general, they found better performance when reducing grid spacing from 50 km to 10 km.

While the studies mentioned above have made major advancements in using WRF to produce simulations useful for fire studies, the fire weather climatology dataset produced in this study is the first of its kind to provide long-term hourly values of meteorological variables on a regular, high spatial resolution, grid over Victoria, Australia based on WRF model output. A statistical bias correction was applied to surface temperature, relative humidity and wind speed to improve the output. In this report we explain and evaluate the performance of WRF model outputs and the applied bias correction in simulating fire weather variables for Victoria, Australia. This evaluation is presented through statistics, meteorological case studies and climatological characteristics of the region.

2 DATA AND METHODS

2.1 REGIONAL MODELLING APPROACH

There are two general types of “downscaling” that can be used to create modelled gridded weather datasets – statistical and dynamical. Statistical relies largely on statistical relationships between predictors and predictands to produce the dataset. Pros to this approach are that it is much less computationally intensive than a dynamical model; it is possible to tailor for specific localities, scales, and problems; and there is flexibility in the statistical methods available. Cons are the observed autocorrelation between the weather at consecutive time steps is not necessarily reproduced; statistical downscaling does not necessarily reproduce a physically sound relationship between different climate elements; and successful statistical downscaling depends on long, reliable observational series of predictors and predictands. Dynamical downscaling makes use of a numerical meteorology model. The pros are individual variables are physically consistent in time and space, and the different variables are internally consistent; a regional model provides for a wealth of output data at high resolution for both the surface and upper atmosphere; and no specific calibration data are required, though model input is needed to establish initial boundary conditions. The cons are dynamical models are very complex and requires substantial

computational resources; near the model boundary domain artifacts and spurious effects can occur (though this was minimal in this project); and some model-produced bias is likely in the output data. For model bias there are established methodologies to correct for this as discussed in Section 2.4.

2.1.1 DATA SOURCES: AWS

AWS data in Australia provide in recent years a historical record of hourly observations of relevance to the bushfire community as well as other interests. Prior to the mid-1990s, the observations were 3-hourly, and at many stations wind speeds were estimates by the observer. Only starting in the mid-1990s when AWS increasingly replaced manual observers did hourly (or better) observations that included anemometer wind speeds become widespread. Details of station inhomogeneties are described in Lucas (2010). For our project, AWS data were used for two primary purposes. One, assessing model estimates using statistical measures of bias and root mean square error, and two, to examine specific meteorological events such as timing of frontal passages.

2.1.2 DATA SOURCES: AWAP

The Australian Water Availability Project (AWAP) dataset contains gridded daily maximum temperature, daily minimum temperature, 24-hour rainfall, and vapour pressure at 0900 and 1500 local time. The dataset has a resolution of 0.05^{o} latitude by 0.05^{o} longitude (~5 x 5 km), with a positional accuracy of 0.01^{o} (~1 km) or better. More information about the development and reliability of the dataset is documented by Jones et al. (2009).

Daily precipitation from the AWAP dataset was used in conjunction with WRF temperature to calculate Drought Factor and the Keetch-Byram Drought Index. AWAP was statistically downscaled from the 5-km grid to match the WRF 4-km grid using the nearest neighbour spatial interpolation method within the NCAR Command Language (NCL) software package.

2.1.3 DATA SOURCES: Fire danger equations

FFDI is an important resultant calculation from the gridded dataset. The equations for the FFDI calculation are well documented, requiring temperature, relative humidity, and wind speed as direct inputs, and the calculated inputs of DF and KBDI. The calculation of FFDI follows Noble et al. (1980), that of KBDI follows Keetch and Byram (1968), and the DF that of Griffiths (1998). These latter calculations have also been described by Finkele et al. (2006), and a description of the inputs can also be found at the website http://www.firebreak.com.au/bkdi_df.html.

2.2 WRF

The mesoscale meteorology model used for this project was the Weather Research and Forecasting (WRF) model described by Skamarock et al. (2008). It is a well-supported and widely used non-hydrostatic model that includes a wide range of choices of physical parameterization schemes. Three integration domains were used in our configuration (Figure 2) with grid spacings of 36 km (outer mesh), 12 km (middle mesh), and 4 km (inner mesh). Each nest has 33 vertical model levels (surface plus 32 sigma levels). Initial state and

lateral boundary conditions for the outer mesh are provided by 6-hourly interval global reanalyses.

Figure 3 shows model terrain height in meters for the 4-km domain. In other words, this is the greatest terrain resolution that the model used for its calculations. The terrain data are the 30s (~ 0.9km) data provided by the National Center for Atmospheric Research (NCAR) as part of the WRF package.

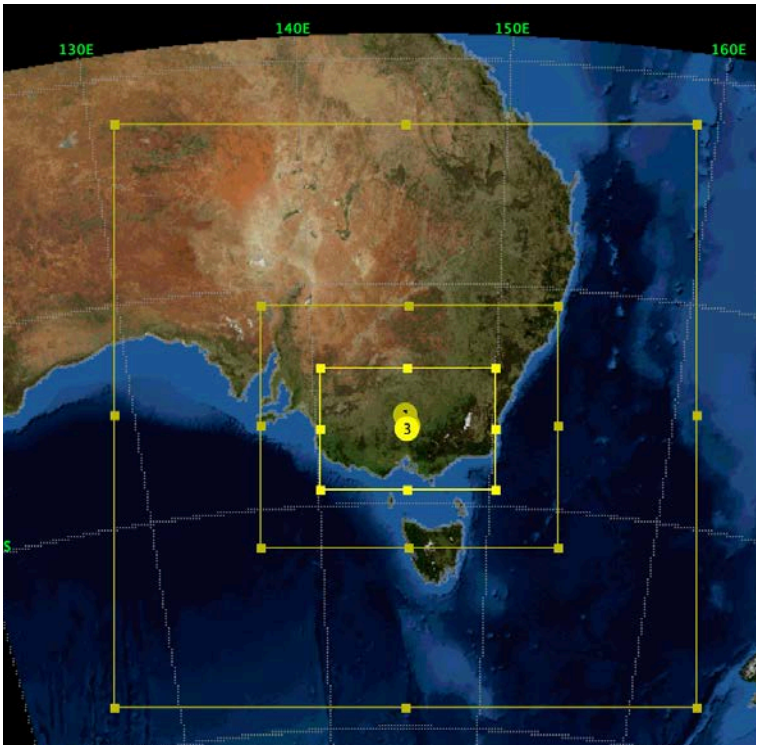

Figure 2. Map showing the domains of the three nested WRF grids centred over Victoria (outer grid spacing 36-km; middle 12-km; inner 4-km).

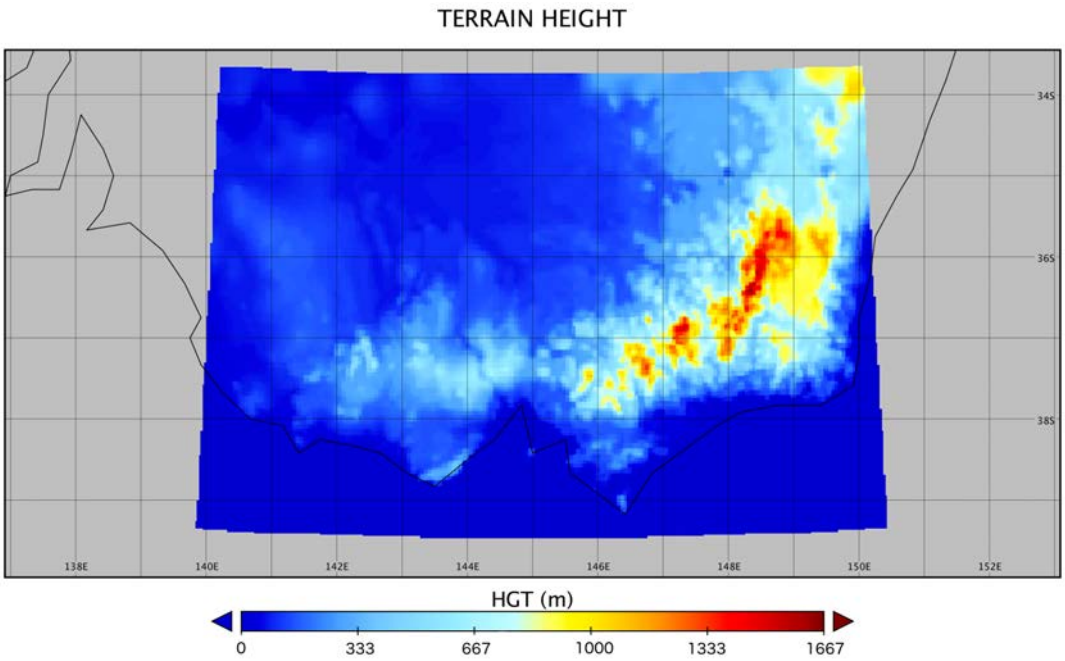

Figure 3. Map showing 4-km inner domain grid resolution in meters. Warmer colors indicate higher terrain.

2.2.1 Model physics parameterisations

Choices of physical parameterisation packages selected are listed in Table 1. While there are many choices in model parameters, we initially chose the WRF community recommended setup, then made adjustments based on detailed model tests discussed in Section 3.6.

Table 1. List of physical parameterisations used in this WRF configuration.

Microphysics: Thompson *et al.* scheme: A new scheme with ice, snow and graupel processes suitable for high-resolution simulations (8).
Longwave Radiation: RRTM scheme: Rapid Radiative Transfer Model. An accurate scheme using look-up tables for efficiency; it accounts for multiple bands, trace gases, and microphysics species.
Shortwave Radiation: Goddard shortwave: Two-stream multi-band scheme with ozone from climatology and cloud effects.
Land Surface: Noah Land Surface Model: Unified NCEP/NCAR/AFWA scheme with soil temperature and moisture in four layers, fractional snow cover and frozen soil physics.
Planetary Boundary layer: Yonsei University scheme: Non-local-K scheme with explicit entrainment layer and parabolic K profile in unstable mixed layer.
Cumulus Parameterization: Kain-Fritsch scheme: Deep and shallow convection sub-grid scheme using a mass flux approach with downdrafts and CAPE removal time scale.
Diffusion Option: Simple diffusion: Gradients are simply taken along coordinate surfaces.
K Option: 2d Deformation: K for horizontal diffusion is diagnosed from just horizontal deformation. The vertical diffusion is done by the PBL scheme.

2.2.2 Initial and Boundary Conditions

We utilized three global reanalyses for initial state and lateral boundary conditions to start each WRF integration and nudge fields through a 15-day process before reinitialising. The National Centers for Environmental Prediction (NCEP) FNL (Final) Operational Global Analysis (NCEP 2000) data are on 1-degree by 1-degree grids prepared operationally every six hours, and were used for the 2003-2012 period. The ECMWF ERA-Interim reanalysis dataset (Dee et al. 2011) were used for the 1979-2002 period. The ECMWF ERA-40 reanalysis dataset (Kållberg et al. 2007) were used for the 1972-1978 period:

- NCEP FNL (Final) Operational Global Analysis ~1-degree 6-hourly (1999-present) 2003-2012
- ECMWF ERA-Interim 80-km 6-hourly (1979-present) 1979-2003
- ECMWF ERA-40 ~1.4 degree 6-hourly (1957-2001) 1972-1978

The 2003-2012 period was used as a primary test period because of the availability of more surface stations for statistical and case study evaluation. The FNL analysis was chosen for this period primarily due to team experience in working with the FNL-WRF combination. This period represented substantial testing of WRF model configuration. While the FNL analysis could have been used to generate WRF output back to 1999, we needed an analysis that was available back to 1972. The ECMWF analysis does this, but in two datasets. We chose the ERA-interim version back to 1979 because its spatial grid size (80-km) is finer resolution and closer to FNL than ERA-40 at ~1.4 degrees. To then be more consistent with ERA-Interim, we chose to use ERA-40 to complete the dataset with 1972.

One year of overlap (2003) was run using both FNL and ERA-Interim. A coarse analysis did not reveal substantial differences in WRF output.

2.2.3 Model Spin Up

There are logistical and data set quality benefits in performing longer (multi-day) rather than shorter (1-2 day) integrations as it is desirable not to have too many discontinuities at the commencement of each new integration due to the need for the inner grid to “spin up” from the smooth global reanalysis fields. One would intuitively expect that the model solution would drift somewhat from reality with time, although the use of lateral boundary conditions from analysis rather than the forecast conditions used in operational forecast models should reduce this effect somewhat. After considerable testing, we chose to generate the data using 15-day integrations, but with the first day of each integration treated as a spin-up period and thus discarded. Therefore, days 2-15 of each integration become Days 1-14 of each two-week data set period.

2.2.4 Nudging

Analysis nudging was implemented for U and V wind components on all three domains. Nudging was performed on all sigma levels throughout the domain, including the PBL. Emphasis was given to the wind components to reduce model perturbations seen in the testing phase output. Time-wise, nudging was done at 6-hour intervals, with a ramping-

down period of 60 minutes. After some analysis, nudging coefficients of 0.0012 were selected.

2.3 BIAS CORRECTION

A statistical bias (mean error of predicted minus observed) from atmospheric models is not uncommon due to combinations of physics parameterizations, spatial resolution and input data (initial boundary conditions including model type and data assimilation). The bias may run consistently above or below a mean observed value, but since it is typically more or less consistent it can be accounted for in the final model output using a statistical correction. For example, if it is known that the model produces 2-meter surface temperatures on average one degree C cooler than observed, one degree can be added to each of the model output timesteps to provide a simple correction without compromising the overall meteorology. Thus, it was expected to have some bias for the Victoria runs. However, we initially attempted to minimize bias through model parameterization choices, statistical analyses and examination of case studies.

To correct bias as best as possible, a quantile mapping (QM) method widely used in global climate model projection analyses was utilized. Quantile mapping (QM) has been an accepted methodology for many years (e.g., Panofsky and Brier 1968), and recently has been used for numerous global climate model projection bias corrections (e.g., Maurer et al. 2010, 2014; Thrasher et al. 2012). QM adjusts a model value by mapping quantiles of the model distribution onto quantiles of the observation distribution. In climate projection analyses, QM is used to correct to future values that are known to have model bias. In our case, we applied QM by comparing individual stations to corresponding WRF grid points, and then once WRF was corrected at these points, the correction was applied across the spatial domain using inverse distance weighting. This process allowed for more localized correction rather than a single derived value such as a mean across the entire domain.

Figure 4 provides a visual schematic of the QM process (adapted from Pierce et al. 2015). The example is for July temperature 1500 local time over the period 2003-2012 for a single station. The blue line shows the observed temperatures and corresponding quantiles, and the red line the WRF model temperatures and corresponding quantiles. The 0.2 quantile value is highlighted by the black horizontal line. The upward blue dashed line indicates that 10°C is the model 0.2 quantile. The left pointing short arrow shows where the 0.2 quantile intersects the observed temperature value, and the downward pointing arrow shows the observed value that should be used as the bias corrected value. In this case, the WRF 10°C becomes 8.9°C. This plot example also shows that less correction is needed for the larger quantiles (warmer temperatures) than the lower end of the distribution. The curves in this illustrative example appear smooth because they were fit with a normal distribution, which is typical for temperature. Weibull and beta distributions were used for wind speed and relative humidity, respectively. We also tested and applied a straightforward empirical distribution method; however, these results did not show an overall improvement, and for some stations the correction yielded poor results.

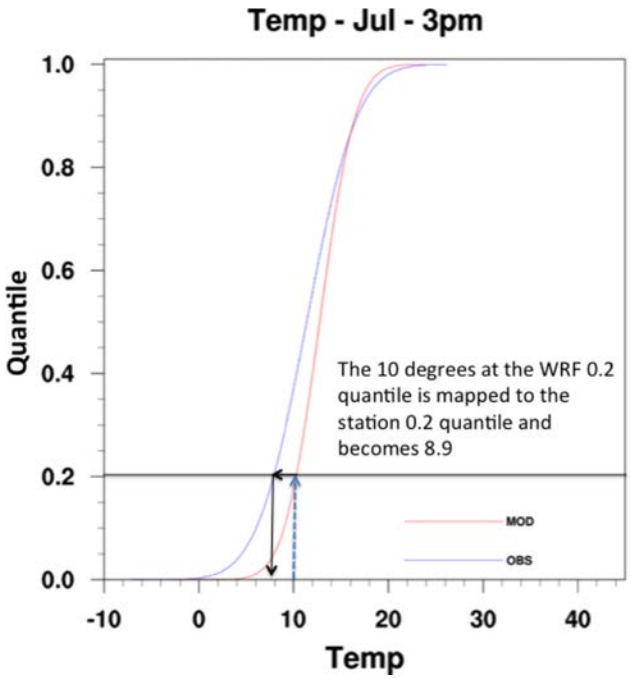

Figure 4. Example illustrative schematic of the quantile methodology.

QM was calculated for temperature, relative humidity and wind speed by hour by month (288 QM functions for each element) to capture the diurnal and seasonal cycles. Up to 63 stations (Figure 5) were used for each hour during the 2003-2012 period given data were available from all stations at that hour. However, each of these elements has different distribution properties. The R software package (R Core Team, 2013) was used to fit the data and determine the quantile values.

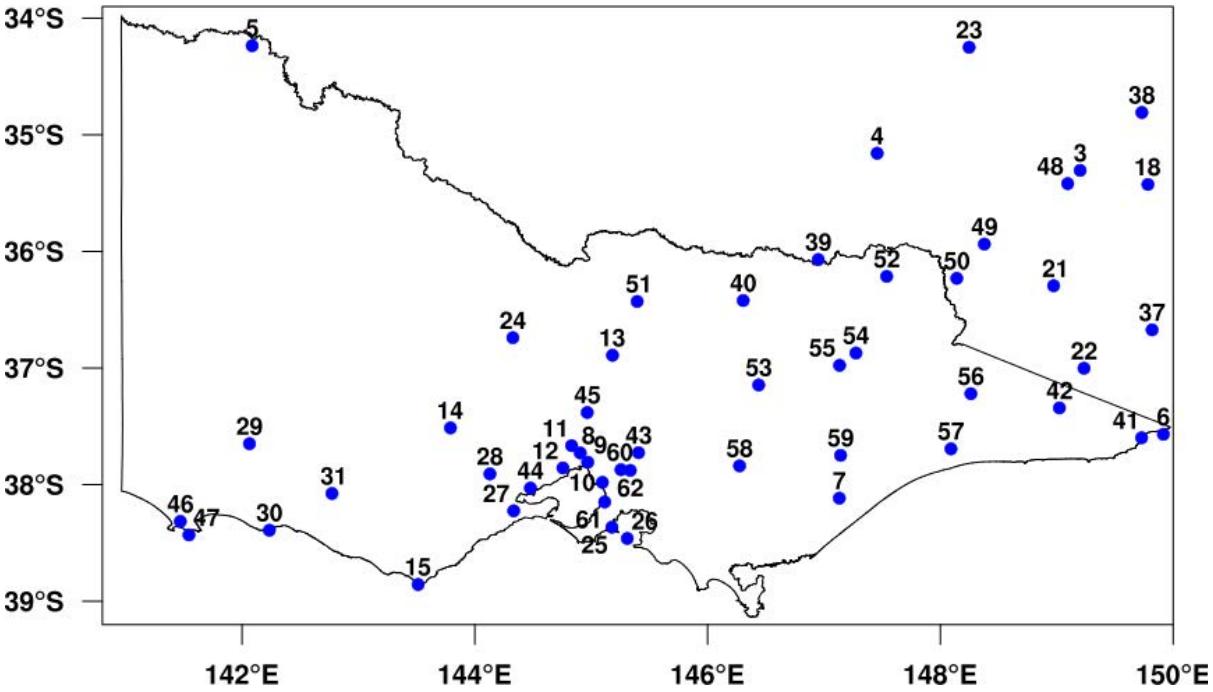

Figure 5. AWS locations for hourly stations used in the development of the quantile mapping for bias correction. Number indicates station index; see Appendix A to match index to station ID and name.

Figure 6 shows an example of the shape (top plot) and the scale (bottom plot) parameters derived for January by hour for 63 stations combined for wind speed using a Weibull distribution, and shown in the form of boxplots. The January diurnal cycle can be seen in the parameters, along with the range of values that distinguishes the stations from each other.

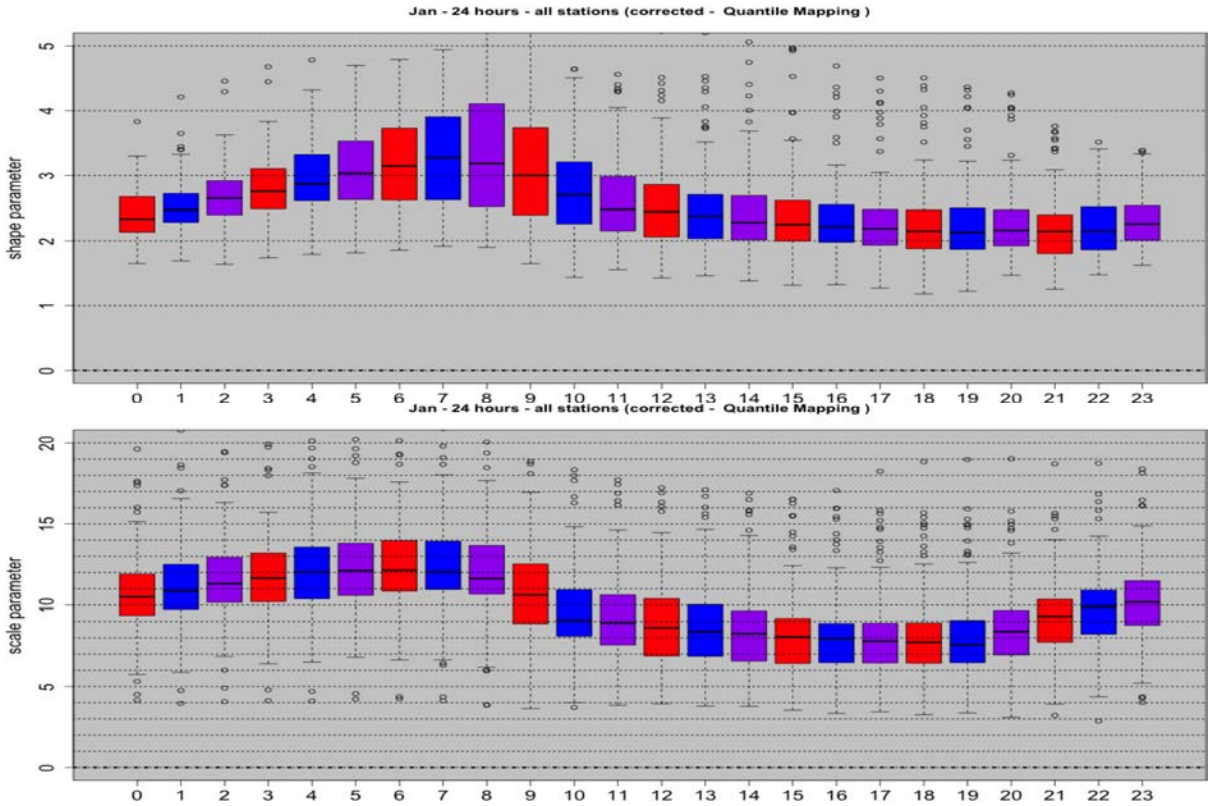

Figure 6. Boxplots of the Weibull shape (top plot) and scale (bottom plot) parameters for January wind speed by hour (UTC) for the 63 stations combined. Shape and scale parameters were determined by hour for each month.

Having determined quantile values for both observed and modeled values, the bias correction based on the difference was applied. Figure 7 shows an example for the January 2003-2012 hourly (UTC) distribution of WRF minus observed for the Avalon Airport station before bias correction (top plot). From the diurnal cycle, it can be seen that WRF tends to over-predict (warm bias) during most of the day, though the median bias is much smaller (1°C or less) and even near zero for hours 13 through 20. The bottom plot in Figure 7 shows the same station, except corrected after quantile mapping. Note that for each hour the median bias value has been corrected to near zero, though some overcorrection took place such that the median bias is slightly on the cool side. Overall the median bias for all hours has been reduced to within 0.5°C. There are still some days that have large errors exceeding ±5°C (the open circles indicating outliers) likely due to a timing issue of fronts and other localized circulation patterns or phenomena that WRF missed. The over correction occurrences are likely related to the more extreme outliers produced by WRF and where they align in the normal distribution fit of the quantiles for the mapping. This highlights that a further examination of statistical fits for the tails of the distribution (e.g., generalized Pareto) could lead to some further improvement in bias correction.

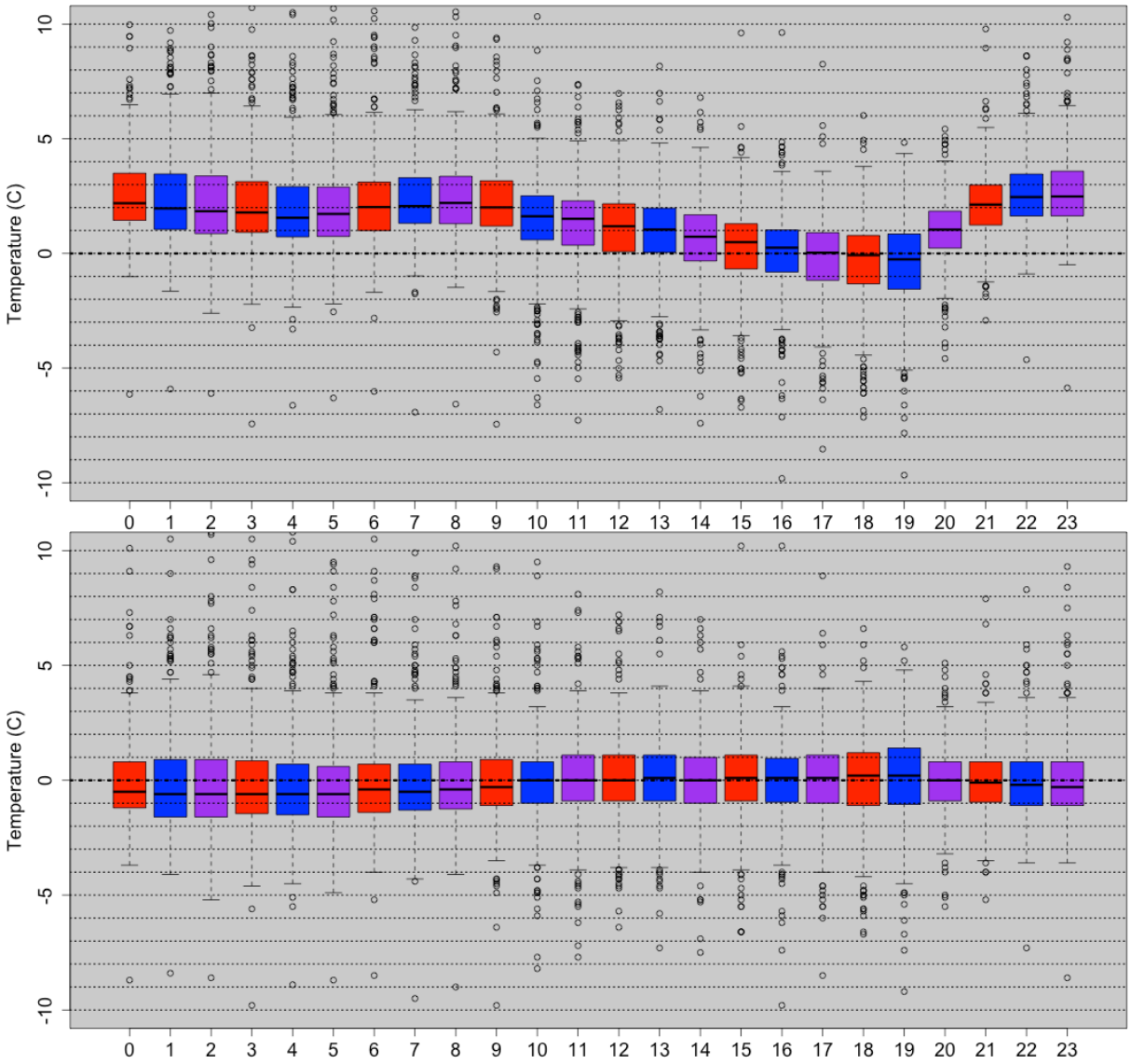

Figure 7. Boxplots of January 2003-2012 hourly (UTC) distribution of WRF minus observed temperature (C) for Avalon airport before bias correction (top plot) and WRF bias corrected minus observed (bottom plot).

Figure 8 shows an example bias correction for the Avalon airport station January hourly relative humidity for the years 2003-2012. The original bias in the top plot shows that WRF under-predicted (dry bias) for most of the day except for hours 13 through 19 where the bias is ±1%. The bottom plot shows the QM bias correction with some very slight overcorrection (for all but two hours the median bias was corrected to within ±1%). There remains within hour variability (shown by the boxes) for the same reasons as described for temperature above.

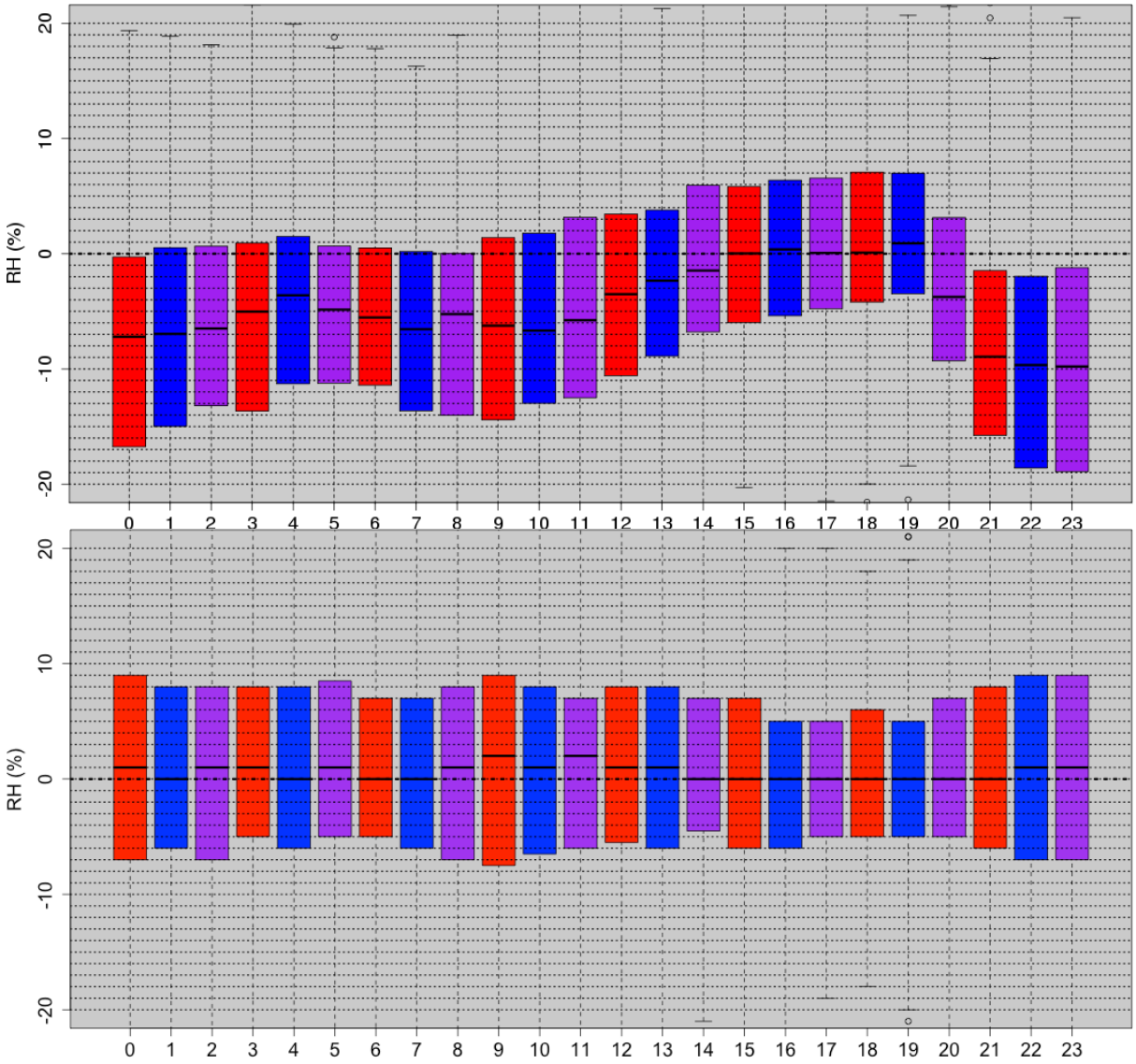

Figure 8. Boxplots of January 2003-2012 hourly (UTC) distribution of WRF minus observed relative humidity (%) for Avalon airport before bias correction (top plot) and WRF bias corrected minus observed (bottom plot).

Figure 9 shows an example bias correction for the Avalon airport station January hourly wind speed for the years 2003-2012. The original bias in the top plot shows that WRF under-predicted (low speed bias) for all hours, though only within 1 knot for hours 4 through 8. The bottom plot shows the QM bias correction with no overcorrection seen in the median values. There remains within hour variability (shown by the boxes) for the same reasons as described for temperature above.

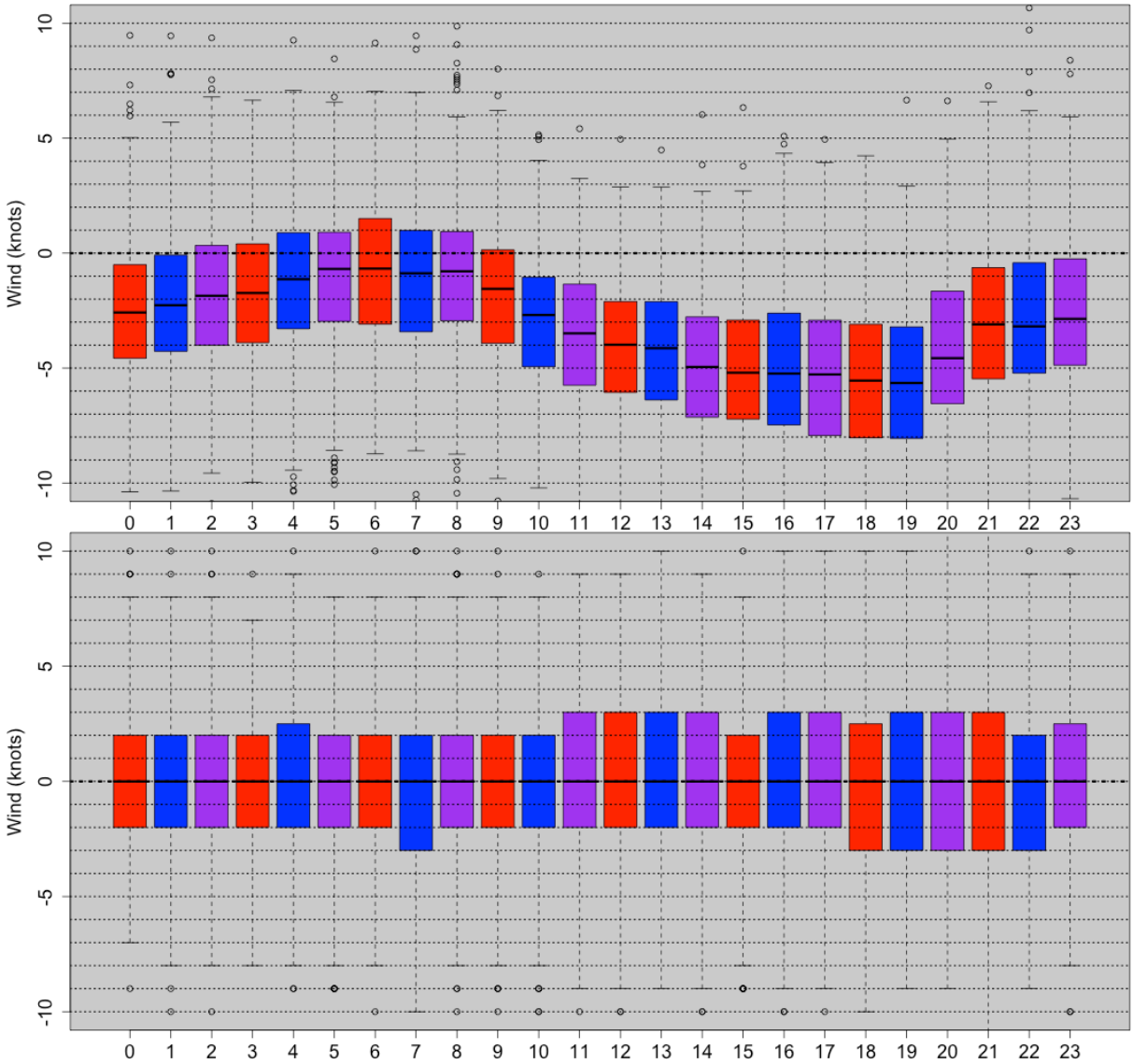

Figure 9. Boxplots of January 2003-2012 hourly (UTC) distribution of WRF minus observed wind speed (knots) for Avalon airport before bias correction (top plot) and WRF bias corrected minus observed (bottom plot).

The top plot in Figure 10 shows example scatterplots for WRF predicted versus Falls Creek observed temperature for January 00UTC. The blue circles show before and the red circles after QM bias correction, respectively. Both scatterplots show a well-defined linear relationship, but the before correction scatter clearly highlights WRF over-predicting temperature. The QM bias correction shows the values nicely aligned along the 45° diagonal. As shown with the boxplots, there remain some points in which the errors could not be substantially reduced. The middle plot in Figure 10 shows scatterplots for Port Fairy. In this case there is little difference between the predicted versus observed points before and after correction, indicating that little QM correction was needed to begin with. As a final example, the bottom plot in Figure 10 shows scatterplots for Avalon Airport, where there was a clear need for bias correction, and several points show large errors between predicted and observed. Many of these larger errors were reduced after correction, and generally the points align better along the diagonal.

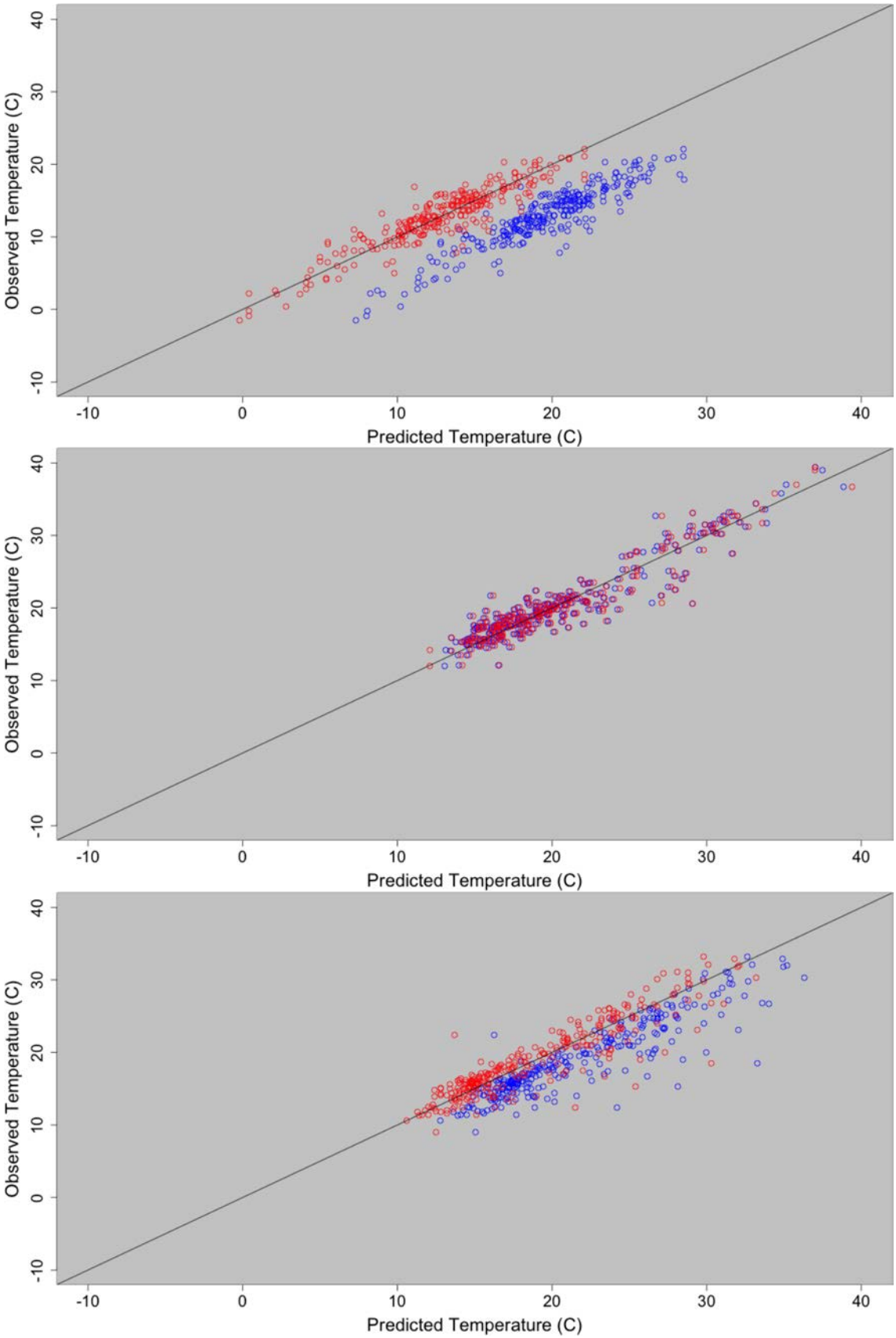

Figure 10. Scatterplots of WRF predicted versus observed temperature (C) for January hour 00 for the years 2003-2012 for the stations Falls Creek (top plot), Port Fairy (middle plot), and Avalon airport (bottom plot). Blue and red circles are before and after, respectively, bias correction.

Figure 11 highlights the need to have bias corrections by hour and month to account for diurnal and seasonal cycles. The top graph for the Essendon station temperature (C) shows each month in different symbols and colors. Except for a very small number of hours in October and November, the overall bias is positive (WRF too warm). Nighttime local hours tend to be warmer by approximately 1C than during the day. The bottom plot in Figure 11 is for the Bairnsdale station. These curves show a substantial seasonal difference along with a diurnal difference. The cool season months tend to have cool temperature bias during the nighttime local hours. The hourly and monthly biases can vary by station, generally due to the local characteristics of the station siting (e.g., elevation, aspect).

Once the QM method was applied to each station for each hour, the "dsgrid2" inverse distance weighting spatial interpolation algorithm in the NCAR Command Language (NCL, 2012) software package was applied to the entire domain for each hour. This allowed for the hourly station bias corrections to be applied spatially across the grid, rather than just using a simple mean for all stations combined. Figure 11 top plot shows an example map of a WRF uncorrected grid minus the corrected grid for January 0300 local time (top plot). This plot is showing the difference across much of Victoria only being ± 1C, suggesting that little bias correction overall was needed for this time. The full range of correction was approximately -1.5 to +2.5C. The Figure 12 bottom plot shows a similar plot except for January 1500 local time. Again only a correction of ± 1C was applied over much of Victoria, but larger corrections were applied to the complex terrain region in the East, and along the coastline. The full range of corrected values was approximately -1.5 to +2.5C. The larger difference over the complex terrain in the afternoon is indicating an overall over-prediction of January afternoon temperature, for which the bias correction could account.

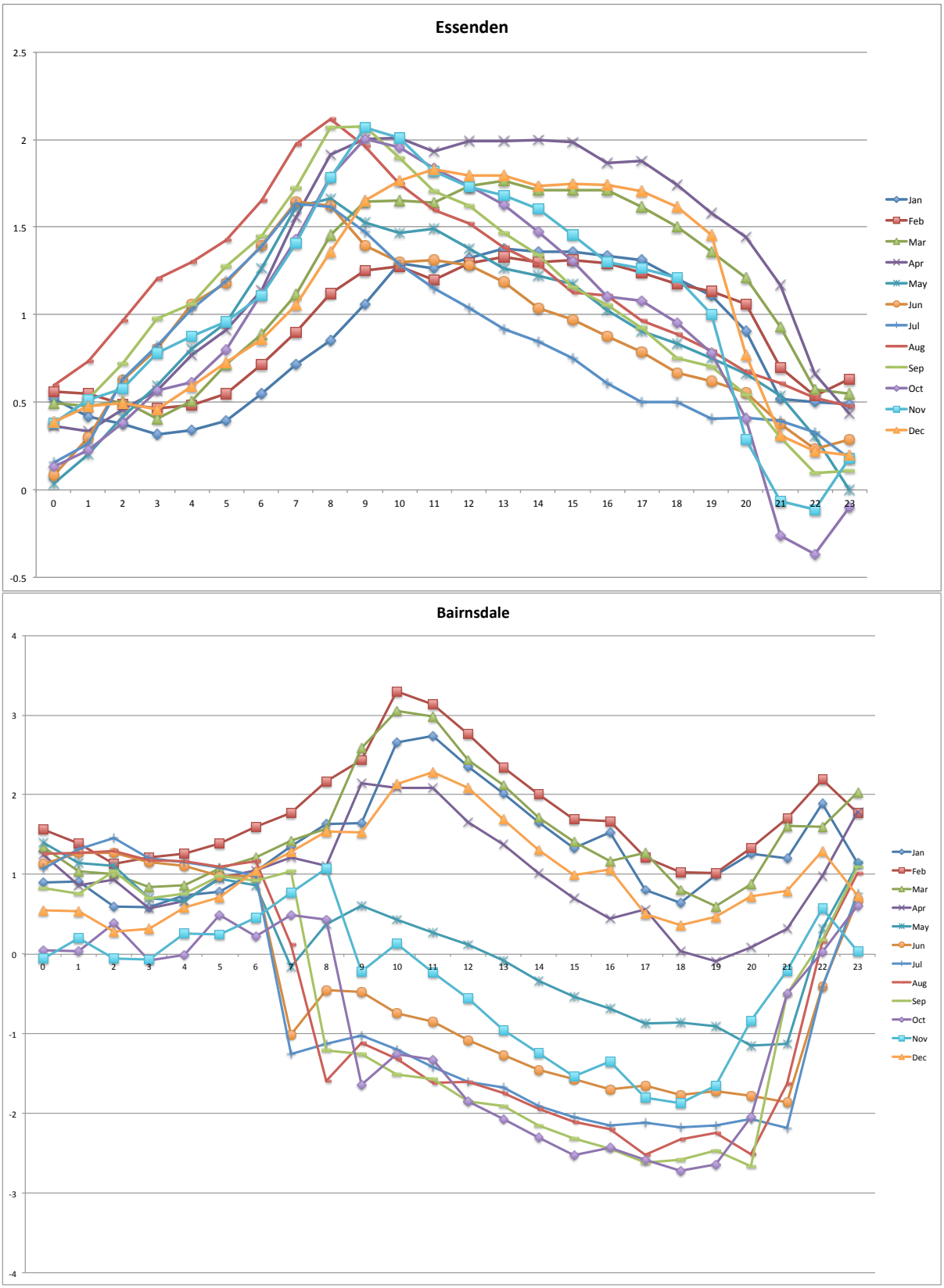

Figure 11. Hourly (UTC) and monthly temperature bias (C) for Essendon (top plot) and Bairnsdale (bottom plot). The colored symbols and lines correspond to a particular month.

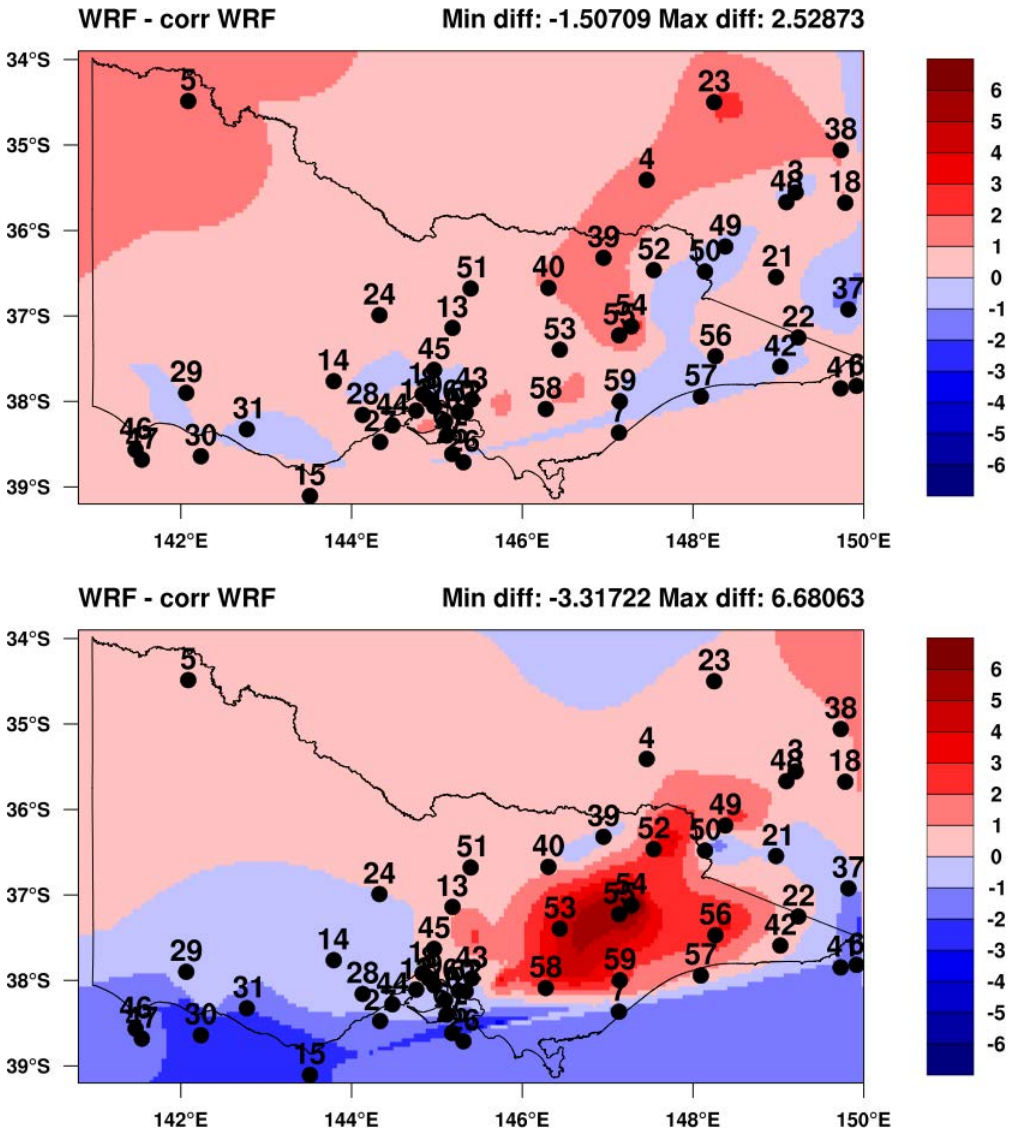

Figure 12. Spatial interpolation examples from the quantile mapping bias correction for January 0300 local time (top) and January 1500 local time (bottom). Shaded values are WRF uncorrected grid point values minus WRF bias corrected grid point values for temperature (C).

2.4 EVALUATION PROCESS

There are no quantitative performance standards defined for a data set such as the one developed in this project, apart from the fact that the climate of the data set should reflect the temporal and spatial variability of the actual Victorian climate to a level sufficient for its intended planning applications, and that the meteorology of actual (fire) weather events should be sufficiently realistic that scenario investigations of these events using, for example, fire behaviour models should produce worthwhile outcomes.

Accordingly, a process was developed as the project proceeded, and can be broadly divided into two, or perhaps three, phases.

The first phase was during the initial and quite exhaustive configuration refinement, or tuning phase, when the model (mostly physics) parameters were tuned to produce stable

meteorologically and climatologically realistic fields, and this focused on relatively short (two-week to 1 season) periods.

The second phase comprised assessments of the first 10 years (2003-2012) of the data set when a stable configuration for the WRF model had been determined.

The third phase comprised the evaluation of the 1972-2002 period.

The type and intensity of the evaluations varied, with greater detail of evaluation over shorter periods being used during Phase 1, detailed evaluations over selected periods during Phase 2, and broader statistical measures with targeted event-based evaluations used in Phase 3. These evaluation strategies matched both the needs of the project, the data volumes from each phase, and also the availability of verifying observations (greatest during the last decade, least during the earliest decade).

2.4.1 Phase 1 – Evaluation method

The evaluation proceeded sequentially in this phase. First a single summer's data (2008-2009) was generated, and the individual hourly fields of wind speed and direction, temperature, relative humidity, and hourly precipitation were visually inspected, together with a number of field or observation error statistics.

The subjective inspections were intended to validate the meteorological integrity of the data for significant weather events, and to identify any possible model instabilities (some of which had been seen in similar earlier exercises) that could be mitigated by tuning of model parameterisations. The objective statistics were used to further inform the meteorological integrity, but also to validate the 2-weekly integration strategy to demonstrate stable characteristics of the WRF model output across these periods – clearly it is undesirable for the WRF model to show any drift in accuracy or variability through days 2-15 of the 15-day integration.

During the tuning phase some 18 configurations were tested, some over a 2-week period during which some possible stability issues were identified, and others over the full 2008-2009 summer season. Because some of the tuning involved testing greater or lesser degrees of horizontal diffusion, and this can affect the detail in a simulation, careful assessment of meteorological detail also was included in each assessment.

Following the decision on final configuration, then for the 2008-2009 summer the attention turned to some other measures – assessing whether there was any trend with integration time from Day 2 through Day 14 of each integration period, was any discontinuity between the end of one integration and the start of the next problematic, and did these diagnostics reveal anything further regarding the stability of the WRF model when used in this configuration.

Aspects of this evaluation are presented in Section 3.2.1

Following the tentative conclusion that the data generated for the summer of 2008-2009 was of a sufficiently high standard, the same model configuration was applied to the 2006-

2007 and the 2009-2010 summers (the first being another severe fire season, while the second was more benign in terms of fire weather, and with higher rainfall).

A similar evaluation of error statistics and synoptic evaluation of the 2006-2007 and the 2009-2010 summer WRF data led to similar conclusions as the 2008-2009 summer evaluation. Accordingly this configuration was adopted for the full 41-year data set.

2.4.2 Phase 2 – Evaluation Method

This phase covered the period from 2003-2012, when a common FNL initialisation was used, and relied on broad evaluation statistics and also on targeted subjective evaluation of selected 2-week periods to seek confirmation of the previously assessed characteristics of the data. As this period coincided with a number of significant fire events (January 2003, January 2006 etc) these events were also assessed subjectively and quantitatively. Some of these results are presented in Sections 3.2.2, 3.3, 3.4, and 3.5 of this report.

2.4.3 Phase 3 – Evaluation Method

This phase examined the full 41-years of the data set, although could not be as detailed as that of Phase 1 due to the magnitude of the data to be examined. Accordingly the focus was on observation-fitting statistics, on the climatology of the data set, and also by examining case studies of notable weather (mostly fire weather) events. Aspects of this phase of the evaluation are presented in Section 3.3, 3.4, 3.5 and Appendix B of this report.

3 RESULTS

3.1 OUTPUTS OF THE UNCORRECTED DATA

3.1.1 Surface Data

The surface data from WRF of primary interest for bushfire applications and that were assessed in this project include temperature, relative humidity, wind speed, wind direction and precipitation. The dataset currently includes the period January 1972 to December 2012 with an hourly temporal resolution and a 4 x 4 km spatial resolution.

3.1.2 Upper level data

While hourly 4-km surface variables were the primary priority of this project, WRF model outputs included hourly 3-dimensional fields of all atmospheric variables. This means that there is the opportunity to assess the climatology of above-surface weather on fire activity that has never been possible at this scale over Victoria before. These studies include the effect of atmospheric stability on fire behavior using indices such as those described by Mills and McCaw (2010), and the potential to perform climatological assessments of foehn/mountain wave events such as those described by Sharples *et al*. (2010) and Badlan *et al*. (2012), or other mesoscale systems that are difficult to analyse climatologically from the observational record.

The upper levels have a horizontal spatial resolution of 4 x 4 km, hourly temporal resolution and 32 atmospheric pressure levels (hPa).

3.2 EVALUATION OF UNCORRECTED DATA

3.2.1 Temperature, Relative humidity and wind speed

During the Phase 1 assessment, considerable attention was focussed on the stability of the numerical product – that is, were there any variations in accuracy with length of time through the 15-day integration periods, and were there any significant discontinuities an the data sets between the last hour of one integration period and the first (after 24-hour spin-up) hour of the next.

To inform on these questions, RMS error of wind speed, temperature and relative humidity between observations and WRF were calculated for each hour through the summer of 2008-2009 together with WRF field variance of these quantities at each hour.

Figure 13 shows the average bias and RMSE for all stations averaged over each hour through the summer of 2008-2009, and also averaged by integration day – that is for the 15 integrations over the 2008-2009 summer, all day 1, day 2, etc. statistics are averaged. While diurnal signals, particularly in the bias, and also some synoptic variation in amplitude are

seen, the important point from this diagram is that there is essentially no trend in error through the 14 days of the integration.

Figure 14 shows the hourly time sequence of these bias and RMSE statistics, but for each individual hour of the twenty two-week integrations. As would be expected there is considerably greater variability than shown in Figure 13, but again there is no trend with time, and, importantly, there are no discontinuities between separate integration periods at the start of each even-numbered week.

This can be seen with greater clarity in Figures 15-17, which shows hourly bias and RMSE values for the individual two-week integration for all stations. Broadly speaking, when the errors are large at the end of one integration they are also large at the start of the next, and when they are small at the end of one integration they are also small at the start of the next. Examples of large errors are for wind speed between panels 3 and 4 and panels 7 and 8 in Figure 14; for temperature between panels 4 and 5 and between panels 7 and 8 in Figure 16; and for relative humidity between panels 7 and 8 in Figure 17. Examples of small values at the end of an integration period and at the start of the next for wind speed include panels 9 and 10 in Figure 15; for temperature between panels 2 and 3 in Figure 17; and for relative humidity between panels 5 and 6 in Figure 17.

This suggests, although does not necessarily prove for all applications, that the discontinuities engendered by the intermittent initialization strategy uses are relatively small. This was further examined by looping hourly image files across the integration discontinuities. This was done across:

- 15 November 2008
- 29 November 2008
- 13 December 2008
- 27 December 2008
- 10 January 2009
- 24 January 2009
- 7 February 2009
- 21 February 2009
- 7 March 2009

While some small degree of step changes could be identified, 0000 UTC is also the time when there are rapid diurnal changes in most parameters, as well as a change from stable to unstable model planetary boundary layer parameterization. Accordingly, at least some of the changes across the 0000 UTC are due to these factors. Overall the continuity was subjectively assessed as more than acceptable for most applications of this data set.

A subjective conclusion is that the integration gaps should have relatively little impact on the utility of the data set for climatological analyses. However, if, for example, a fire spread model is to be run across these periods, care should be taken to carefully assess the impacts of any possible inconsistency.

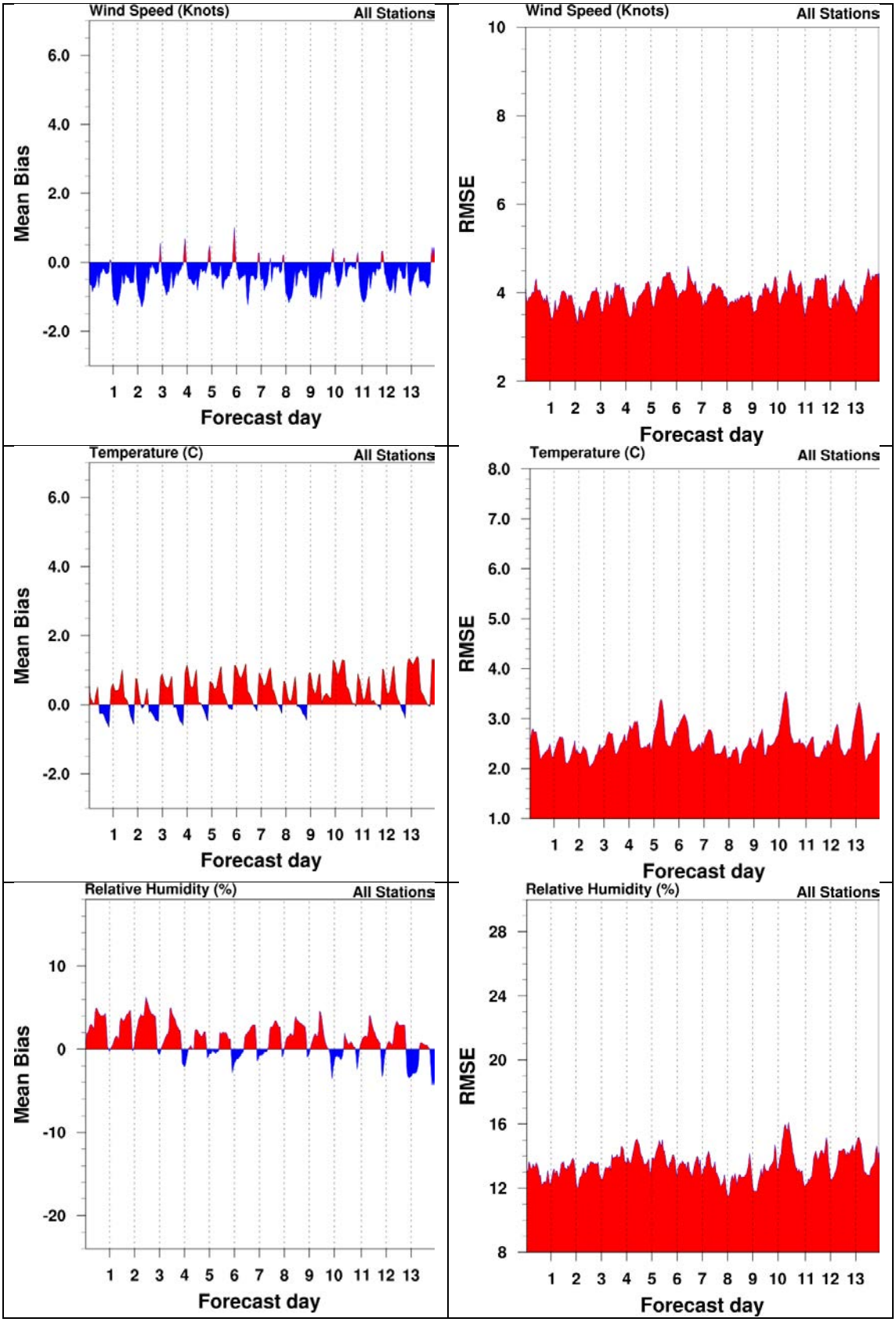

Figure 13. Mean bias (left panels) and RMSE (right panels) of wind speed (m/s; top), temperature (C; middle panels), and relative humidity (%; bottom panel)

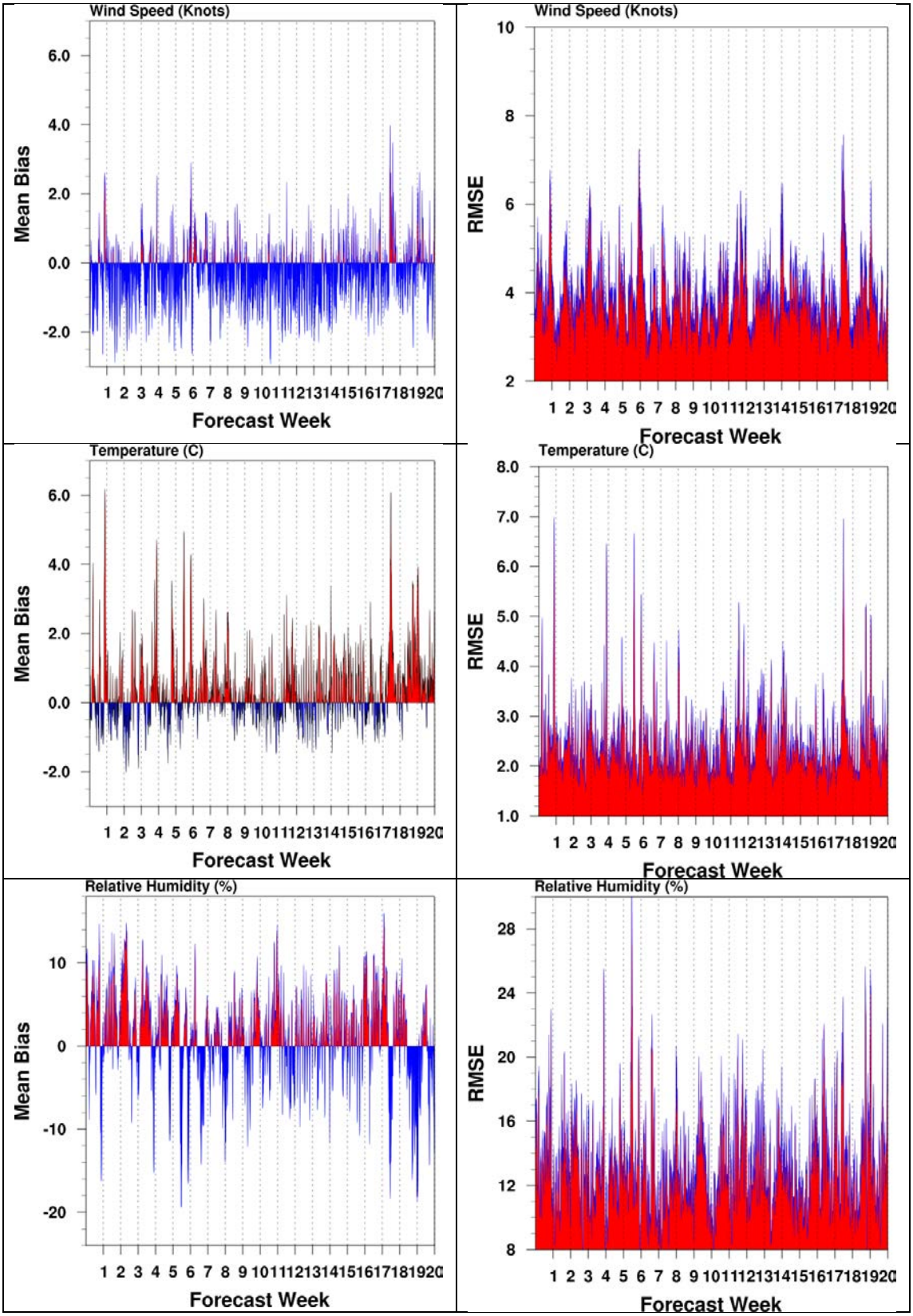

Figure 14. All station bias (left panels) and RMSE (right panels) for wind speed (knots; top panels), temperature (C; middle panels) and relative humidity (%; bottom panels) averaged for each hour through the 10 2-week integration periods of the 2008-2009 summer.

Appendices for the Fire weather climatology dataset for Victoria

TABLE OF CONTENTS

APPENDIX A – AWS STATIONS USED IN THE BIAS CORRECTION ANALYSIS

TABLE A1. The AWS stations, elevation, latitude and longitude used in the bias correction analysis

Index	Name	Elevation (m)	Lat	Lon
1	MOUNT GAMBIER AERO	63	-37.7473	140.774
2	BANKSTOWN AIRPORT AWS	6.5	-33.9181	150.986
3	MONTAGUE ISLAND LIGHTHOUSE	52	-36.2519	150.227
4	CANBERRA AIRPORT	578.4	-35.3049	149.201
5	WAGGA WAGGA AMO	212	-35.1583	147.457
6	MILDURA AIRPORT	52.8	-34.2358	142.087
7	GABO ISLAND LIGHTHOUSE	15	-37.5679	149.916
8	EAST SALE AIRPORT	4.6	-38.1156	147.132
9	ESSENDON AIRPORT	78.4	-37.7278	144.906
10	MELBOURNE REGIONAL OFFICE	32.2	-37.8075	144.97
11	MOORABBIN AIRPORT	12.1	-37.98	145.096
12	MELBOURNE AIRPORT	113.4	-37.6655	144.832
13	LAVERTON RAAF	20.1	-37.8565	144.757
14	MANGALORE AIRPORT	140.8	-36.89	145.183
15	BALLARAT AERODROME	435.2	-37.5128	143.791
16	CAPE OTWAY LIGHTHOUSE	82	-38.8556	143.513
17	CAPE JAFFA THE LIMESTONE	17	-36.9655	139.716
18	BATHURST AIRPORT AWS	744.5	-33.412	149.654
19	BRAIDWOOD RACECOURSE AWS	665.2	-35.4253	149.783
20	GREEN CAPE AWS	19.4	-37.2622	150.05
21	ULLADULLA AWS	35.7	-35.3635	150.483
22	COOMA AIRPORT AWS	930	-36.2939	148.973
23	BOMBALA AWS	760.5	-37.0016	149.234
24	YOUNG AIRPORT	379.6	-34.2493	148.247
25	BENDIGO AIRPORT	208	-36.7395	144.327
26	CERBERUS	12.7	-38.3646	145.178
27	RHYLL	13.4	-38.4612	145.31
28	GROVEDALE GEELONG AIRPORT	33.4	-38.2242	144.334
29	SHEOAKS	236.7	-37.9075	144.13
30	HAMILTON AIRPORT	241.1	-37.6486	142.064
31	PORT FAIRY AWS	10	-38.3906	142.235
32	MORTLAKE RACECOURSE	130	-38.0753	142.773
33	RENMARK AERO	31.5	-34.1983	140.677
34	CONDOBOLIN AIRPORT AWS	192.6	-33.0682	147.213
35	FORBES AIRPORT AWS	230.4	-33.3627	147.921
36	RICHMOND RAAF	19	-33.6004	150.776
37	BADGERYS CREEK AWS	81.2	-33.8969	150.728
38	BEGA AWS	41	-36.6722	149.819

39	GOULBURN AIRPORT AWS	640	-34.8085	149.731
40	ALBURY AIRPORT AWS	163.5	-36.069	146.951
41	WANGARATTA AERO	152.6	-36.4206	146.306
42	MALLACOOTA	22	-37.5976	149.729
43	COMBIENBAR AWS	640	-37.3417	149.023
44	COLDSTREAM	83	-37.7258	145.407
45	AVALON AIRPORT	10.6	-38.0287	144.478
46	WALLAN KILMORE GAP	527.8	-37.3808	144.966
47	PORTLAND CASHMORE AIRPORT	80.9	-38.3147	141.47
48	CAPE NELSON LIGHTHOUSE	45.4	-38.4306	141.544
49	TUGGERANONG ISABELLA PLAINS	586.7	-35.4184	149.094
50	CABRAMURRA SMHEA AWS	1482.4	-35.9371	148.378
51	KHANCOBAN AWS	340	-36.2304	148.141
52	SHEPPARTON AIRPORT	113.9	-36.4289	145.395
53	HUNTERS HILL	981	-36.2136	147.539
54	MOUNT BULLER	1707	-37.145	146.439
55	FALLS CREEK	1765	-36.8708	147.275
56	MOUNT HOTHAM	1849	-36.9767	147.134
57	GELANTIPY	755	-37.22	148.262
58	MOUNT NOWA NOWA	350	-37.6924	148.091
59	MOUNT BAW BAW	1561	-37.8383	146.275
60	MOUNT MOORNAPA	480	-37.7481	147.143
61	SCORESBY RESEARCH INSTITUTE	80	-37.871	145.256
62	FRANKSTON AWS	6	-38.1481	145.116
63	FERNY CREEK DUNNS HILL	561	-37.8775	145.336

APPENDIX B – FIRE EVENT CASE STUDIES

BLACK SATURDAY – 7 February 2009

This event is so well documented and reviewed that only a brief presentation is included, in spite of its massive impact.

Figure B1 shows the WRF fields at 0200 UTC 7 February 2009. This earlier than typical time of day for maximum fire danger is chosen because winds through central and western Victoria on that day were highest rather earlier than later in the afternoon. The very high temperatures, low relative humidity, and high wind speeds are particularly evident. Another feature of note is the cool change, which is just through Cape Otway and Warrnambool at this time, in good agreement with observations. The point value WRF fields at Melbourne Airport show that the temperature is well simulated, as is the wind speed, but the relative humidity is biased too moist by some 10%.

The FFDI field shows values above 100 through western Victoria ahead of the cool change, with values above 120 southwest of Melbourne. The over-prediction of relative humidity at Melbourne Airport contributes to a FFDI value of 97 there, some 40 points lower than if the relative humidity had been correctly simulated.

Figure B2 shows the wind field at 0700 UTC (1800 EDT) on 7 February 2009, when the wind change is past Wilsons Promontory, has just passed Melbourne Airport (observed time 1723 EDT), and also shows the observed change in change-line orientation just a little to the northwest of Melbourne.

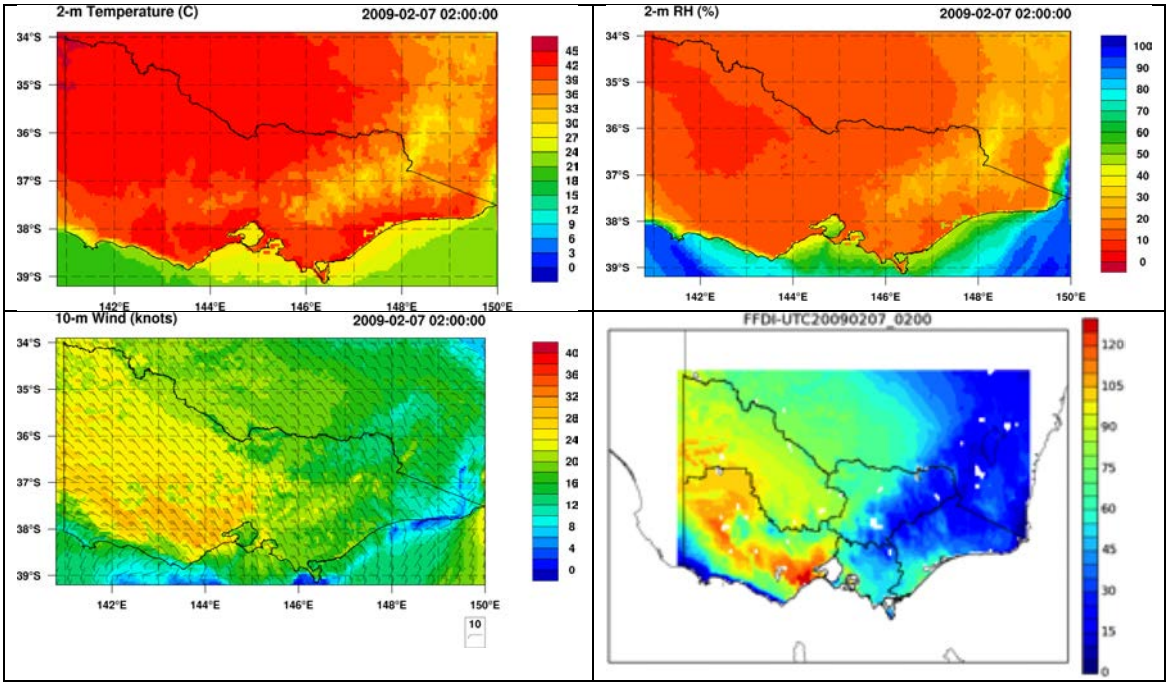

Figure B1. WRF fields of 2m temperature (top left), 2m relative humidity (top right), 10-m wind (bottom left) and FFDI (bottom right) at 0200 UTC (1300 EDT) 7 February 2009.

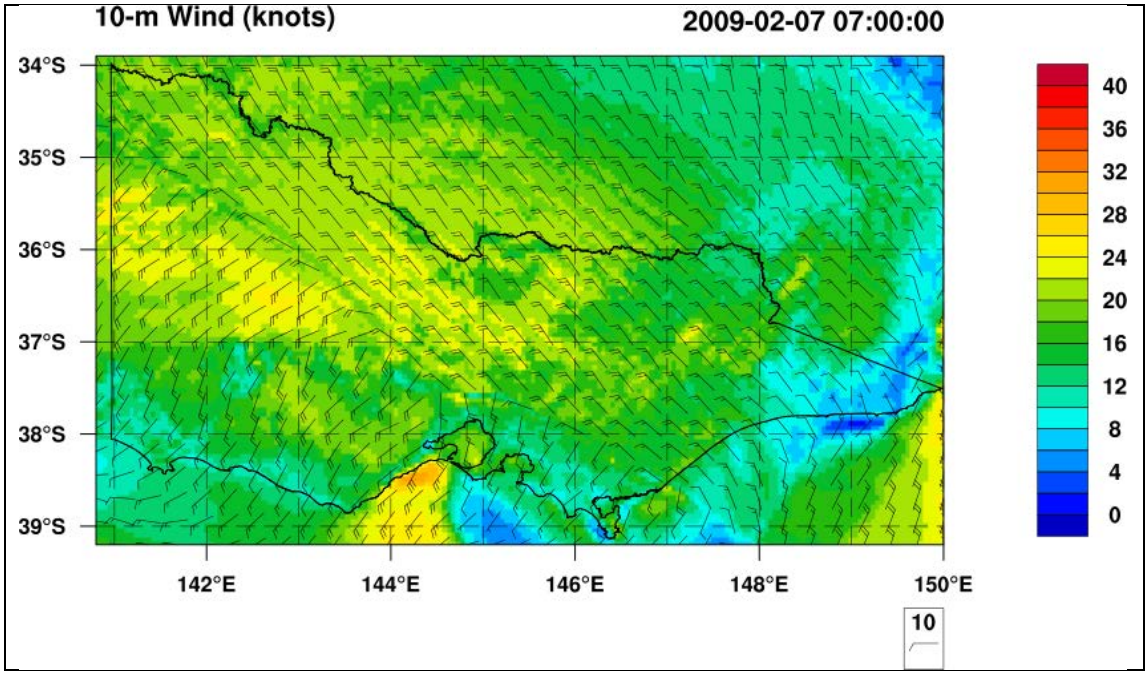

Figure B2. WRF wind field at 0700 UTC (1800 EDT) 7 February 2009.

BRISBANE RANGES FIRE – 22 January 2006

As well as the fire in the Brisbane Ranges, this was also the day of the Mt Lubra Fire in the Grampians, and there were also fires in other areas, including Ngarcat NP in South Australia. The MODIS satellite image for the afternoon of 22 January 2006 (Fig. B3) shows the smoke plumes from these fires.

The WRF fields of temperature, relative humidity, wind, and FFDI are shown in Fig. B4, with the plotted AWS data from Sheoaks in Fig. B5. The WRF simulation has captured the high temperatures, low humidity, and high wind speeds very well with simulated temperatures and relative humidity matching the observed ~40C and ~20% well, and wind speeds in the area of the Brisbane Ranges being 20-25 knots (37-46 km/hr). At Sheoaks the WRF wind speeds are under-predicted by some 9 km/hr at 0500 UTC (39 vs 48 km/hr), but the meteogram (Fig. B5) shows that over the 2-hour period centred on 0500 UTC the wind speed averaged around 44 km/hr, reducing the over-forecast by nearly 50%. In addition, there appears to be some evidence that some of these observations are "SPECI" observations, and so report a 1-minute average wind speed, again affecting this comparison.

The WRF shows an extensive area of FFDI between 50 and 75 extending from western Victoria to the surf coast, and including the Grampians, ahead of the cool change. Values over the Brisbane Ranges, including at the location of the Sheoaks AWS, are around 55.

Figure B6 shows the wind field at 0700 UTC (1800 EDT) 22 January 2006, when the WRF simulated wind change is just about to pass the location of Sheoaks. The structure appears very realistic, but the change passage is an hour, or a little more, early.

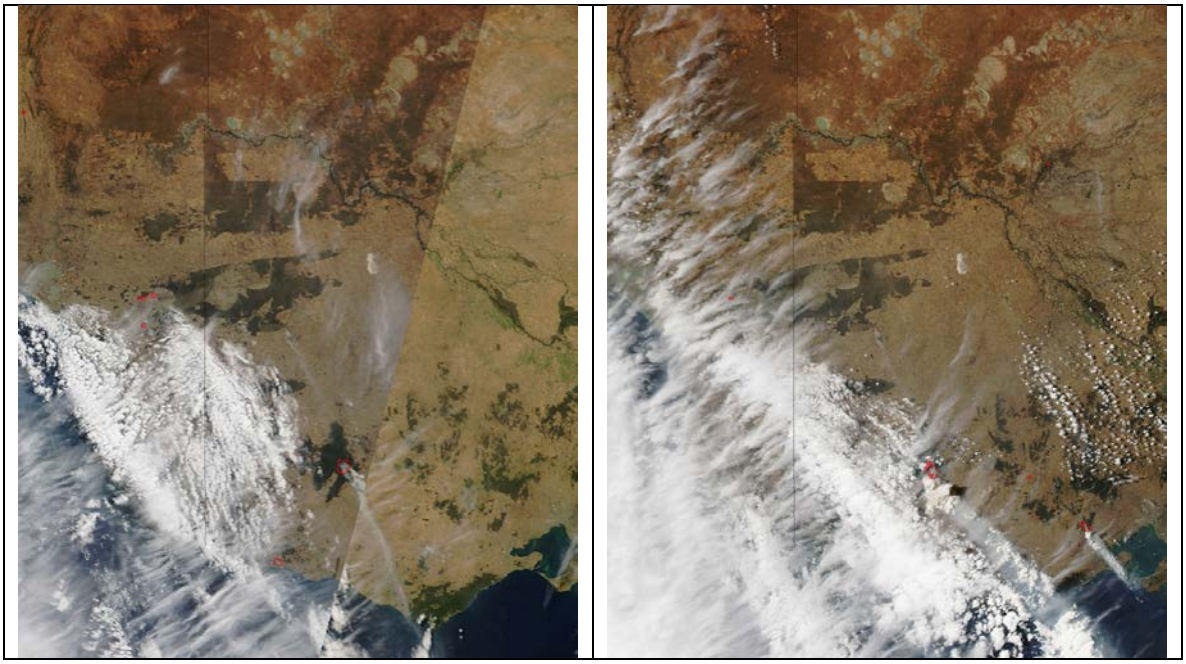

Figure B3. MODIS satellite images at approximately 11am (left) and 2pm (right) on 22 January 2006.

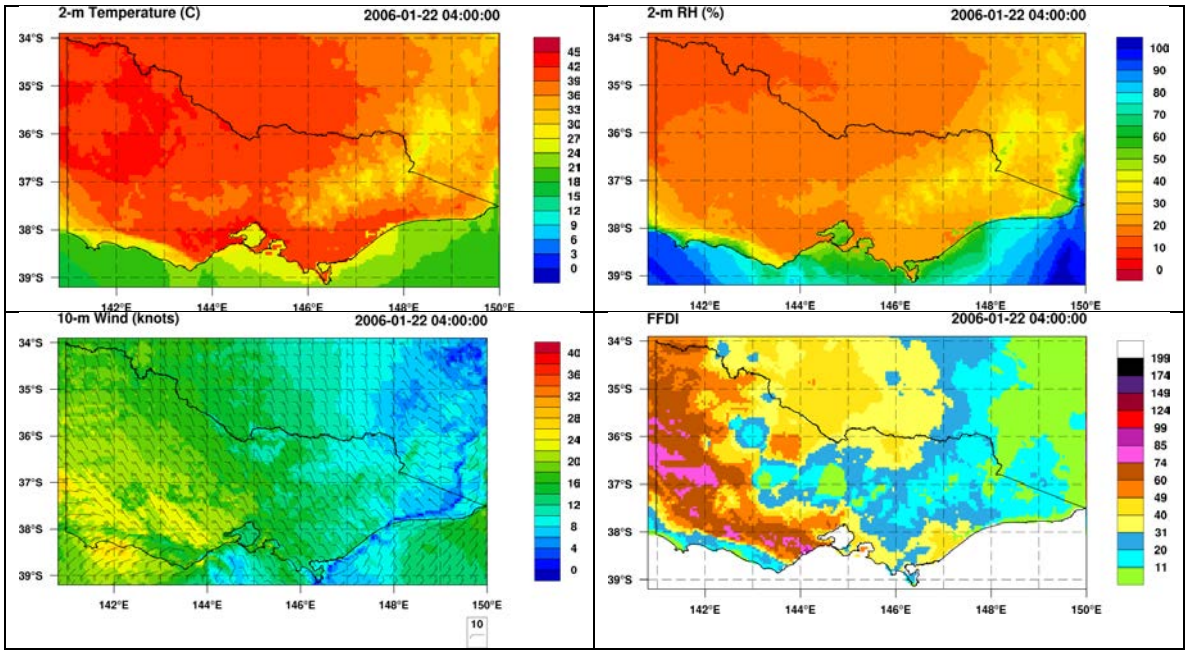

Figure B4. WRF fields of 2m temperature (top left), 2m relative humidity (top right), 10-m wind (bottom left) and FFDI (bottom right) at 0400 UTC (1300 EDT) 22 January 2006.

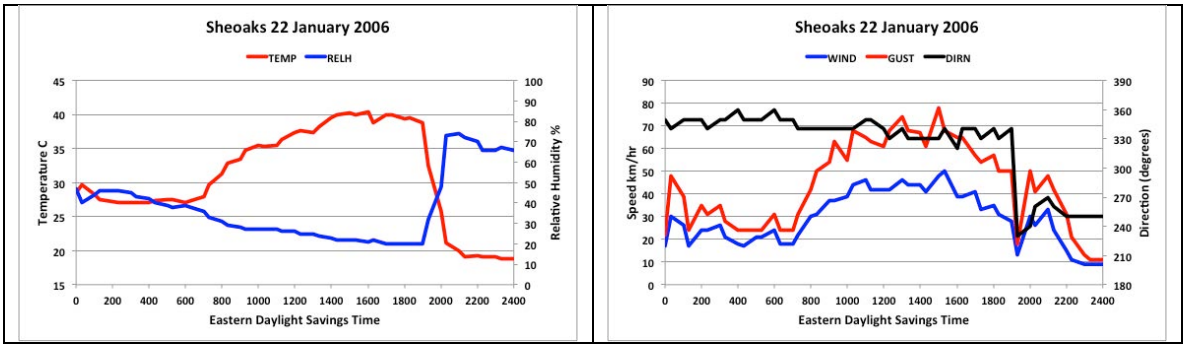

Figure B5. Sheoaks AWS observation time-series of temperature and relative humidity (left), and 10-m mean and gust wind speed and direction for 24 hours from 0000 22 January 2006 (EDST).

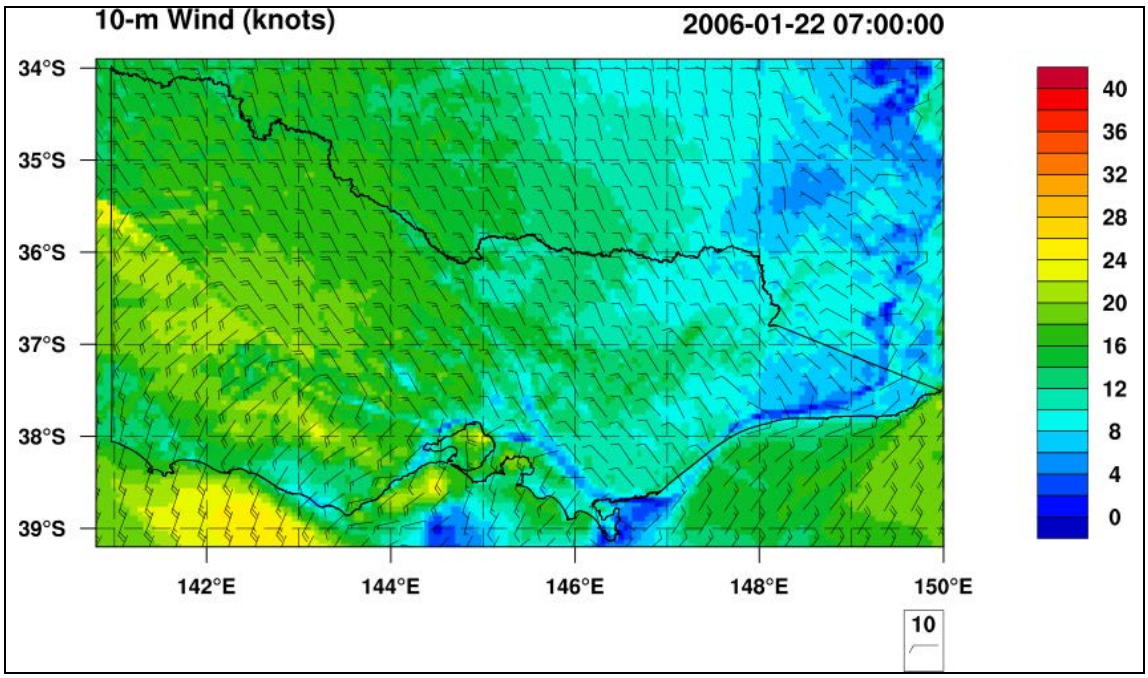

Figure B6. WRF wind field at 0700 UTC (1800 EDT) 22 January 2006.

ALPINE FIRES BREAKOUT – 30 January 2003

This was a day in which the Alpine fires showed a great increase in activity, with huge smoke plumes developing in strong northwesterly winds. The observations from Mt Hotham are shown in Fig. B7. An important feature is the very strong winds overnight, and which persisted well into the day. Due to the elevation the highest observed temperatures were just above 20C, and lowest relative humidity around 30%, but with the high wind speeds this gave an FFDI in the 25-30 range assuming a Drought Factor of 8 as used by the WRF calculation.

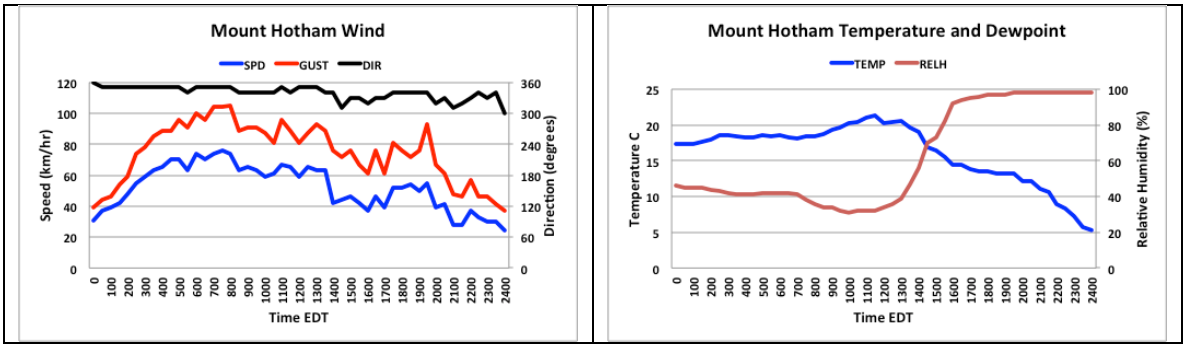

Figure B7. Observations of wind direction, speed and gust speed (left) and temperature and relative humidity (right) from the Mt Hotham AWS from midnight to midnight (EDT) 30 January 2003.

The WRF fields show a number of interesting features. Figure B8 shows the wind field at 2200 UTC 29 January (0900 EDT 30 January 2003. Very strong winds are seen over the Alps, indicative of topographically-induced mountain wave/downslope winds. Additionally a southwesterly change is moving through central Victoria.

This change is further advanced to the north of the state. An initial wind change was observed to pass through Wangaratta between 2230-2330 UTC. Thereafter it veered slightly to WNW for a couple of hours before backing steadily again. WRF showed this behaviour very realistically, with the change there occurring between 0000 and 0100 UTC in the WRF data.

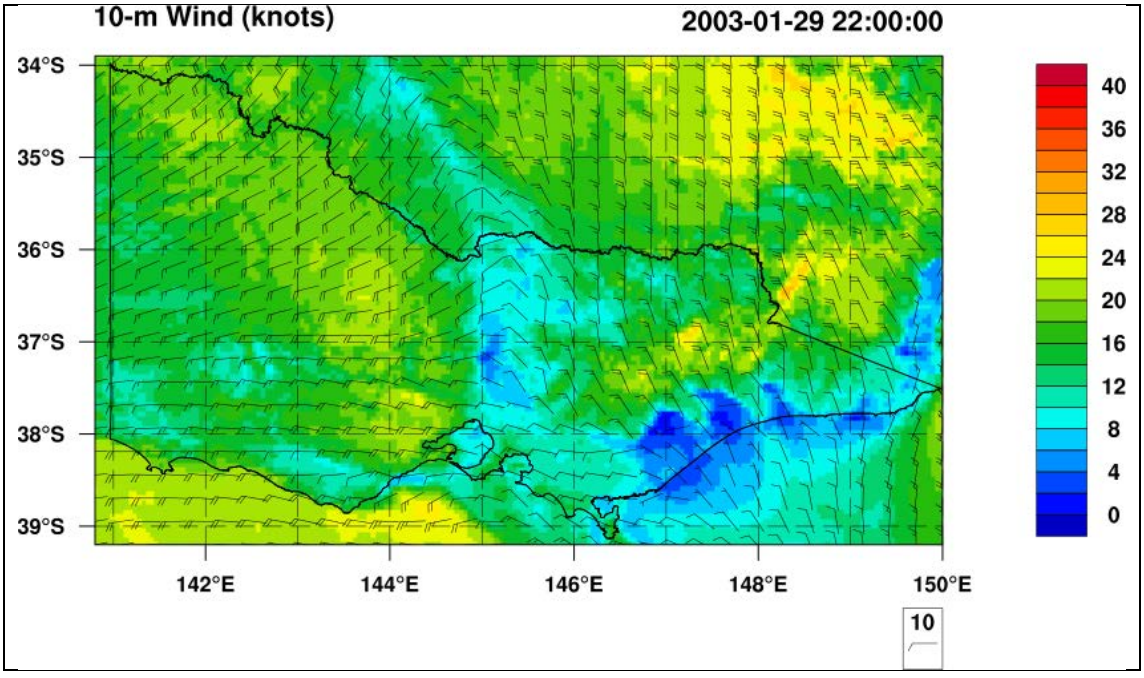

Figure B8. WRF wind field at 2200 UTC 29 January (0900 EDT 30 January) 2003.

The fire weather fields from WRF at 0000 UTC (1100 EDST) 30 January 2003 are shown in Fig. B9. Temperature, relative humidity and wind speed are of the same order as those

observed at the Mt Hotham AWS (Table 4), with corrected temperature being a little higher and corrected wind speed a little lower than that observed. It is notable, though, that the time-sequence of AWS observations at Mt Hotham is highly variable. This is consistent with the spatially variable pattern of wind speed over the highest terrain in Fig. B9, suggestive of topographically modified flow fields.

The FFDI pattern shows a band of highest FFDI extending southwards from central NSW, matching the location of the highest temperatures and lowest relative humidity, and crossing the Alps in the vicinity of Mt Hotham, but attenuated in magnitude with increasing elevation.

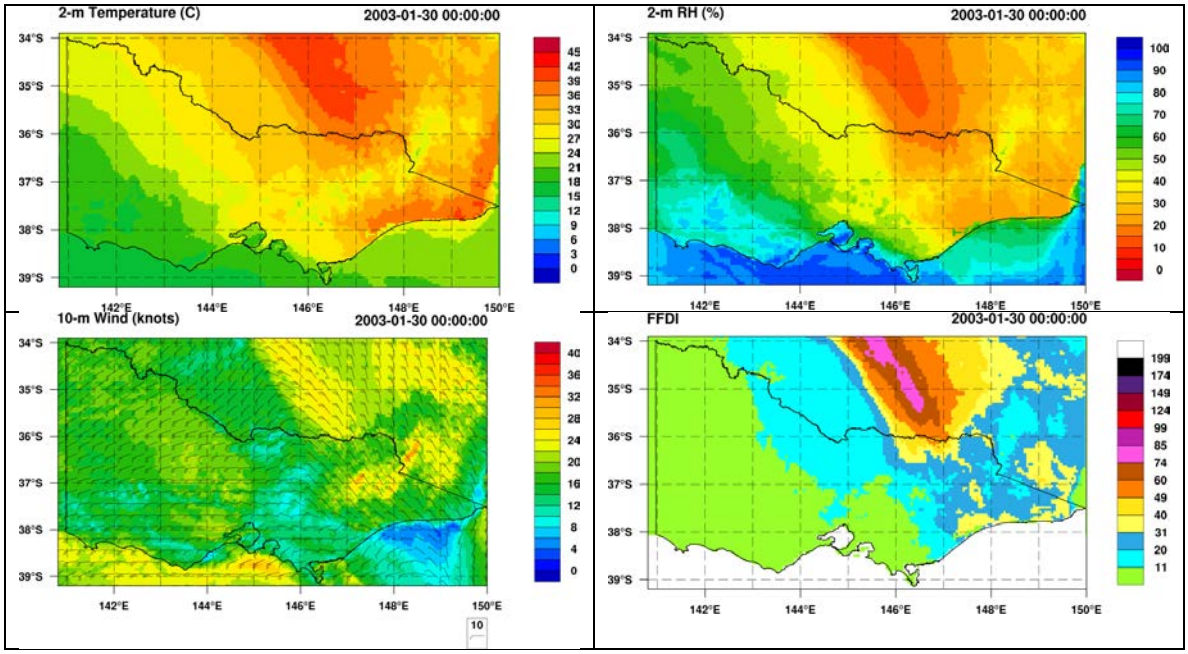

Figure B9. WRF fields of 2m temperature (top left), 2m relative humidity (top right), 10-m wind (bottom left) and FFDI (bottom right) at 0000 UTC (1100 EDT) 30 January 2003.

It is also seen in Fig. B9 that the southern portion of the wind change has moved eastwards from its position two hours earlier, and is approaching Bairnsdale at this time. The AWS observations from Bairnsdale are shown in Fig. B10. A somewhat complex change structure is seen, but with the change finally passing through Bairnsdale at around 0330 UTC (1430 EDT) 30 January 2009. The WRF fields indicate the change passage through Bairnsdale at 0400 UTC (Fig. B11), and also simulate the observed (Fig. B10, left) increase in wind speed after the change passage. At this stage, the parts of the change north and south of the ranges are clearly separate structures, with little change in wind direction over the higher parts of the Victorian Alps. The pattern in Fig. B10 is also very similar to that shown in Mills (2005a) from the Bureau of Meteorology's then operational mesoscale NWP model. This change was modelled by WRF at Gelantipy at 0500 UTC, and observed there between 0400 and 0430 UTC.

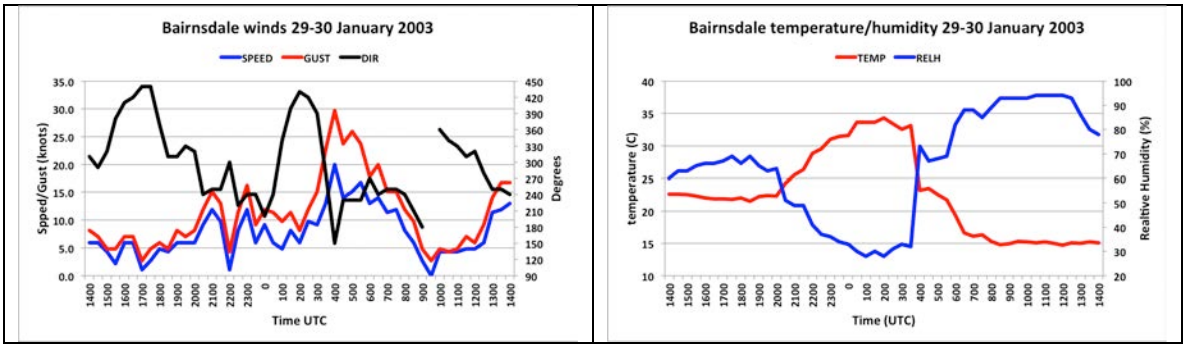

Figure B10. Observations of wind direction, speed and gust speed (left) and temperature and relative humidity (right) from the Bairnsdale AWS from midnight to midnight (EDT) 30 January 2003.

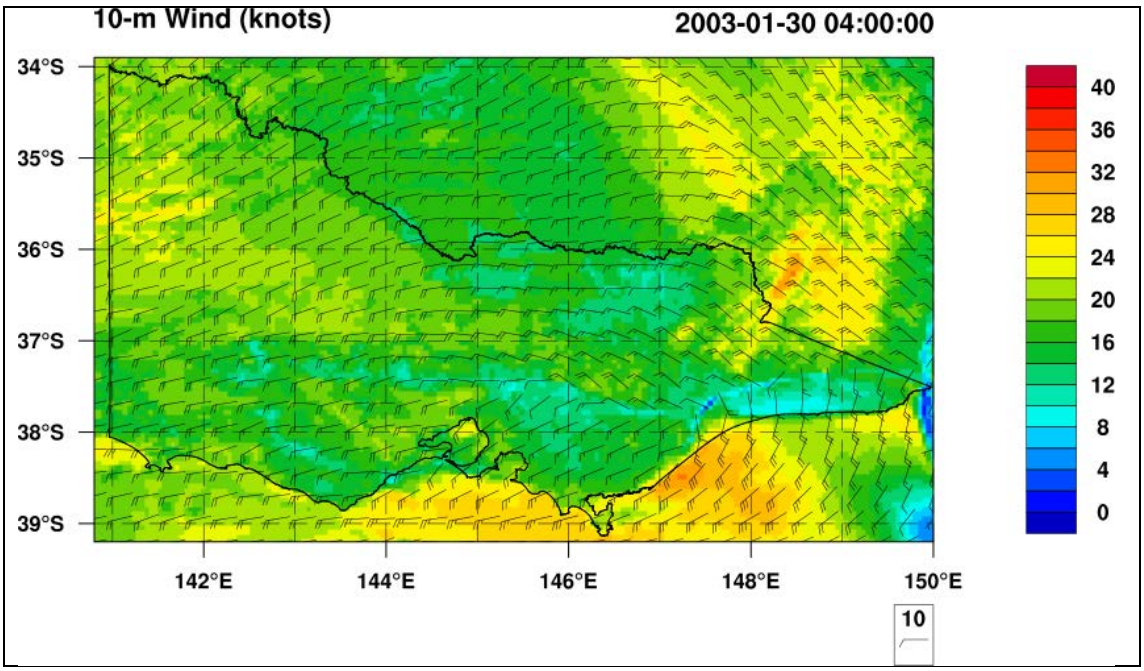

Figure B11. WRF wind field at 0400 UTC (1500 EDT) 30 January 2003.

CANBERRA – 18 January 2003

This is the day that the fires ignited by lightning on 8 January 2003 showed extreme fire behaviour and caused huge damage to life and property in Canberra. The particular aspects that we wish to concentrate on are:

- The fire weather at Canberra on the afternoon of 18 January;
- The arrival of the cool change from the east in the late evening;
- The deep atmospheric dry band that was hypothesised to be the major contributor to the steep drop in humidity on the afternoon of 18 January.

Figure B12 shows the time series of Canberra Airport AWS observations through 18 January 2003.

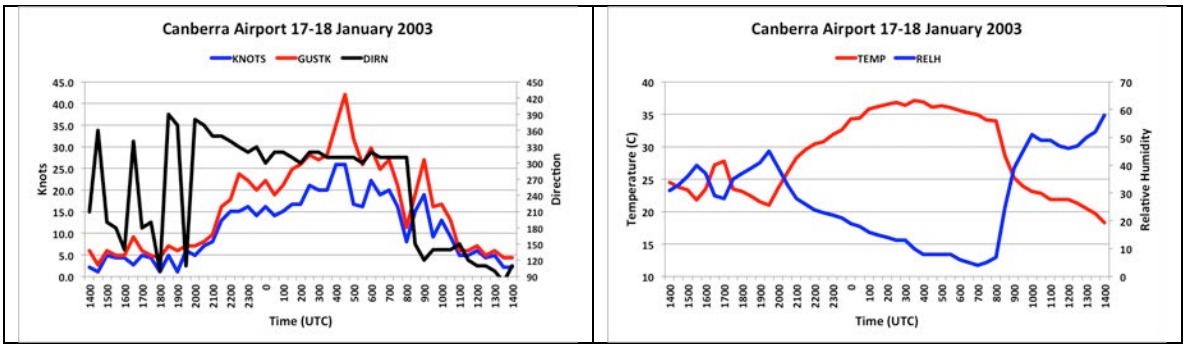

Figure B12. Observations of wind direction, speed and gust speed (left) and temperature and relative humidity (right) from the Canberra Airport AWS from midnight to midnight (EST) 18 January 2003.

Figure B13 shows the WRF 2m temperature, relative humidity, and 10m wind speed fields at 0400 UTC 18 January 2003, near the time of maximum FFDI. The high temperatures, low relative humidity, and 20-25 knot (37-46 km/hr) winds in the area are evident. The temperature is very well simulated (Table 4), but relative humidity is too moist compared to the AWS observations at Canberra Airport, and the wind speed is only some 66% of observed, leading to lower FFDI values than those based on the observations. The wind speed observation at 0400 UTC was, though, a SPECI and so a 1-minute average. The mean of the wind speed observations from 0300-0500 was 40 km/hr, reducing the difference between WRF and AWS values. The band of near-surface dry air that Mills (2005a) associated with a satellite water-vapour image showing a mid-tropospheric dry band can also be seen at 0400 UTC west and northwest of Canberra.

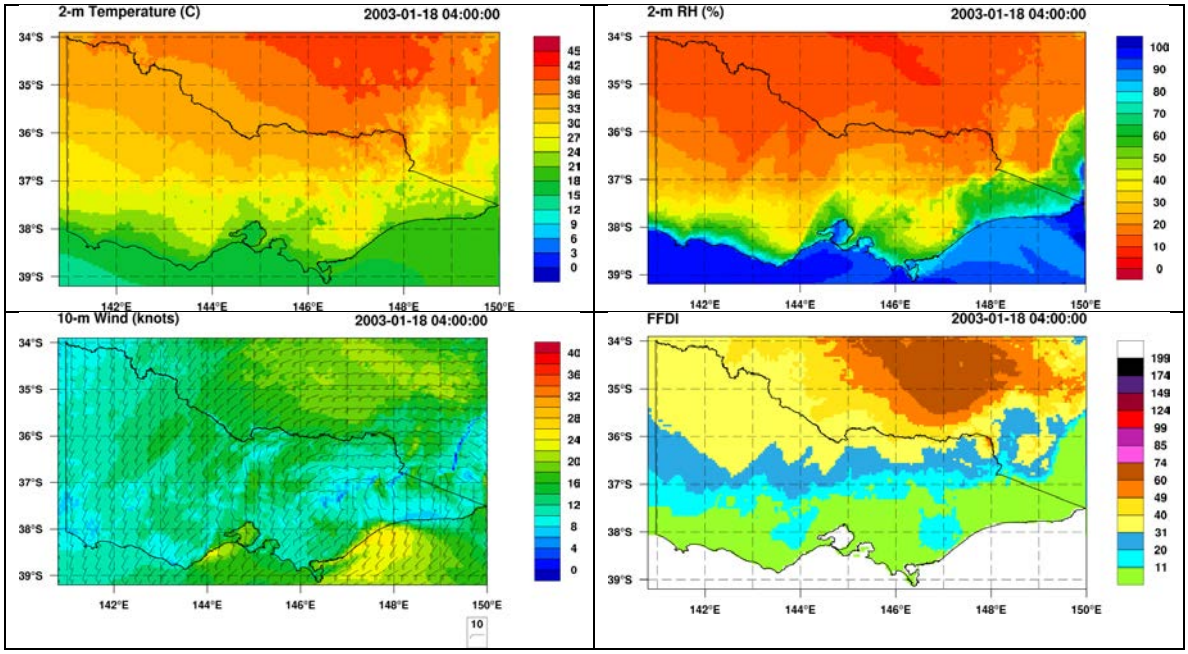

Figure B13. WRF fields of 2m temperature (top left), 2m relative humidity (top right), 10-m wind (bottom left) and FFDI (bottom right) at 0400 UTC (1500 EDT) 18 January 2003.

This is better seen at 0000 UTC (Fig. B14), where the WRF relative humidity pattern shows a strong correspondence to the position of the upper atmosphere dry band (seen as dark in the satellite image), although the WRF values are biased high compared to the very low values observed as the dry band passed through surface stations such as Wagga Wagga (Mills 2005a).

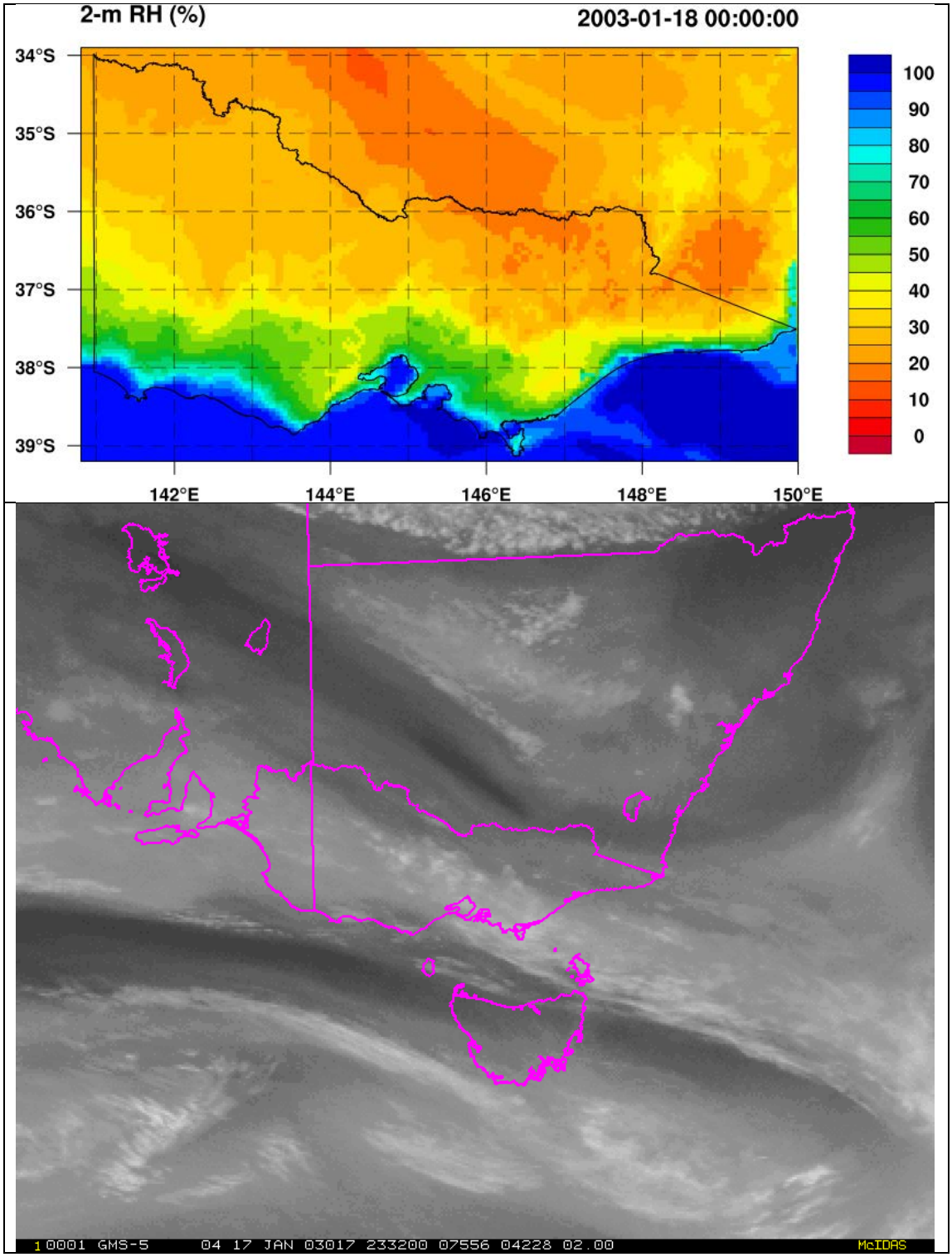

Figure B14. WRF relative humidity at 0000 UTC 18 January 2003 (top), and GMS-5 water vapour channel imagery at 2332 UTC 17 January 2003 (bottom).

Finally, Fig. B15 shows an excellent WRF simulation of the arrival of the easterly cool change, both in terms of timing (less than 30 mins error) and structure.

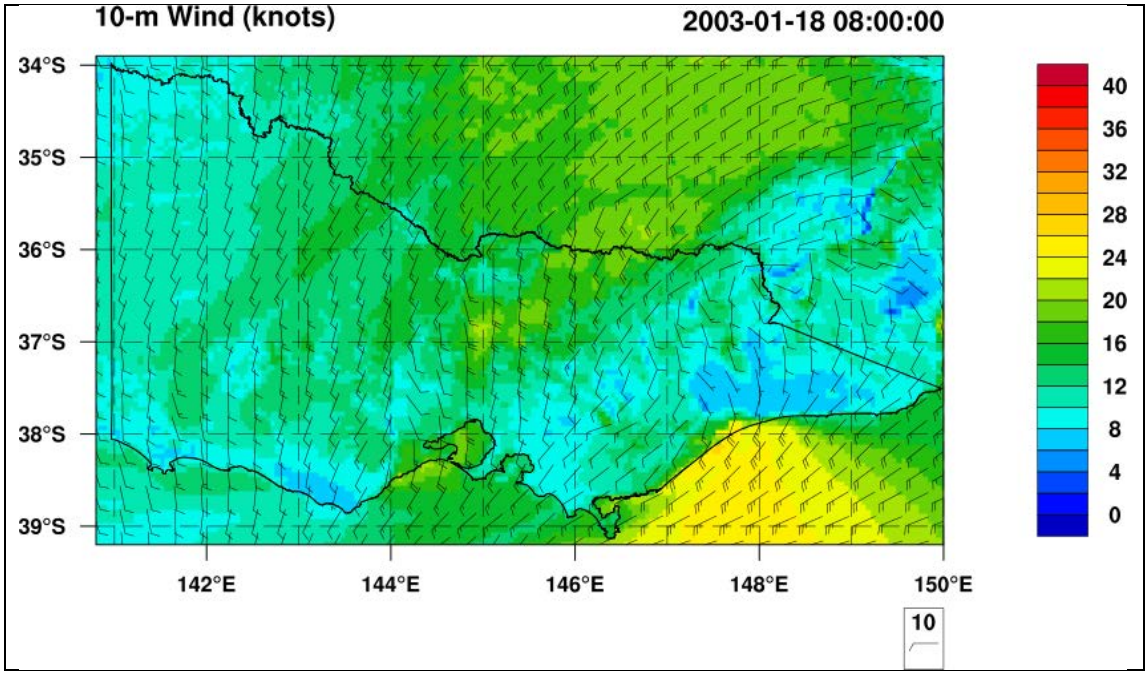

Figure B15. WRF wind field at 0800 UTC (1900 EDT) 18 January 2003.

MELBOURNE SMOKE FUMIGATION – 11 January 2001

To quote from Hess et al (2006) "*On 11 January 2001 thick smoke was transported behind a cold front from the Lavinia Nature Reserve in the northeast corner of King Island, some 250 km to the northeast (see Fig. 1 for locations) to the Melbourne area. This event led to the highest level of particulate recorded (at the time) in Melbourne since the Ash Wednesday bushfires and the Melbourne Dust Storm of 1983. The smoke from the King Island fire arrived in the Melbourne suburbs during the evening. Earlier that afternoon smoke from a smaller fire at Winchelsea (100 km southwest of Melbourne) arrived with the cold front.*"

We concentrate on two aspects of this case. First the fire weather representative of the Winchelsea fire, and second the wind change timing. Grovedale (Geelong Airport) AWS observations show at 1400 EDT 11 January 2001 pre-change temperature, relative humidity and wind speed of 39.4C, 12%, and 41 km/hr. The WRF fields are shown in Fig. B16, and indicate hot, dry and windy conditions in the area. WRF point values at 0300 UTC shows (Table 4) temperature less than a degree low, but relative humidity 5% too high and wind speed some 11 km/hr too low. However, the average wind speed from 0200 to 0330 UTC (0400 UTC was post cool change) was 34 km/hr, indicating much closer agreement for the WRF. The wind change is also evident just reaching the coast south of Geelong. A zone of higher FFDI, approaching 50, is seen in the area just west of Geelong (Fig. B16).

Figure B17 shows the wind field at 0500 UTC, showing the wind change to have just passed through Moorabbin Airport, where the observed wind change occurred between 0500 and 0530 UTC, indicating a change timing error of less than an hour.

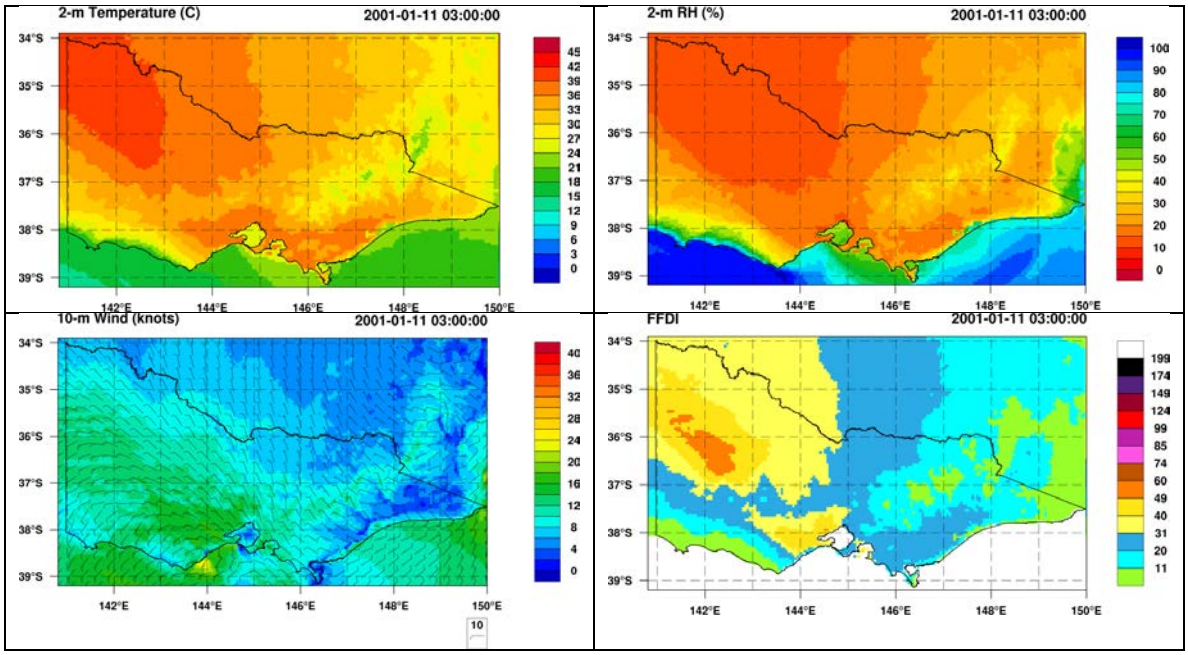

Figure B16. WRF fields of 2m temperature (top left), 2m relative humidity (top right), 10-m wind (bottom left) and FFDI (bottom right) at 0300 UTC (1400 EDT) 11 January 2001.

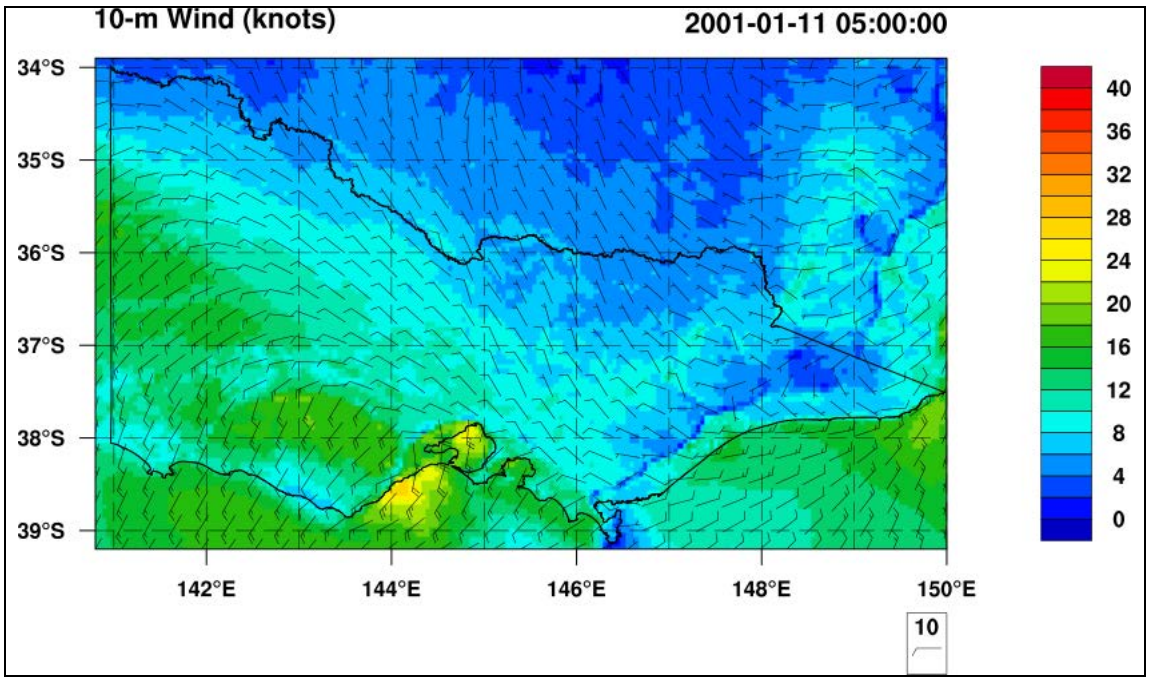

Figure B17. WRF wind field at 0400 UTC (1500 EDT) 11 January 2001.

LINTON FIRE – 2 December 1998

The fire started near Linton (37.68S, 143.57E) at around 1300 EDT on 2 December 1998. At 1400 EDT weather conditions were reported by the CFA to be temperature 28C, relative humidity 24%, and wind 44 km/hr. Importantly, a wind change arrived on the eastern flank of the fire ground at 2040 EDT (0940 UTC) 2 December 1998 (statistics from CFA 1999).

The WRF temperature, relative humidity and wind fields at 1400 EDT (0300 UTC) 2 December 1998 are shown in Fig. B18. The temperature and wind speeds are very close to those reported, while the relative humidity is some 15% high. WRF FFDI values are around 10. While the meteorological parameters contribute to these low values, the Drought Factor is also relatively low, around 5 at the location of Linton.

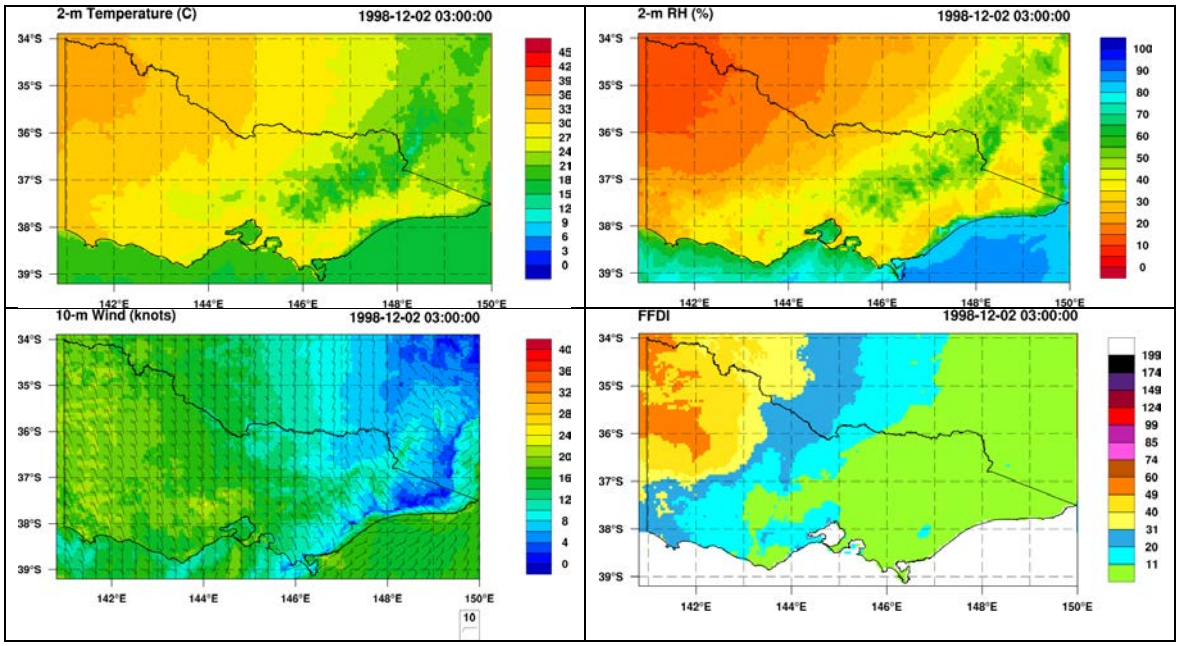

Figure B18. WRF fields of 2m temperature (top left), 2m relative humidity (top right), 10-m wind (bottom left) and FFDI (bottom right) at 0300 UTC (1400 EDT) 2 December 1998.

The WRF wind field at 1000 UTC (2100 EDT) is shown in Fig. B19. The wind change is immediately west of Linton, and hourly animations of the wind field suggest that the wind change timing error was less than 1 hour.

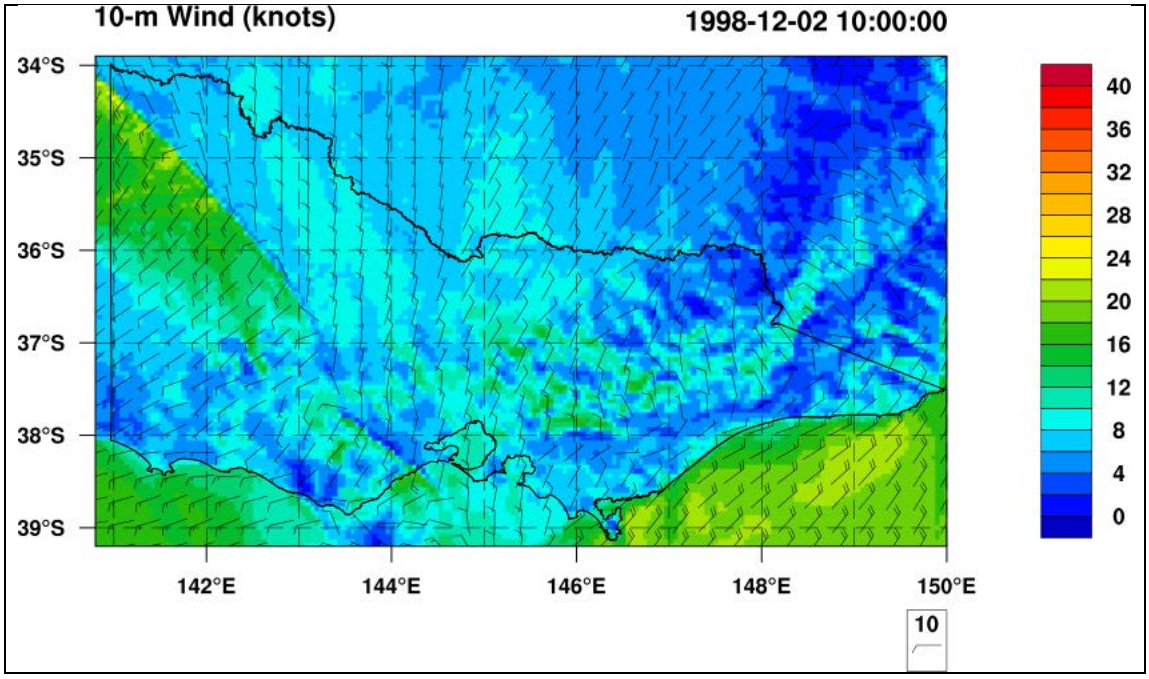

Figure B19. WRF wind field at 1000 UTC (2100 EDT) 2 December 1998.

DANDENONG RANGES FIRE – 21 January 1997

This fire started during the morning of 21 January 1997, and was affected by the passage of a wind change in the early evening. Fires also occurred on the Mornington Peninsula, and smoke from these fires was advected over the eastern suburbs of Melbourne under a strong post-frontal inversion. The meteorology of the cool change was reported by Mills (2002).

The WRF temperature, relative humidity and wind fields at 1400 EDT (0300 UTC) 21 January 1997 (the last time reported from the Scoresby AWS before a gap in observations) are shown in Fig. B20. The Scoresby observations (Table 4) at 0300 UTC show that the temperature is a little low in WRF, the relative humidity a little high, and the wind speed under-forecast. While not affecting the temperature and the relative humidity observations, the observation at this time (and the previous 3 half-hourly observations) were "SPECI", and so may show higher wind speeds than would be reported from a 10-minute average. The developing wind change is seen along the Surf Coast east of Cape Otway.

The change moved through Moorabbin Airport just after 1800 EDT (0700 UTC) 21 January 1998, and the WRF wind field for that time (Fig. B21) shows that the simulated change is just a little earlier than that observed. Interestingly, Mills (2002) makes the point that at Aireys Inlet there was a lull in the wind speed around the time of change passage, followed by a surge in speed of the post-frontal winds, and this structure is seen in Fig. B21.

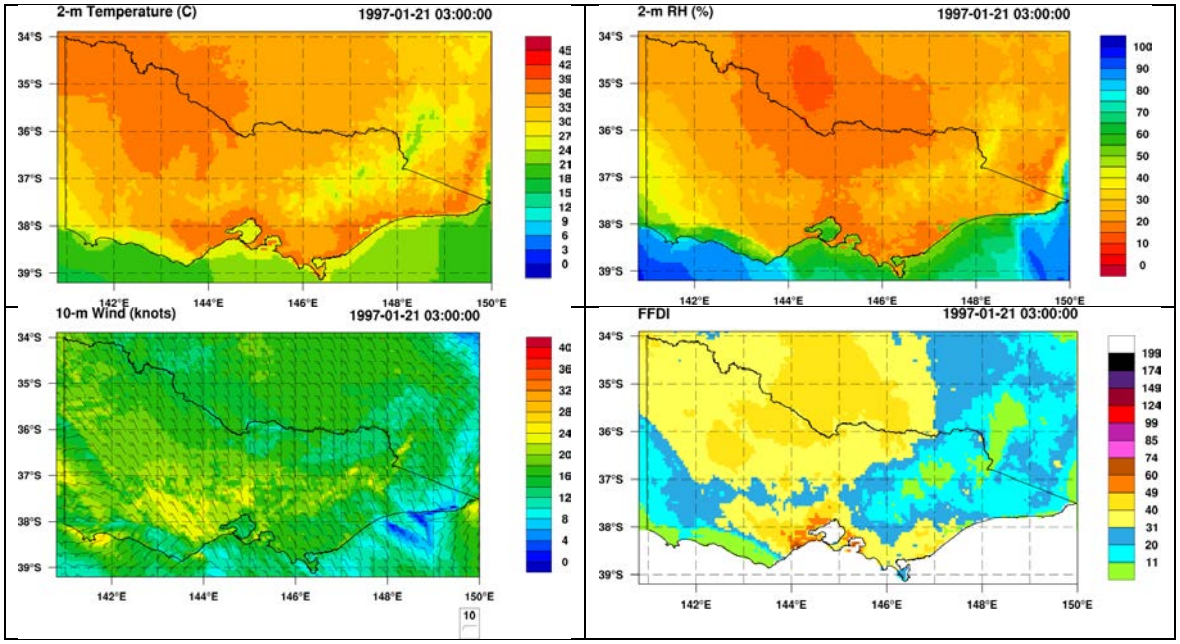

Figure B20. WRF fields of 2m temperature (top left), 2m relative humidity (top right), 10-m wind (bottom left) and FFDI (bottom right) at 0300 UTC (1400 EDT) 21 January 1997.

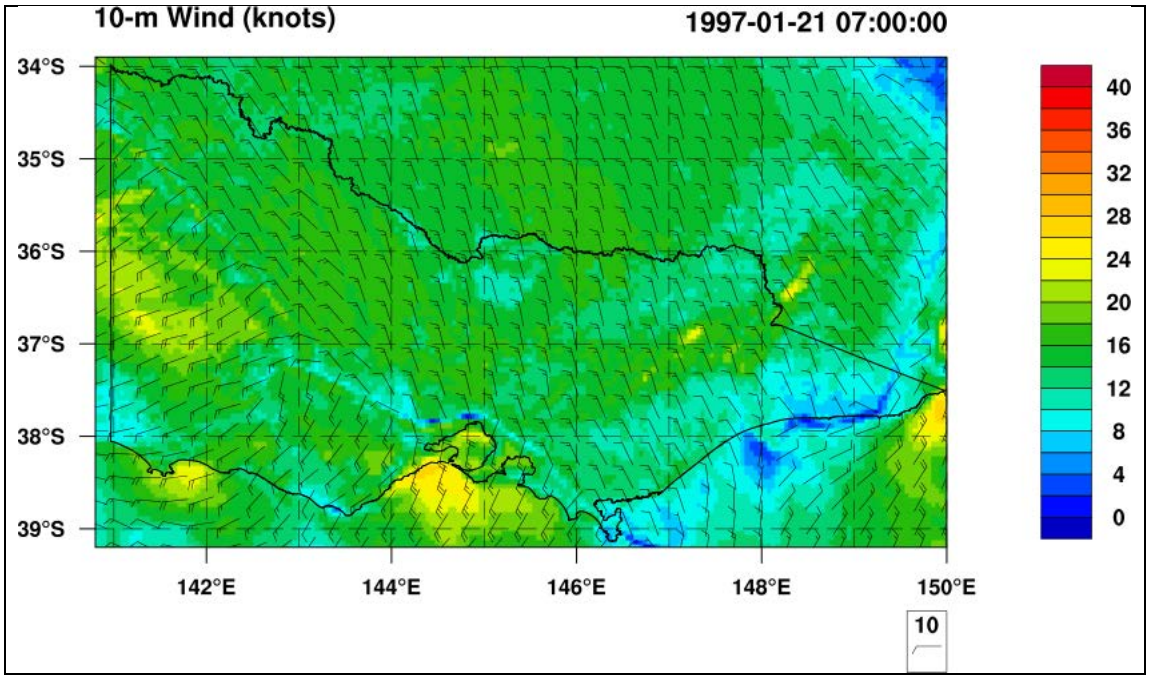

Figure B21. WRF wind field at 0700 UTC (1800 EDT) 21 January 1997.

BERRINGA FIRE – 25 February 1995

Berringa is somewhat south of Ballarat. It was an interesting fire because while conditions were hot and dry, it was a sub-synoptic wind change that shifted a long, narrow grass fire which had started in (then) Extreme fire weather conditions, but which were decreasing as wind speed decreased, into a very dry forest. The marked increase in fuel load then led to

greatly increased fire activity, and a pyrocumulus cloud was measured on radar to reach 9600m.

There are two aspects to be assessed: first, the fire weather ahead of the mesoscale wind change (typically 37C, 5%, 290/30 km/hr in mid-afternoon (Chatto, 1999), but with wind speeds declining to ~15 km/hr just before the wind change at Berringa at 0730 UTC, and second, the structure and timing of the wind change.

WRF temperature, relative humidity, and wind fields at 0400 UTC are shown in Fig. B22. Forecast fields well match the observations, with wind speeds perhaps just a little low, but also showing a decline with time when looped hour by hour.

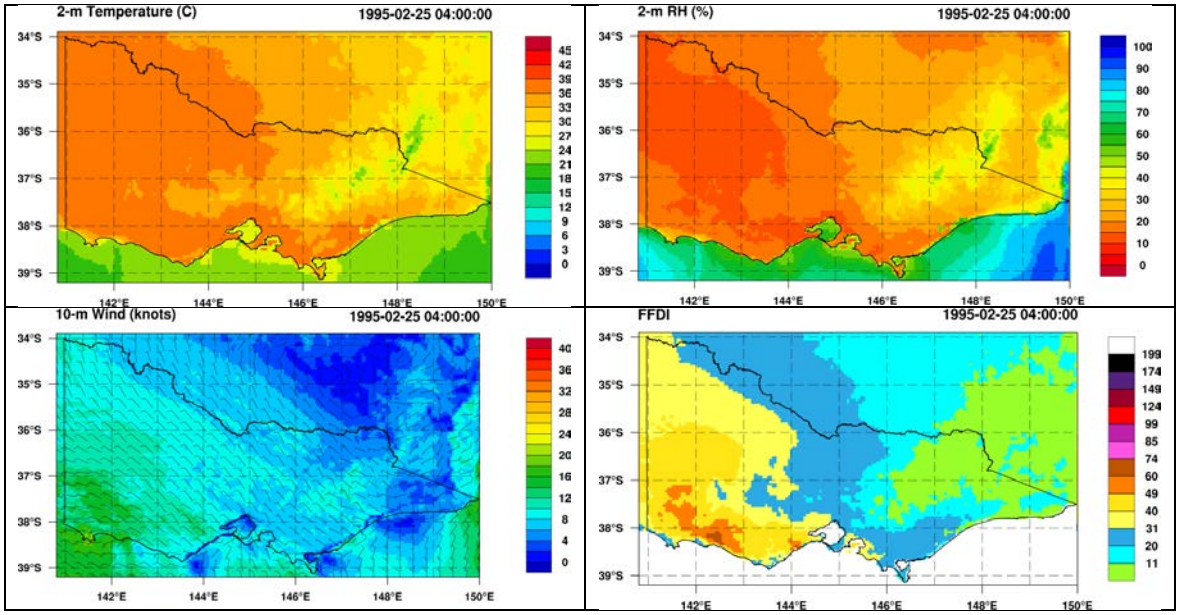

Figure B22. WRF temperature, relative humidity, and wind speed and direction at 0400 UTC 25 February 1995.

The wind change at 0730 UTC was a crucial component of the fire weather on the day. WRF has done an outstanding job here (Fig. B23), with the change reaching Berringa (near 37.8S, 143.8E) just before 0800 UTC. It also shows an increase in post-change wind speeds, as was observed by the portable AWS at the fire (Chatto 1999).

A summary assessment of WRF for this case would be excellent. It will be interesting to follow up this event with the 3-D fields to look at the stability aspects of the atmosphere. Mills and McCaw (2010) also show a potential impact of an unusual jet stream structure that focused ascent over the fire area around the time of the wind change development.

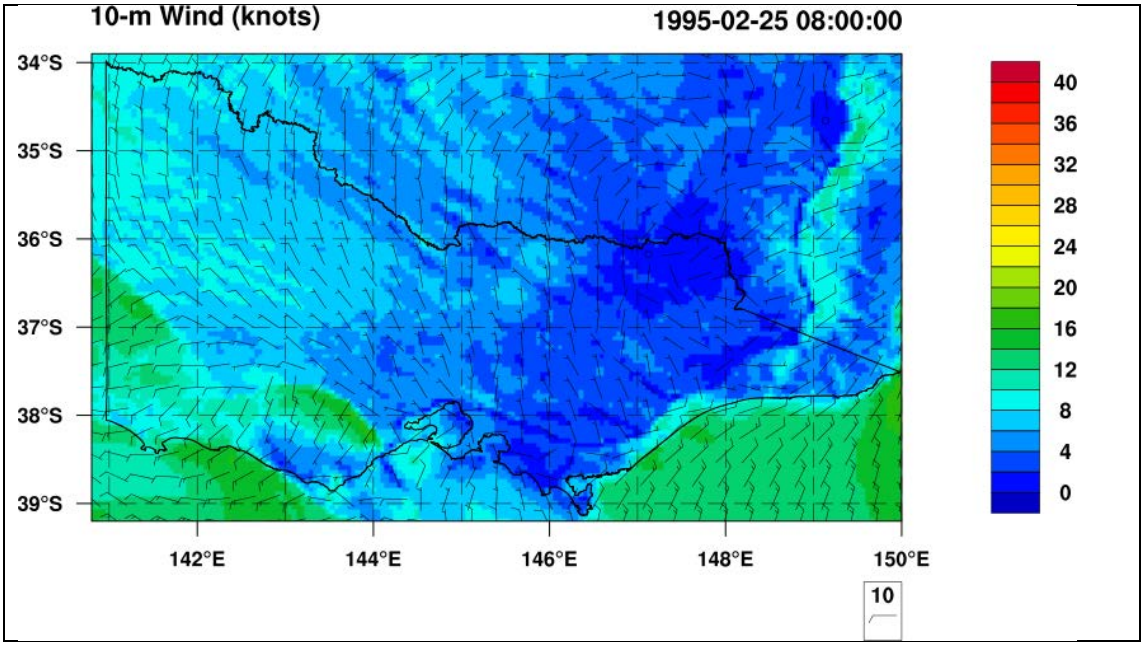

Figure B22. WRF wind field at 0800 UTC (1900 EDT) 25 February 1995.

STRATHBOGIE RANGES – 27-30 December 1990

Country Fire Authority (1991) describes this event from a fire management perspective, while less formal, but reasonably comprehensive, notes were prepared by the Bureau of Meteorology (unpublished). The key day was 27 December, when a small low-pressure system formed just off the southeast coast of South Australia and moved eastwards across southern Victoria. Associated with the low was a trough system extending northwards. The wind shift with this trough passage was not as marked as with many dry cold fronts, but very strong northwesterly winds mixed to the surface in the late morning, and then backed to the west-southwest later in the day.

The Bureau of Meteorology notes also mention an abrupt decrease in relative humidity accompanied this increase in wind speed during morning heating.

Figure B23 shows the WRF wind speed, temperature and relative humidity fields at 0400 UTC. Temperatures in the Strathbogie region are around 35C, relative humidity between 10 and 15%, and wind speeds at least 30 kts (60 km/hr). The WRF conditions, interpolated to Benalla, are slightly more extreme than the 3pm observation at Benalla (Station 082002) (Table 4), but essentially excellent. (Note the values quoted in CFA (1991) do not match those in the Bureau of Meteorology archives, with the CFA report quoting a wind speed of 65 km/hr).

The WRF has an FFDI value of 73 at 3pm at Benalla, but the spatial field shows a band of very high values reaching over 100, matching the high temperatures, low humidities, and high wind speeds, extending southward into Victoria, and time series shows this to move eastwards across the northern part of the state.

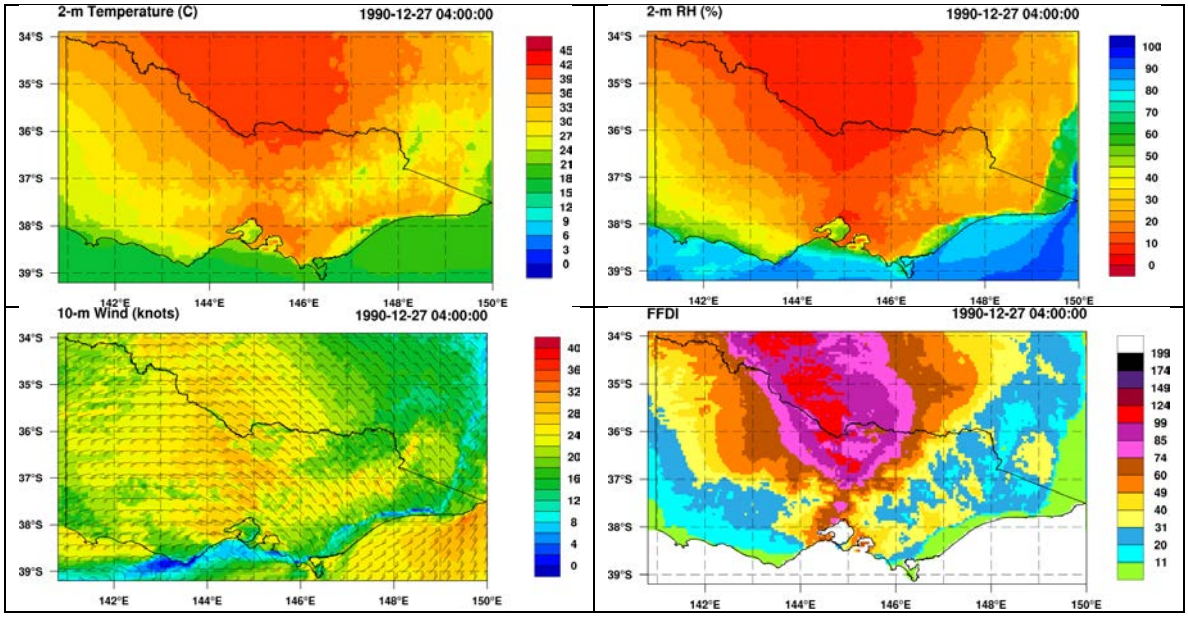

Figure B23. WRF temperature, relative humidity, and wind speed and direction at 0400 UTC 27 December 1990.

The Bureau of Meteorology notes also mention an abrupt decrease in relative humidity accompanied this increase in wind speed during morning heating. This behaviour is well-replicated in the WRF simulations.

Interestingly, Fig. B24 shows the upper air profiles at Laverton at 0000 UTC and 1200 UTC 27 December 1990. Particularly at 0000 UTC it is evident that strong northwesterly winds are present above the surface inversion, and that this would break when the temperature reached around 30C, when a sharp increase in wind speed would be expected to occur.

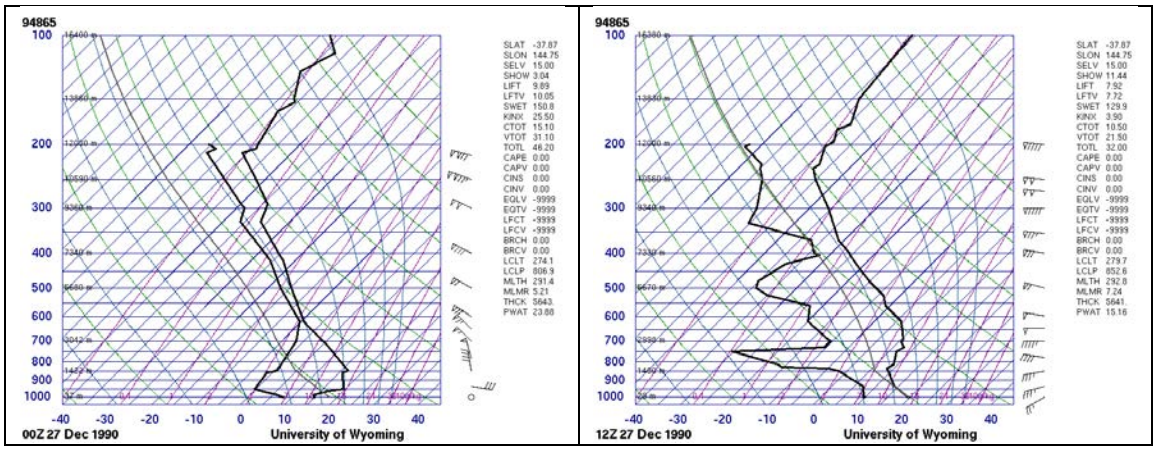

Figure B24. Laverton radiosonde profiles at 0000 and 1200 UTC 27 December 1990.

BEMM RIVER – 14 October 1988

This is an interesting case as it is in far East Gippsland, unlike all the other cases in this Appendix, and also is early in the fire season, in mid-October. Buckley (1992), quoted by Kilic

(personal communication), reports weather conditions around noon of temperature 30C, relative humidity 27%, and a wind speed of 95 km/hr. It is unclear whether this extra-ordinarily high wind speed was a measurement or an estimate, and so in the comparison of observed and WRF parameters we have used the observation at Orbost at 3pm (0400 UTC) for comparison – here the wind speed was reported as 45 km/hr. However, there are no observations around noon, and the WRF fields indicate highly variable weather conditions in that region.

The WRF meteorological fields at 0300 UTC show hot, very dry, and very windy conditions in far east Gippsland at that time, and while the wind speeds do not match the reported 95 km/hr, they are around 30 knots (55 km/hr), and there are indications of mountain wave effects, suggesting that higher speeds would be likely for shorter periods, and with considerable spatial and temporal variability.

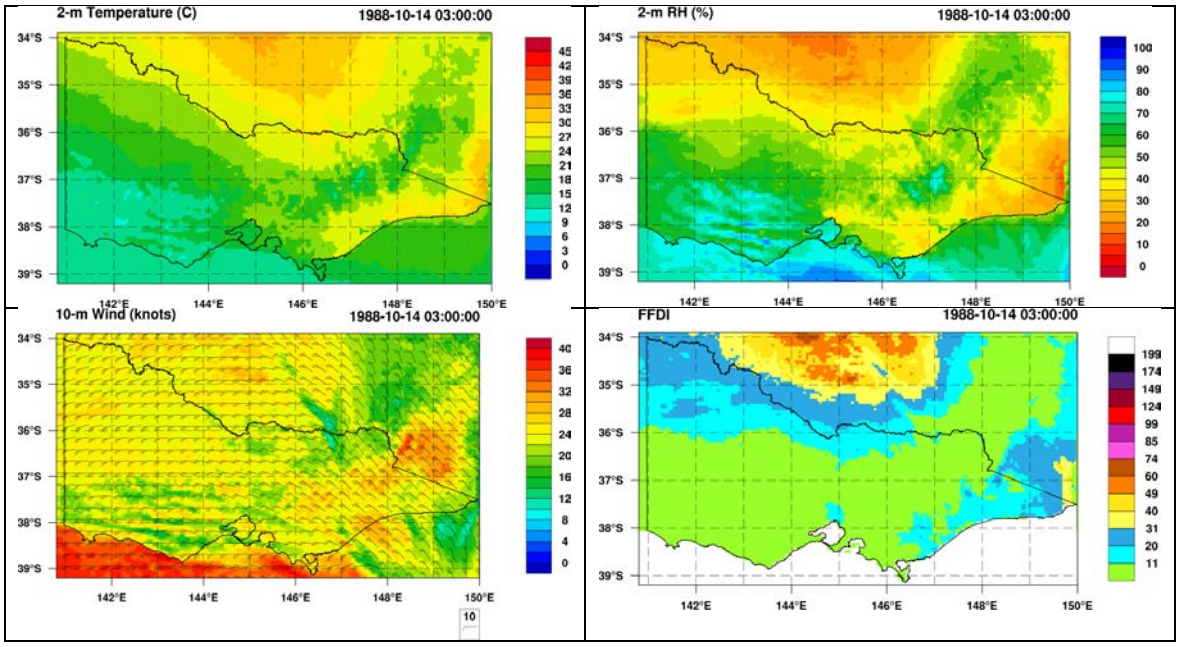

Figure B25. WRF temperature, relative humidity, and wind speed and direction at 0300 UTC 14 October 1988.

The FFDI field, and the point values interpolated at Orbost (Table 4) suggest that the FFDI was below 20 over much of the region, due to the Drought Factor not being particularly high.

Figure B26 shows the WRF wind and relative humidity patterns across Victoria at 0700 EDT 14 October, and there are strong indications of foehn/downslope winds overnight, and with very low overnight relative humidity recovery indicated across much of southern Victoria, and particularly in East Gippsland.

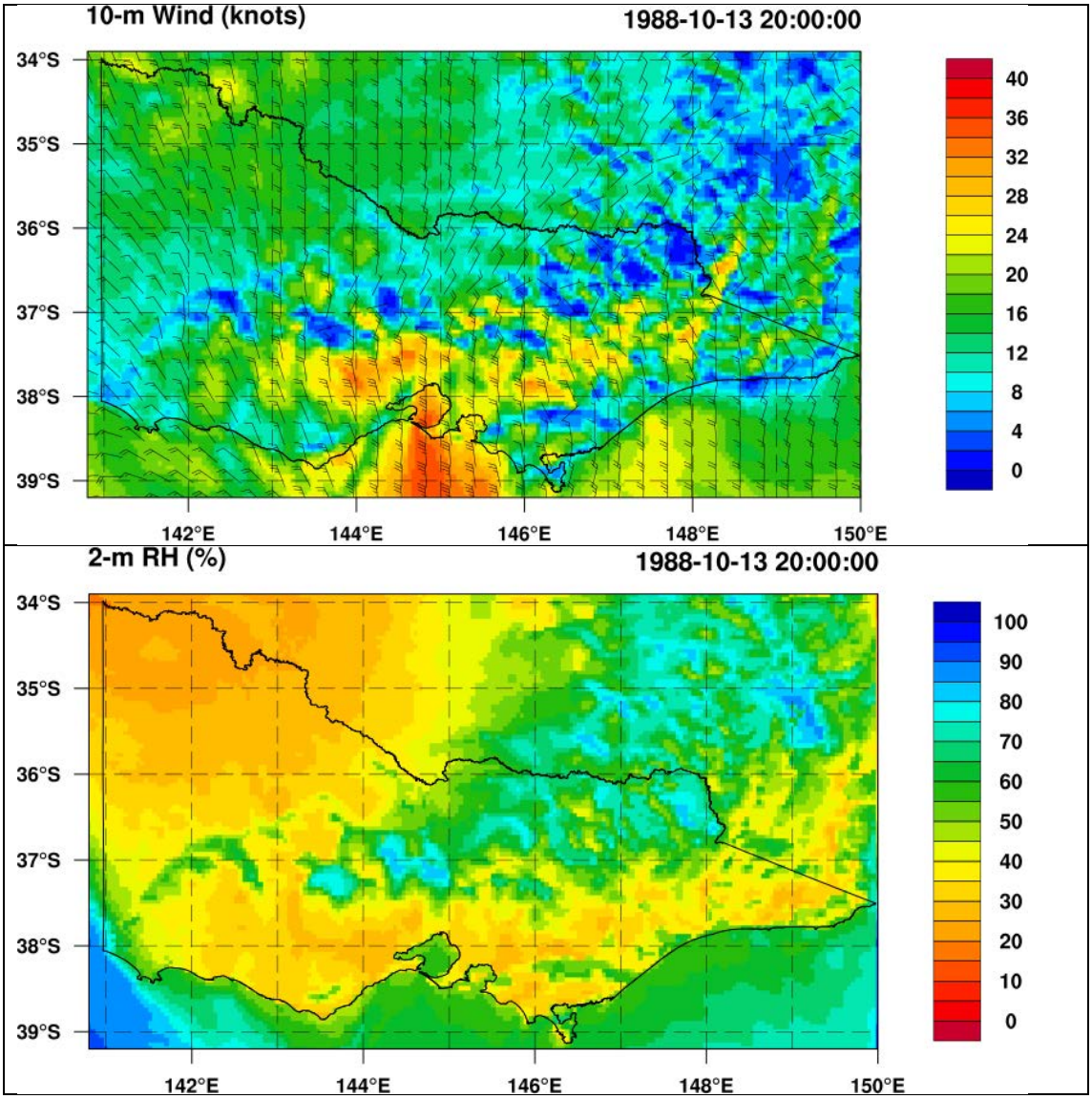

Figure B26. WRF wind and relative humidity at 2000 UTC 13 October (0700 EDT 14 October) 1988.

ASH WEDNESDAY – 16 February 1983

The WRF temperature, relative humidity and wind fields at 0500 UTC (1600 EDT) 16 February 1983 are shown in Fig. B27. The temperature compares well with Melbourne Airport observations (Table 4), but relative humidity, while very low, is not as low as observed, and the wind speed is biased low. The stronger wind speeds in western Victoria at this time are quite realistic. Mills (2005b) describes many of these features. Later in the afternoon and evening the WRF wind speeds in central Victoria do weaken compared with observations.

The WRF FFDI field at 0500 UTC (Fig. B27) shows FFDI in the 60's at Melbourne Airport, somewhat lower than given from AWS observations. In western Victoria the high wind speeds near the change line show FFDI values near or above 100 over a large area. Notably,

given the impact of the Deans Marsh fire that started about 0400 UTC, there is a small region of FFDI above 100 extending to the coast east of Cape Otway.

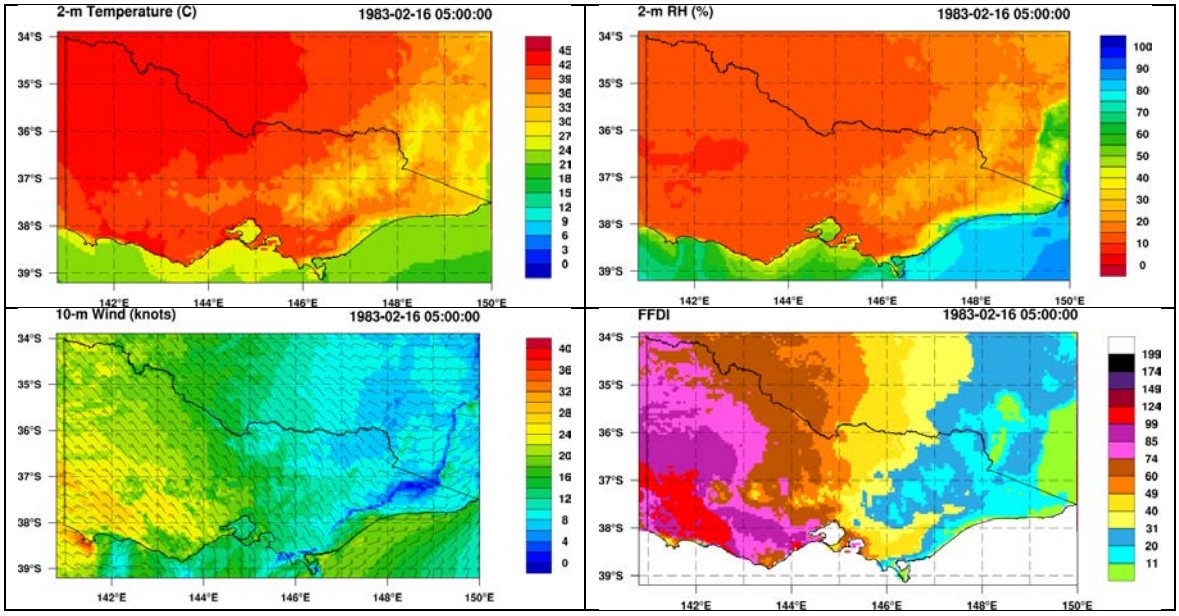

Figure B27. WRF temperature, relative humidity, and wind speed and direction at 0500 UTC 16 February 1983.

The Ash Wednesday change reached Melbourne rather later in the day than is frequently the case, passing through Melbourne Airport between 0930 and 1000 UTC. Wind speeds peaked at Melbourne Airport in the early afternoon, around 45 km/hr, and then slowly declined to around 30 km/hr before the change. There was a sharp increase in speed following the change, with mean speeds around 60 km/hr for about half an hour, followed by a slow decline, but remained above 30 km/hr for many hours (all interpolated from the Dines Anemograph chart reproduced as Fig.82 of the Bureau's Ash Wednesday report).

WRF simulations show the early afternoon speed well reproduced at Melbourne Airport (Fig. B27). The WRF winds across the time of the simulated wind change show that the change moved through that site between 1000 and 1100 UTC (Fig. B28).

Figure B28 shows wind speeds higher after the cool change than before, in agreement with observations, but in the Melbourne basin somewhat lower than observed.

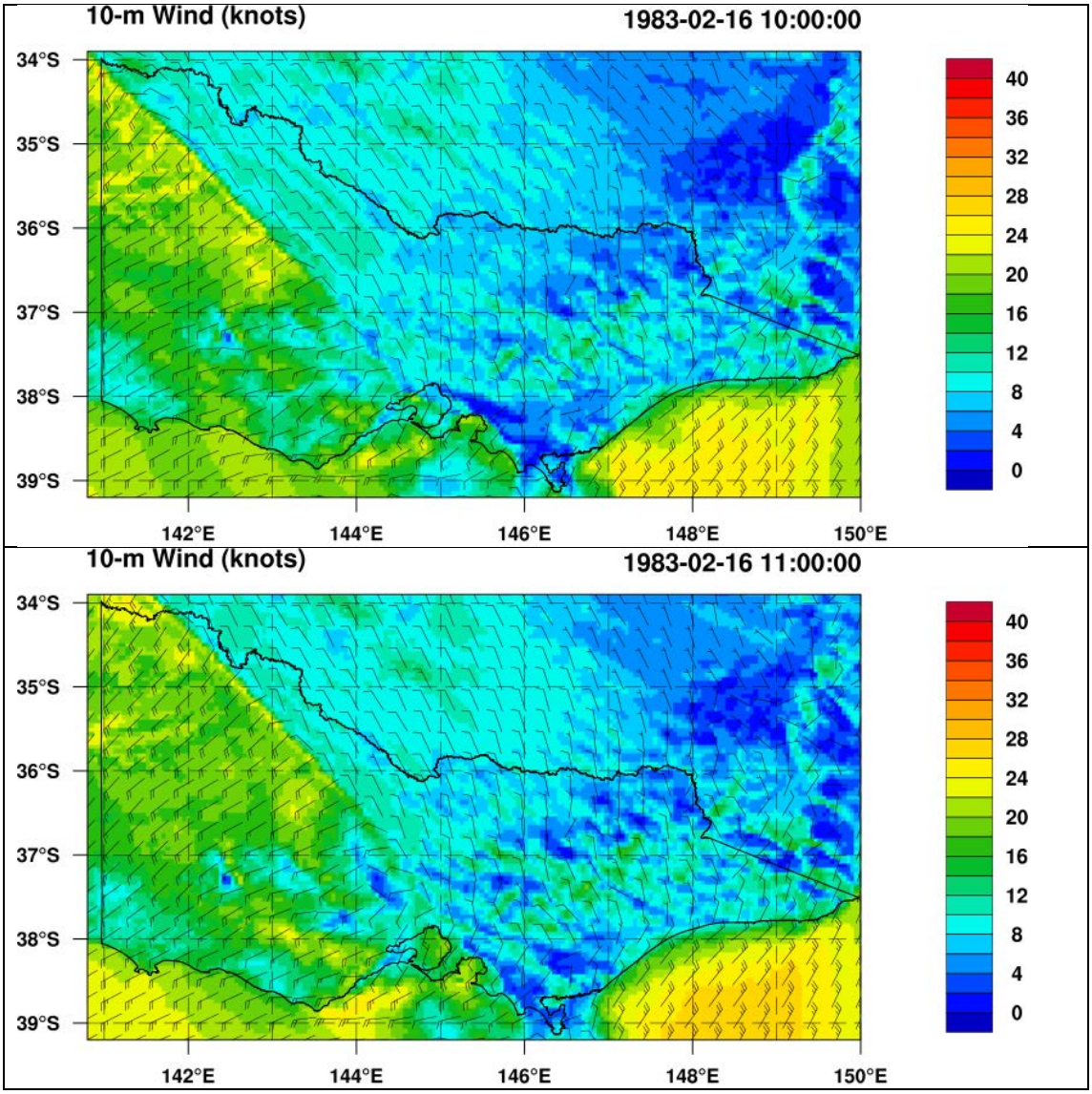

Figure B28. Wind speed and direction at 1000 and 1100 UTC 16 February 1983.

The Bureau of Meteorology Ash Wednesday (Bureau of Meteorology 1984) report includes a table of wind change times at a large number of locations, and provided by a diverse range of observers. Selected values are listed in Table B1 and compared subjectively with the WRF simulations. These verifications, allowing for some error in estimates and the hourly interval in WRF, and the spacing between wind barbs, indicate excellent performance.

In addition, some of the structural aspects of the change, such as the only slow backing of the wind in the southwest of Victoria (e.g., Mt Gambier), but with sustained and even increasing wind speeds as the wind backed, and the sharp change with increased wind speeds following the change at Mildura (two stations where anemometer records allow this interpretation) are very encouraging.

Table B1. Observed (Bureau of Meteorology 1984) and interpolated WRF change times

Station	Change Time (EDST)	Change Time (UTC)	WRF Time (UTC)
Hamilton	1800	0700	0700
Nhill	1800	0700	0700
Cape Otway	1810	0710	0600
Horsham	1823	0723	0730
Lorne	1900	0800	0700-0800
Anglesea	1924	0824	0800-0900
Avalon	1958	0858	0930
Melbourne Airport	2040	0940	1030
East Sale	2230	1130	1200
Mangalore	2230	1130	1130
Orbost	2400	1300	1500
Mildura	2035	0935	1115

MELBOURNE DUST STORM – 8 February 1983

This was another strong, dry, cold front that produced extreme fire weather over Victoria, in addition to the very well documented dust storm. Occurring just a week before Ash Wednesday, its significance as an extreme fire weather event has been somewhat overlooked.

The WRF temperature, relative humidity, and wind fields are shown in Fig. B29. As with the Ash Wednesday case the temperature and relative humidity are in good agreement with the observations at Melbourne Airport (Table 4), but relative humidity is a little too high, although still very dry, and wind speeds are biased just a little low.

FFDI values (Fig.B28) show values above 90 in western Victoria before the cool change.

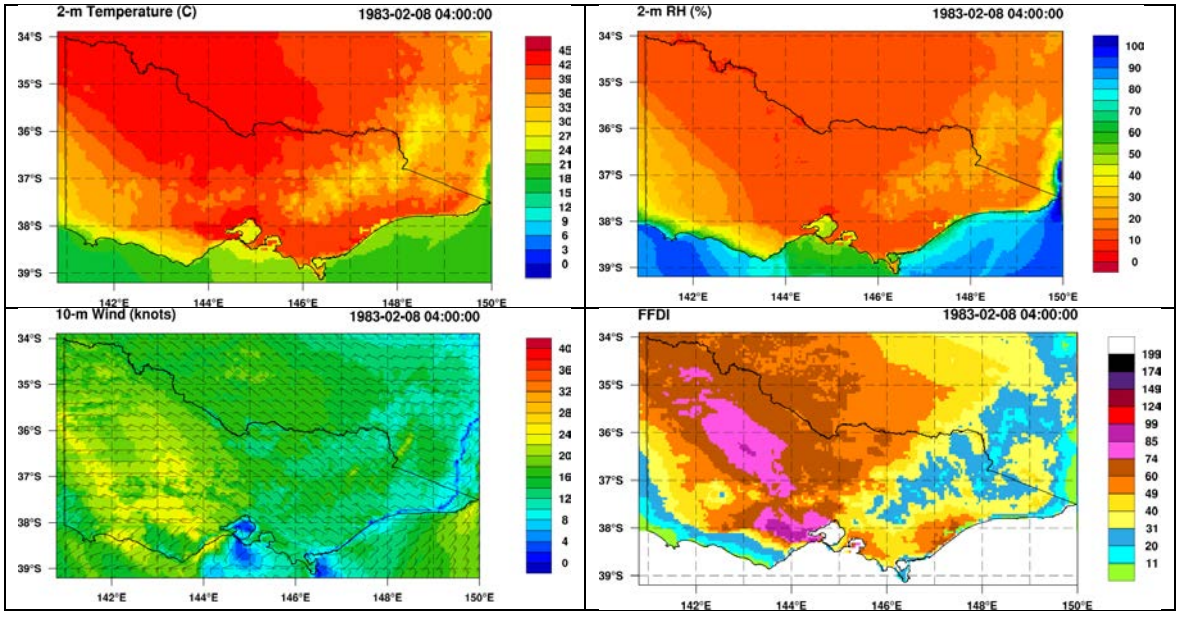

Figure B28. WRF temperature, relative humidity, and wind speed and direction at 0500 UTC 8 February 1983.

The wind change moved through Melbourne Airport between 0400 and 0430 UTC. The WRF simulations indicate change passage between 0500 and 0600 UTC (see Fig. B29). A notable feature of the change was a marked increase in speed following the change (see Garratt 1984), and the model does show some indication of this structure over wide areas of Victoria.

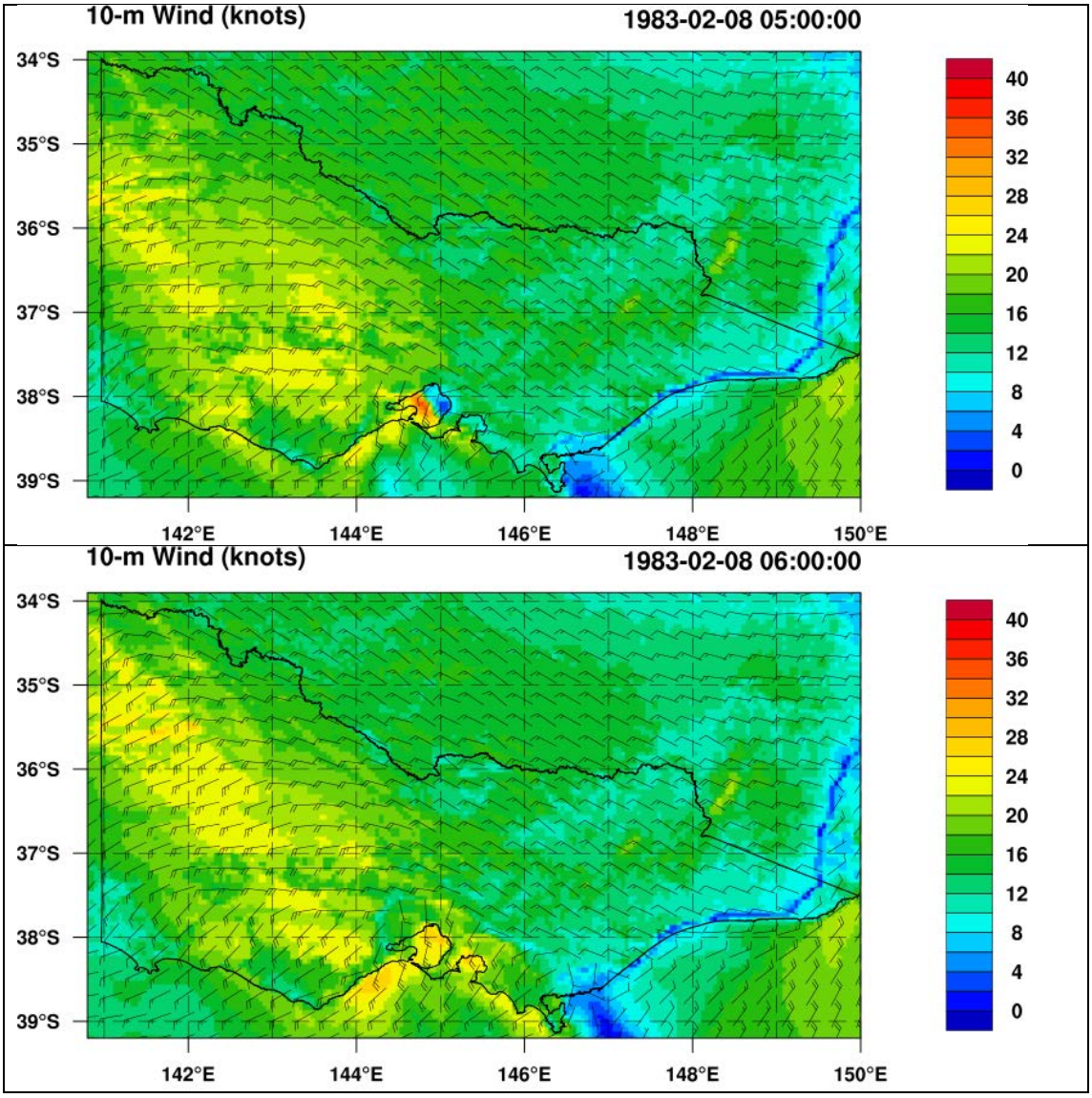

Figure B29. Wind speed and direction at 0500 and 0600 UTC 8 February 1983.

WESTERN DISTRICT FIRES – 12 February 1977

This was the multi-fire event documented by McArthur, Cheney, and Barber (1982). We have relied on the wind change timings and the meteorological observations in their report for verification.

The WRF fields at 0500 UTC are shown in Fig. B30. These fields qualitatively well match the reported 38C temperature and 15% relative humidity typical of the western district on that

day. It also shows strong pre-frontal winds, above 25 knots, with the winds decreasing closer to the cool change, as was reported. These are very typical of McArthur et al (1982) descriptions of the probable weather in the western district prior to the arrival of the cool change. FFDI values are above 50 over a wide area of western Victoria.

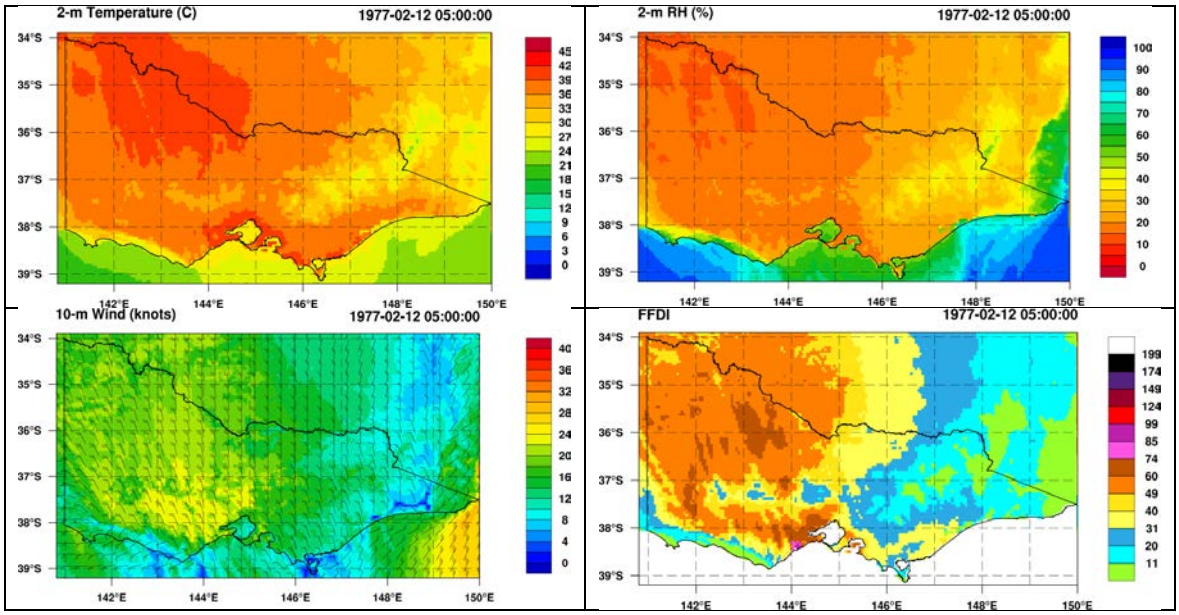

Figure B30. WRF temperature, relative humidity, and wind speed and direction at 0500 UTC 12 February 1977.

Wind change timing was a little slow, as seen in Table B2 below, where wind change times reported by McArthur et al compared with those interpolated from the WRF loop. The shape of the change is also a little different to that shown in McArthur et al (1982), (see Fig. B31) but the interpretation of McArthur may not necessarily be completely correct given the limitations of the observing network at the time, and also the developments in understanding of fronts since that time.

This timing performance is rather less good than that of many fronts that were identified in earlier assessments of the 1997-2013 period. The general simulation of extreme fire weather ahead of the cool change is sound, and several features of the day are well represented.

Table B2. Observed (from McArthur et al 1982) and interpolated WRF cool change timings at the listed locations on 12 February 1987.

Location	Observed change (UTC)	WRF change (UTC)
Hamilton	0300	0700
Horsham	0600	1000
Ararat	0740	1030
Geelong	0800	1100
Laverton	0830	1130
Melbourne Airport	0930	1330

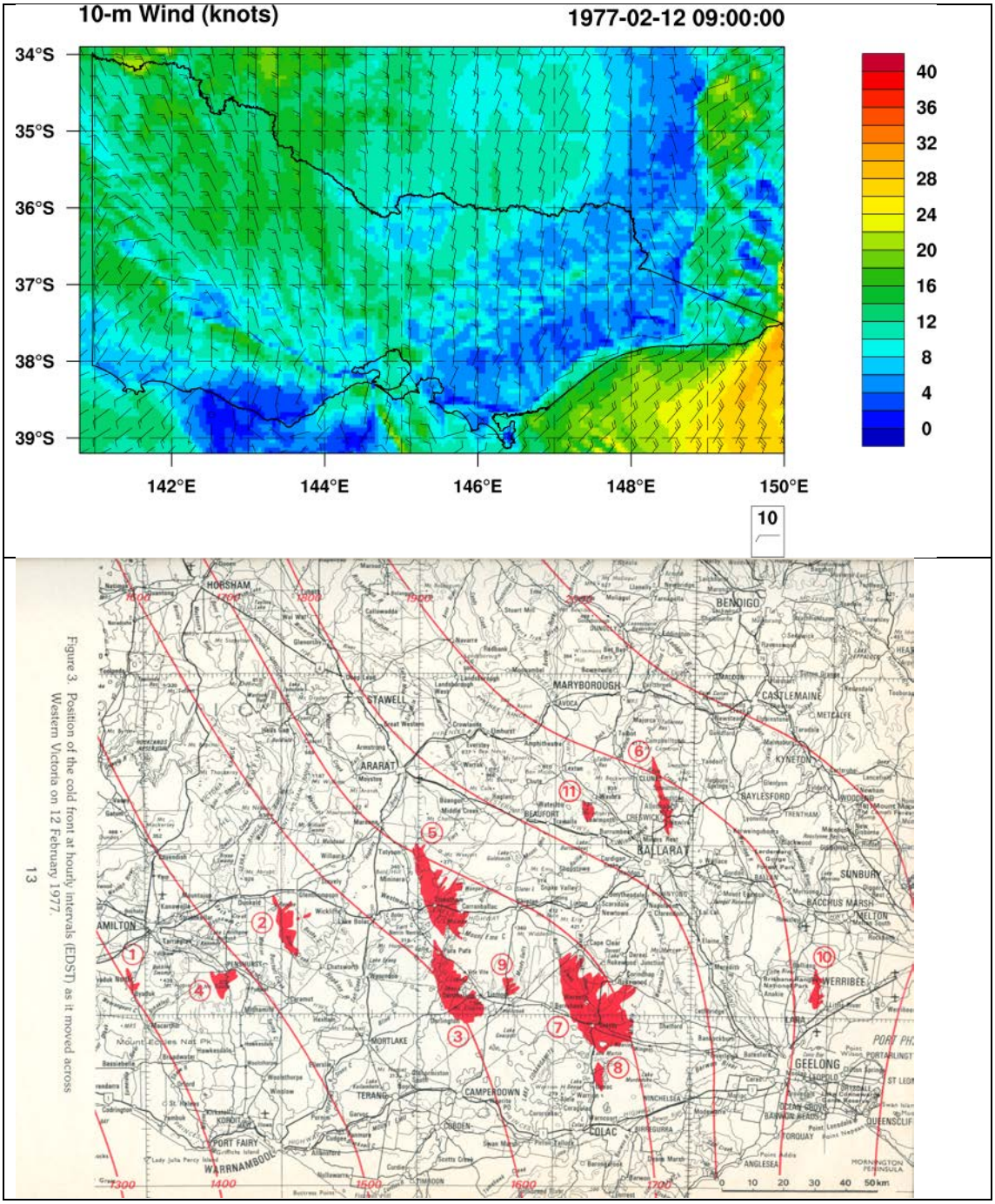

Figure B32 WRF wind field at 0900 UTC 12 February 1977 (upper) and McArthur et al (1982) wind shift isochrones.

LIST OF FIRE WEATHER CASES

Black Saturday	7 February 2009
Brisbane Ranges Fire	22 January 2006
Alpine Fires Breakout	30 January 2003
Canberra	18 January 2003
Melbourne Smoke Fumigation	11 January 2001
Linton Fire	2 December 1998
Dandenong Ranges	21 January 1997
Berringa Fire	25 February 1995,
Strathbogie Ranges	27-30 December 1990,
Bemm River	14 October 1988
Ash Wednesday	16 February 1983
Melbourne Dust Storm	8 February 1983
Western District Fires	12 February 1977

LATITUDES AND LONGITUDES OF LOCATIONS REFERRED TO IN FIRE WEATHER CASE STUDIES

BAIRNSDALE AIRPORT ,-37.8817, 147.5669,
BENALLA , -36.55, 146.00,
CANBERRA AIRPORT ,-35.3088, 149.2003,
GELANTIPY ,-37.2200, 148.2625,
GROVEDALE ,-38.2241, 144.3345,
MELBOURNE AIRPORT ,-37.6655, 144.8321,
MOUNT HOTHAM ,-36.9767, 147.1342,
ORBOST ,-37.6922, 148.4667,
SCORESBY ,-37.8710, 145.2561,
SHEOAKS ,-37.9075, 144.1303,
STREATHAM , -37.6833,143.050,
WANGARATTA AERO ,-36.4206, 146.3056

REFERENCES

Buckley, A.J., 1992. Fire behavior and fuel reduction burning: Bemm River wildfire October 1988. *Australian Forestry*, **55**, 135-147.

Bureau of Meteorology, 1984. Report on the meteorological aspects of the Ash Wednesday fires – 16 February 1983, 143pp.

Chatto, K. (Ed), 1999. Development, behavior, threat and meteorological aspects of a plume-driven bushfire in west-central Victoria: Berringa fire. February 25-26, 1995. Research Report No 48, CFTT Creswick Research Station, Department of Natural Resources and Environment. 66pp.

Country Fire Authority, 1991. Report on investigations into the major fires 27 December 1990. 52pp.

Country Fire Authority, 1999. Reducing the risk of entrapment in wildfires. A case study of the Linton Fire. 16pp.

Garratt, J.R., 1984. Cold fronts and dust storms during the Australian summer 1982-83. *Weather*, **39**, 98-103.

Hess, G.D., Tory, K.J., Lee, S., Wain, A.G. and Cope, M.E., 2006. Modelling the King Island bushfire smoke. *Aust. Meteor. Mag*., **55**, 93-103.

McArthur, A.G., Cheney, N.P., and Barber, J., 1982. The fires of 12 February 1977 in the western district of Victoria. CSIRO and CFA Report.

Mills, G.A., 2002: A case of coastal interaction with a cold front. *Aust. Meteor. Mag*., **51**, 203-221.

Mills, G.A., 2005a. On the sub-synoptic scale meteorology of two extreme fire weather days during the Eastern Australian fires of January 2003. *Aust. Meteor. Mag*., **54**, 265-290.

Mills, G.A., 2005b. A re-examination of the synoptic and mesoscale meteorology of Ash Wednesday 1983. *Aust. Meteor. Mag*., **54**, 35-55.

Mills, G.A., and L. McCaw 2010. *Atmospheric Stability Environments and Fire Weather in Australia – extending the Haines Index*. CAWCR Technical Report No20, 158pp.

APPENDIX C - EXAMPLES OF MESOSCALE CIRCULATIONS

Southwesterly surges in northwestern Victoria

Occasionally strong surges in southwesterly winds were observed passing through the Mallee in northwestern Victoria. One such example is that of 1 January 2006. The time-series of wind observations from Mildura Airport is shown in Fig. C1. A cold frontal wind shift to the southwest was recorded between 0430 and 0500 EDT, and winds only backed very slowly thereafter. However, wind speeds increased steadily through the day, peaking at around 35 km/hr at 1730 EDT, with gusts above 50 km/hr, and with speeds declining thereafter. The WRF wind field at 0600 UTC (1700 EDT) shows a band of strong winds oriented northwest-southeast across much of northern Victoria, and being located across Mildura at this time. Time-looping of the wind fields shows this strong wind band propagating to the northeast with time, consistent with the peaking and then decline of the winds at Mildura - see the wind field in Figure C2.

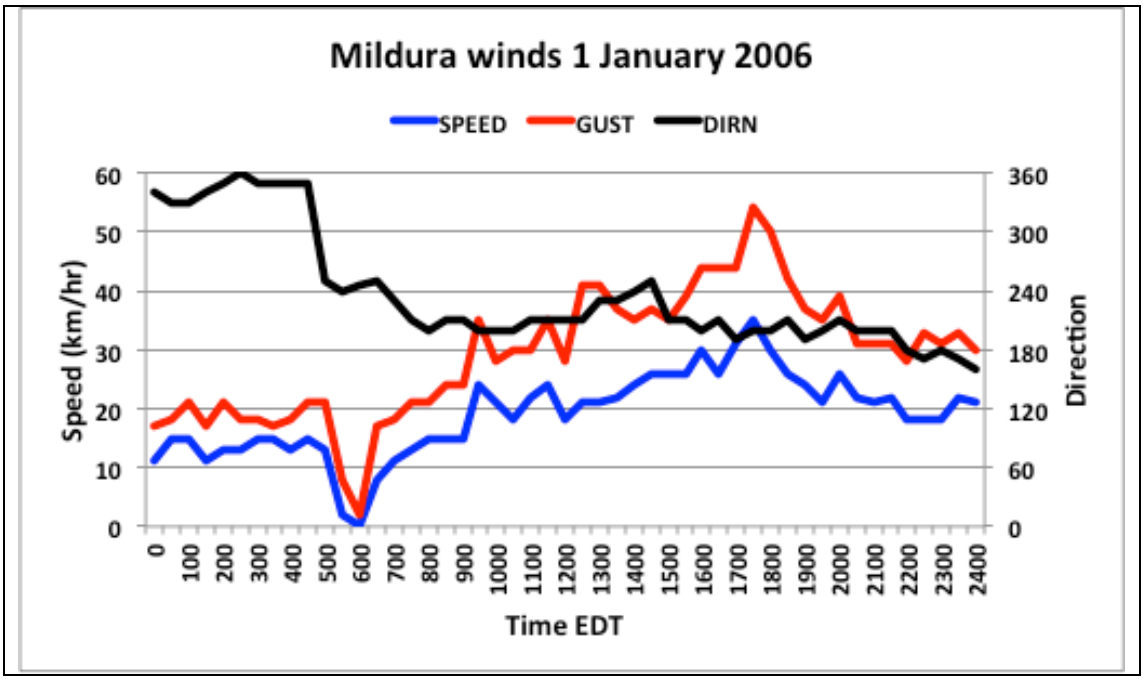

Figure C1. Time-series of mean 10-m wind speed (blue), gust speed (red), and wind direction (black) at Mildura on 1 January 2006.

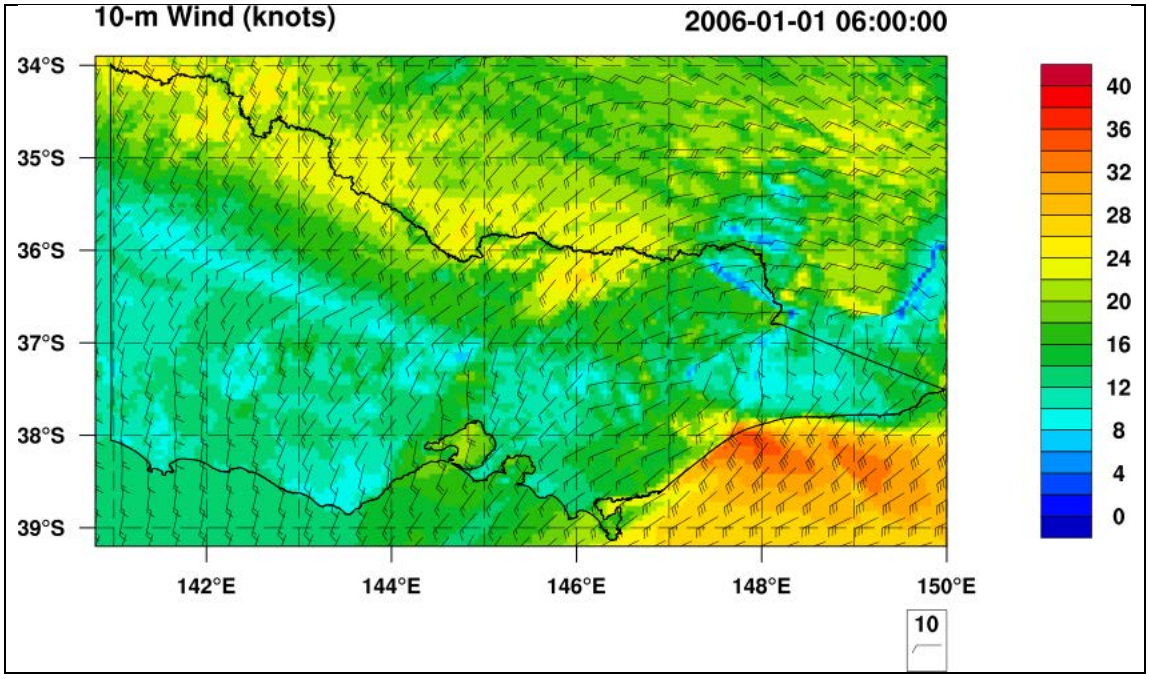

Figure C2. WRF wind field at 0600 UTC (1700 EDT) 1 January 2006

Foehn winds over the Otway Ranges

A feature that became apparent from inspection of the WRF wind fields was the simulation of regular small wind speed maxima over the coast just east of Cape Otway in strong northwesterly flow. An example is shown in Fig. C3, at 2100 UTC 4 September 2012. While large areas of strong winds, mostly along and in the lee of the Great Dividing Range, are seen, the feature on which this section focuses is circled, and shows a minimum of wind speed just inland of the coastal ranges east of Cape Otway, and a narrow band of stronger winds along the coast.

Given that the flow was a strong northerly, it is a physically realistic hypothesis that the Otway Ranges are inducing a “blocked foehn” flow in this region (see Sharples et al 2010), and a vertical cross-section through the WRF fields (Fig. C4) supports this hypothesis. The potential temperature contours descend on the southern side of the Otway ranges, with a band of strong winds descending in their lee, while weaker winds are “blocked” below the level of the topography on the northern (windward) side.

It remains to demonstrate that the WRF model has not only simulated a physically realistic flow, but also that observations confirm this feature. Figure C5 shows the meteograms of wind speed, gust, and direction from the AWS at Warrnambool, Aireys Inlet, and Geelong Racecourse on the 5 September 2012 (local time). The locations of these AWS are listed at the end of this section. Focussing on the morning hours, it is seen that Aireys Inlet shows mean winds speeds a little stronger than those at Warrnambool, and much stronger gust speeds, while both mean and gust speeds are much lower at Geelong Racecourse, consistent with the spatial variation of wind speed seen in the WRF simulation.

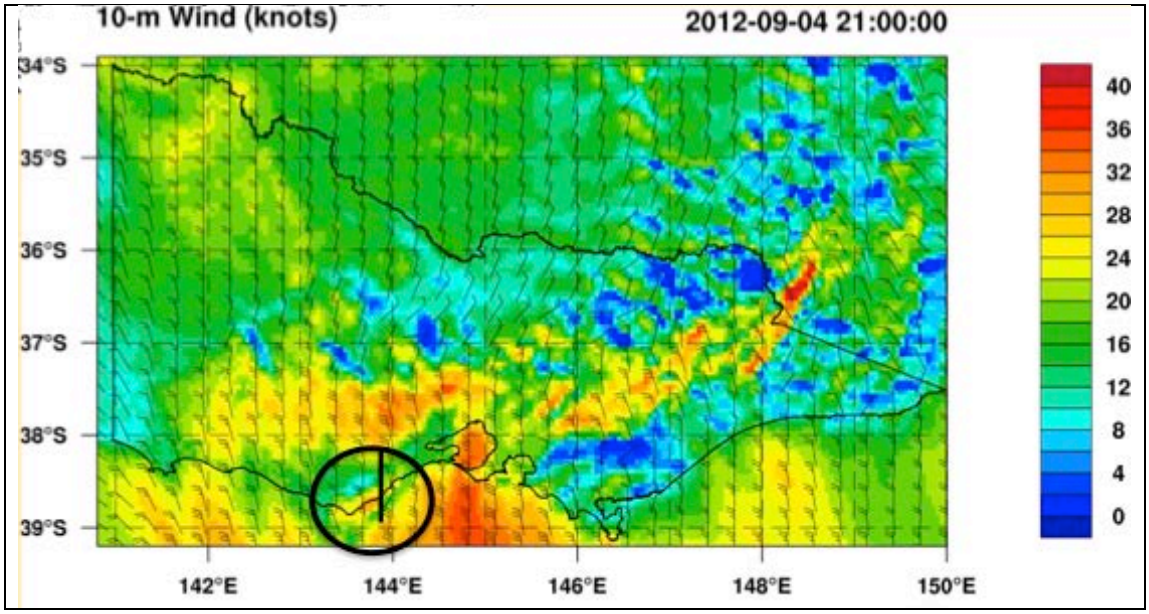

Figure C3. WRF 10-m wind field at 2100 UTC 4 September 2012.

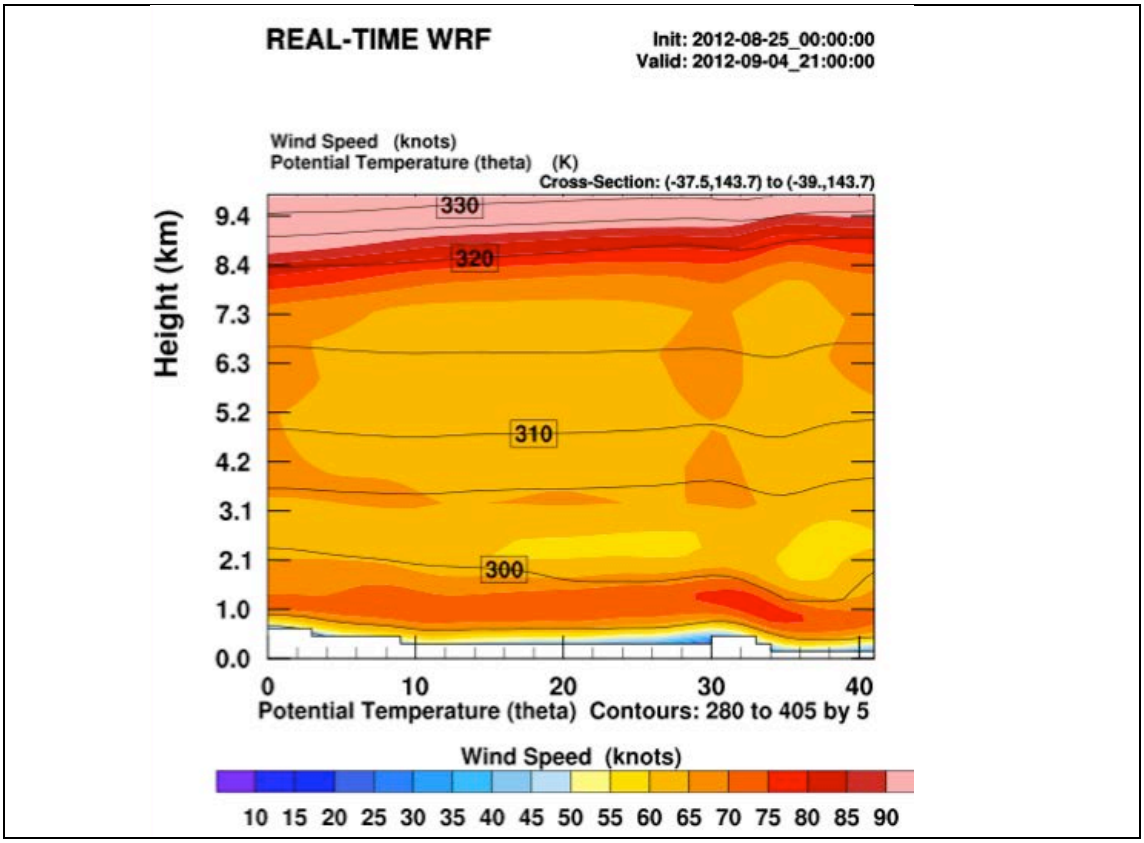

Figure C4. Vertical cross-section of potential temperature (contours) and wind speed (shaded) from north (left) to south (right) along the line shown circled in Fig. D3.

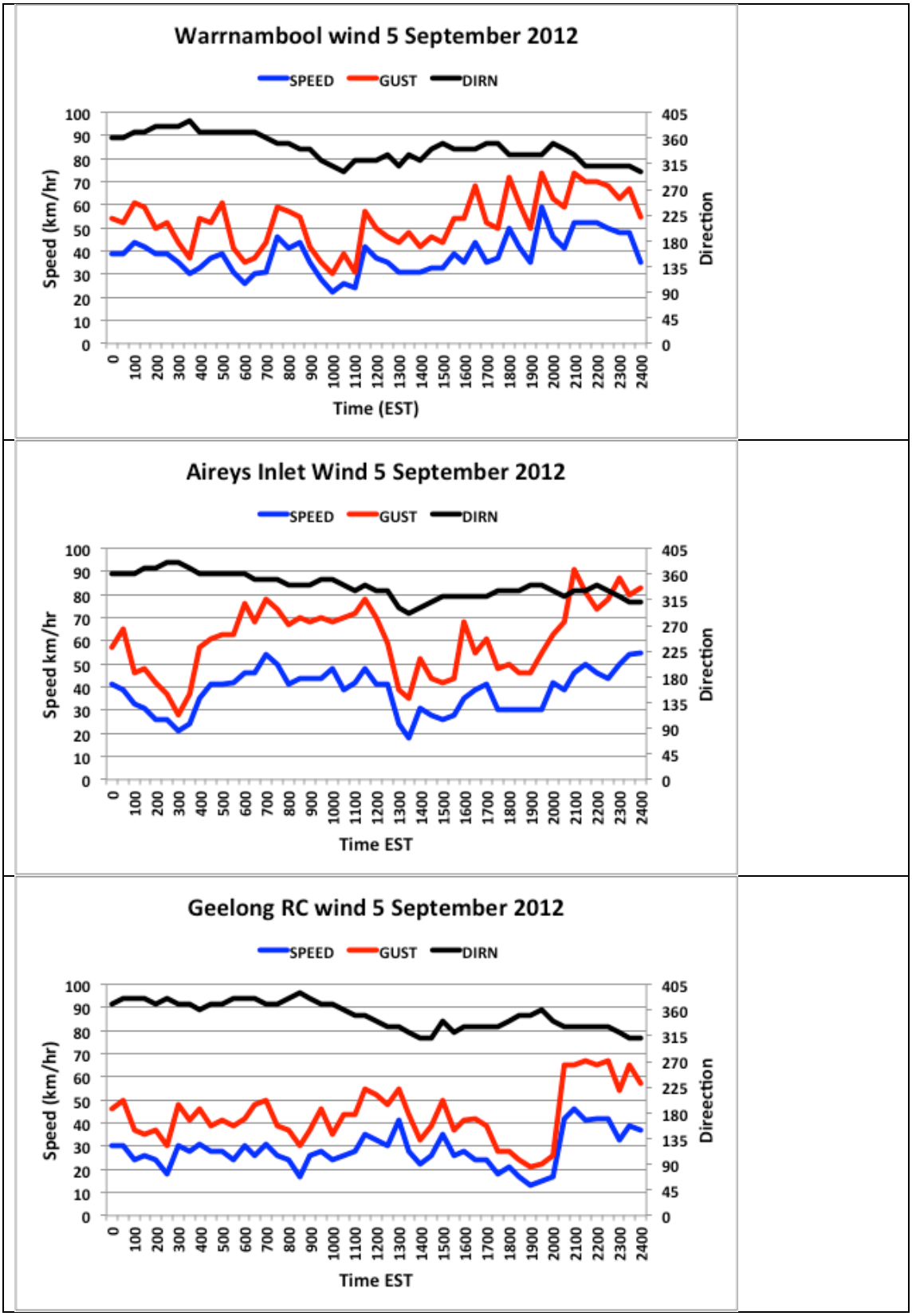

Figure C5. Mean (blue) and gust (red) 10-m wind speeds (km/hr) and wind direction (black) from midnight to midnight 5 September 2012 at Warrnambool, Aireys Inlet, and Geelong Racecourse.

Support for the low-level wind and temperature structure shown in the WRF vertical cross-section in Fig. C3 is provided by the vertical profiles of temperature and wind at Melbourne Airport at 0000 UTC (1000 EST) 5 September 2012 in Fig. C6. A low-level inversion below a well-mixed layer to around 700 hPa is seen in the temperature profile, while a low-level jet peaking at nearly 80 knots just below the inversion is seen.

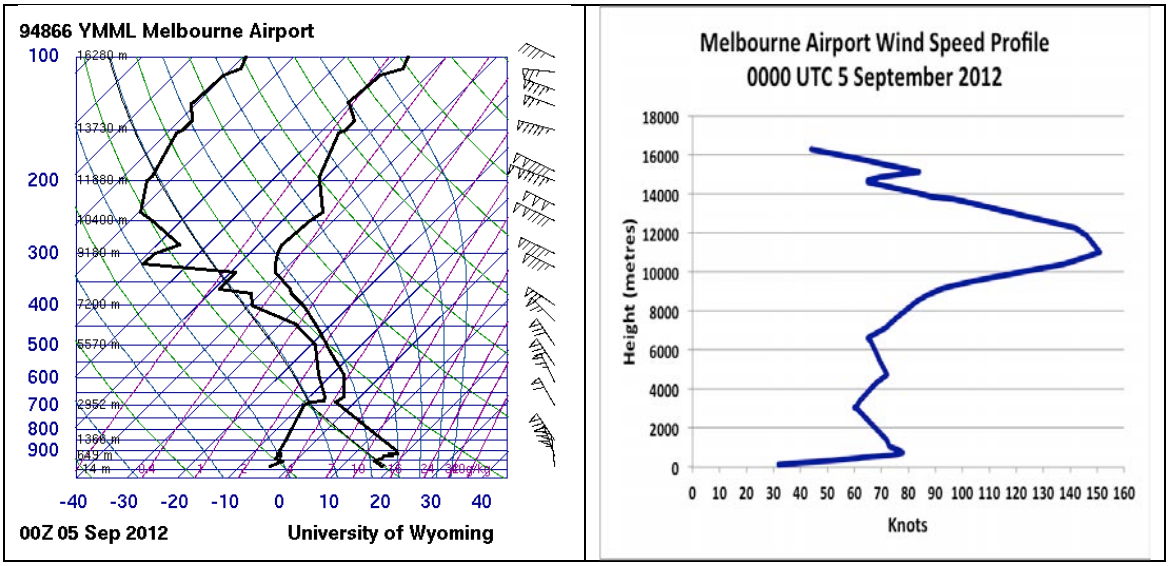

Figure C6. Vertical temperature (left) and wind speed (right) profiles from the Melbourne Airport radiosonde at 0000 UTC 5 September 2012. Data from the University of Wyoming http://weather.uwyo.edu/upperair/sounding.html .

There are other regions of strong winds, many larger than that on which the above discussion has focused at this time. North of the Otway Ranges there is a relative minimum in the wind speed, but a large area of very strong winds is seen south of the Central Highlands. Figures C7 and C8 show the meteograms of wind speed and direction at Mt Gellibrand and Melbourne Airport for 5 September 2012, and both show very strong winds at the time of the WRF wind field shown in Fig. C3. It is also interesting that at Melbourne Airport the winds are observed to increase after 0900 UTC, in contrast to the other stations where winds decrease during the daylight hours, while at all stations there is an increase in wind speed again late in the evening of 5 September.

Returning to the discussion of the flows around the Otway Ranges, while the Aireys Inlet observations support the patterns shown in the WRF fields, this case, and several others seen during the evaluation process, show that the maximum speeds seen in this “Otway Foehn” pattern are generally simulated between Cape Otway and Aireys Inlet, where there are no observations, indicating the value of this gridded data set for climatological analyses.

AWS locations:

087184, BREAKWATER (GEELONG RACECOURSE ,-38.1737, 144.3765,
090035, COLAC (MOUNT GELLIBRAND) ,-38.2333, 143.7925,
090186, WARRNAMBOOL AIRPORT NDB ,-38.2867, 142.4522,
090180, AIREYS INLET ,-38.4583, 144.0883,
090015, CAPE OTWAY LIGHTHOUSE ,-38.8556, 143.5128

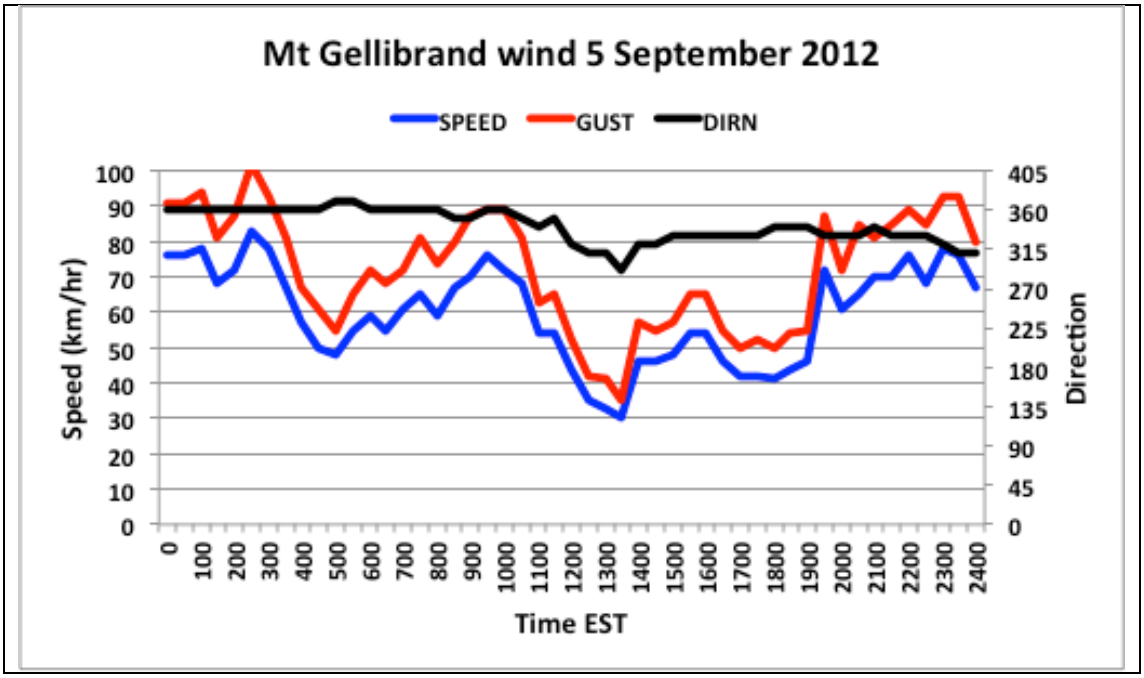

Figure C7. Mean (blue) and gust (red) 10-m wind speeds (km/hr) and wind direction (black) from midnight to midnight 5 September 2012 at Mt Gellibrand.

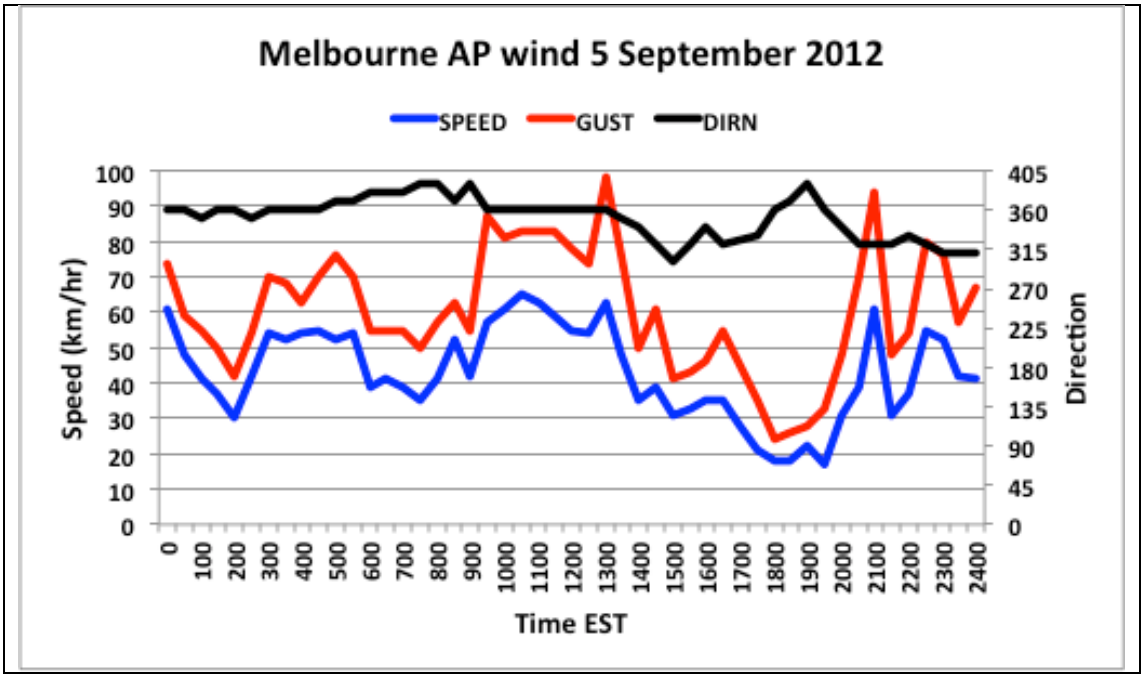

Figure C8. Mean (blue) and gust (red) 10-m wind speeds (km/hr) and wind direction (black) from midnight to midnight 5 September 2012 at Melbourne Airport.

The Winchelsea Convergence

Mills and Morgan (2006) described a convergence feature that forms between southwesterly and southeasterly flows near Geelong some hours after a northwesterly to southwesterly cool change, and then propagates westwards. The WRF wind field at 0600

UTC 20 January 2004, the day of Mills and Morgan's archetype Winchelsea Convergence pattern is shown in Fig. C9. The convergence line is seen as the arc of minimum wind speed (blue colours) stretching northwards and then east from the Surf Coast to north of Melbourne, and with a convergence between south-southeasterlies just west of Geelong (east of the convergence), and southwesterlies to its west. This pattern replicates very closely the patterns published by Mills and Morgan (2006) using the Bureau of Meteorology's then-operational mesoscale (5km grid) NWP model, and supported by radar observations.

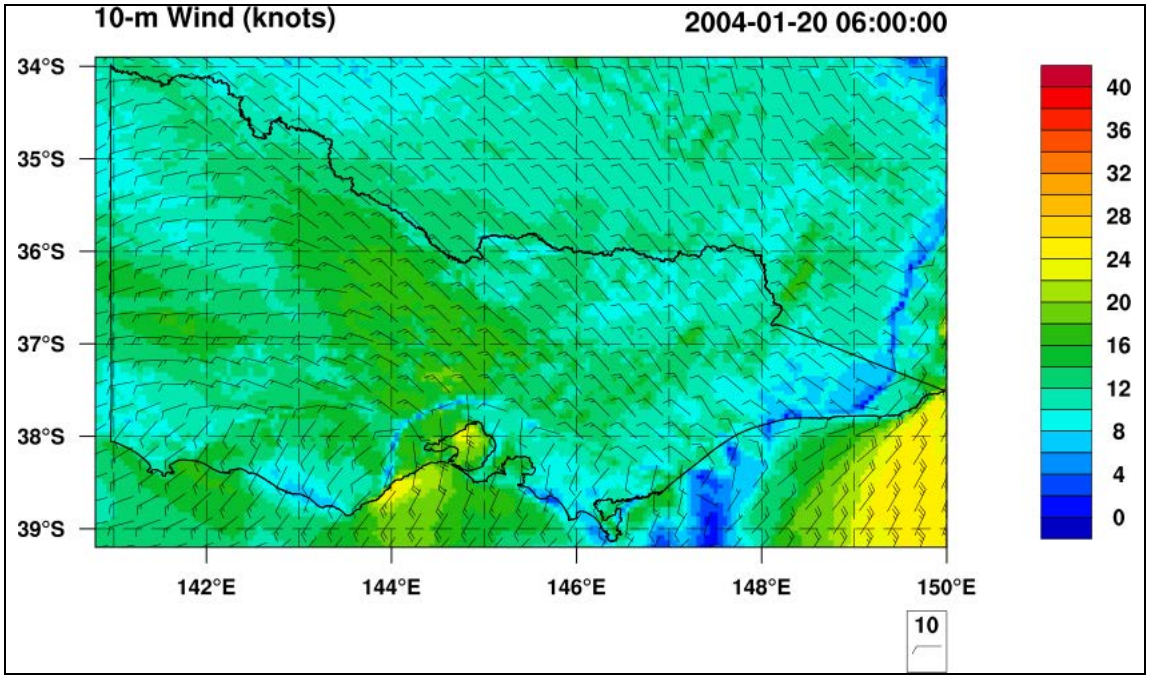

Figure C9. WRF 10-m wind field at 0600 UTC 20 January 2004.

Another example from the WRF data set is shown in Fig. C10, for an event that occurred on 11 January 2007. The AWS wind observations from the Sheoaks AWS for the day are shown in Fig. C11, with the cool change from northwesterlies to southwesterlies occurring between 0530 and 0630 EDT, and the westward-propagating southeasterly change passing through the AWS between 1430 and 1500 EDT (0330-0400 UTC). The WRF simulation is perhaps 1 hour late with this change when compared with the observations, but has simulated an excellent pattern.

The WRF simulations (not shown) also show the initial early morning wind change moving through Sheaoks within an hour of the observed time, and simulate the stronger winds that were observed before the change (Fig. C11).

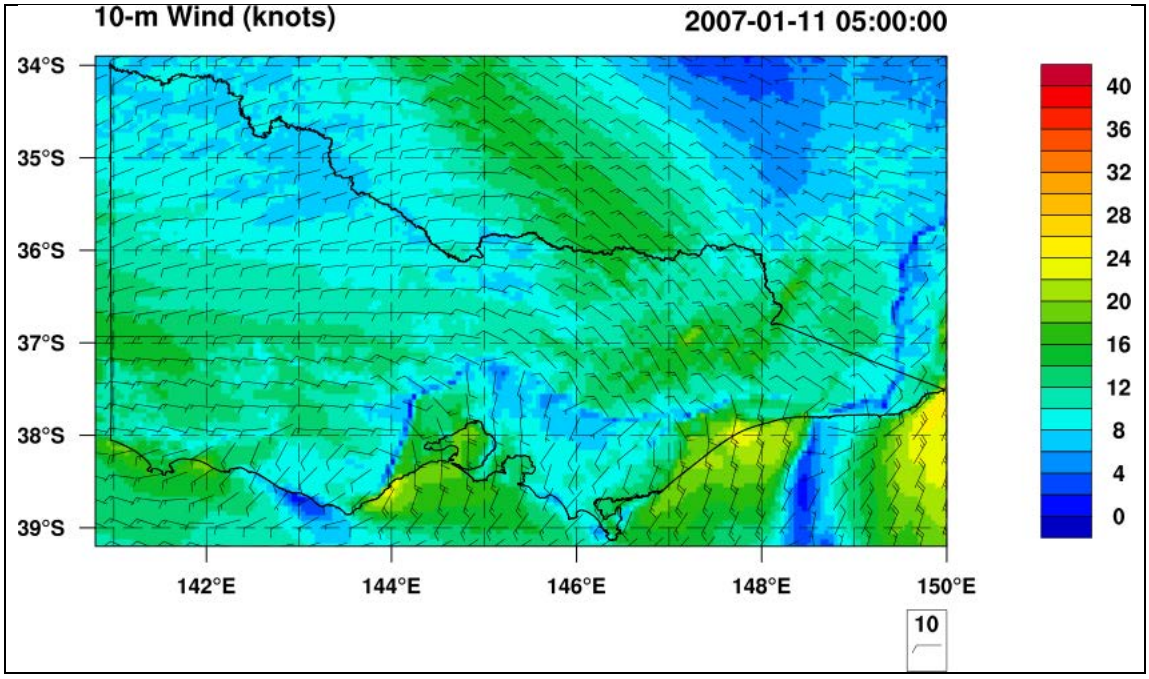

Figure C10. WRF 10-m wind field at 2100 UTC 11 January 2007.

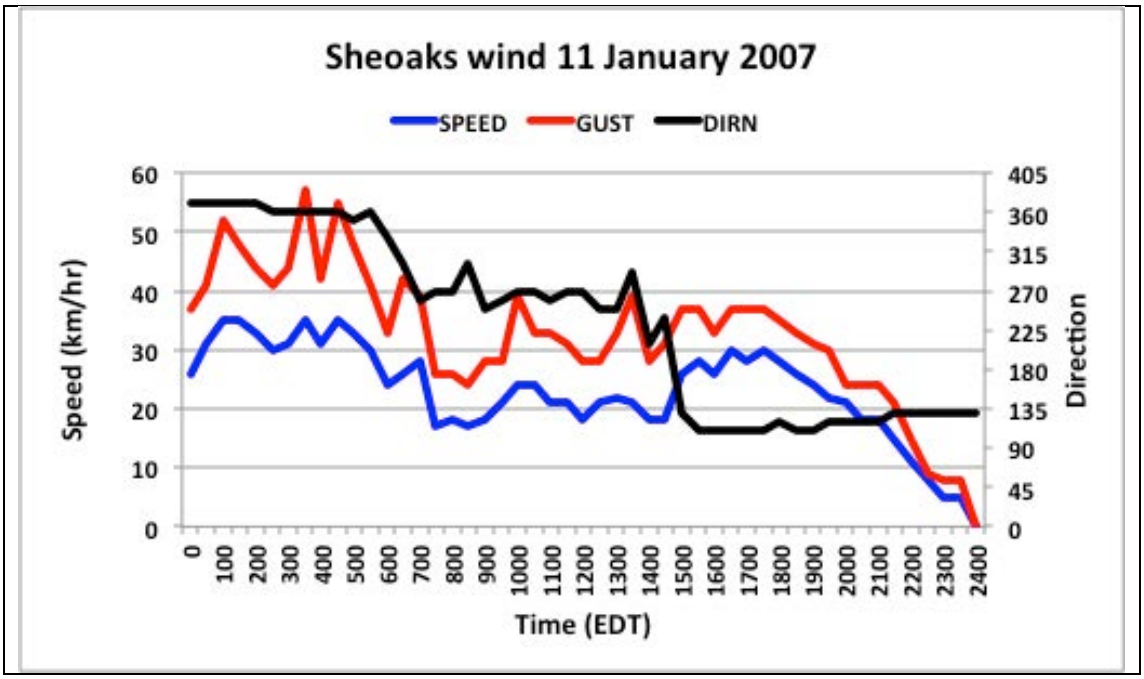

Figure C11. Mean (blue) and gust (red) 10-m wind speeds (km/hr) and wind direction (black) from midnight to midnight 5 September 2012 at Sheoaks.

AWS station:
087168, SHEOAKS, -37.9075, 144.1303

Cellular Convection over western Victoria

During Phase 1 of the evaluation considerable effort was placed on deciding what was possible model "noise" or "instability" and what was potentially realistic mesoscale detail. An example of one of these decisions is presented in Fig. C12, which shows the WRF wind field for 0500 UTC 10 February 2009. Over much of western Victoria a "speckled" pattern is seen in the wind speed, with little blobs of higher wind speed, seen as yellow, scattered across the area. When animated, these appear to propagate across the landscape. The question is, are these artefacts of the WRF model, or potentially useful detail?

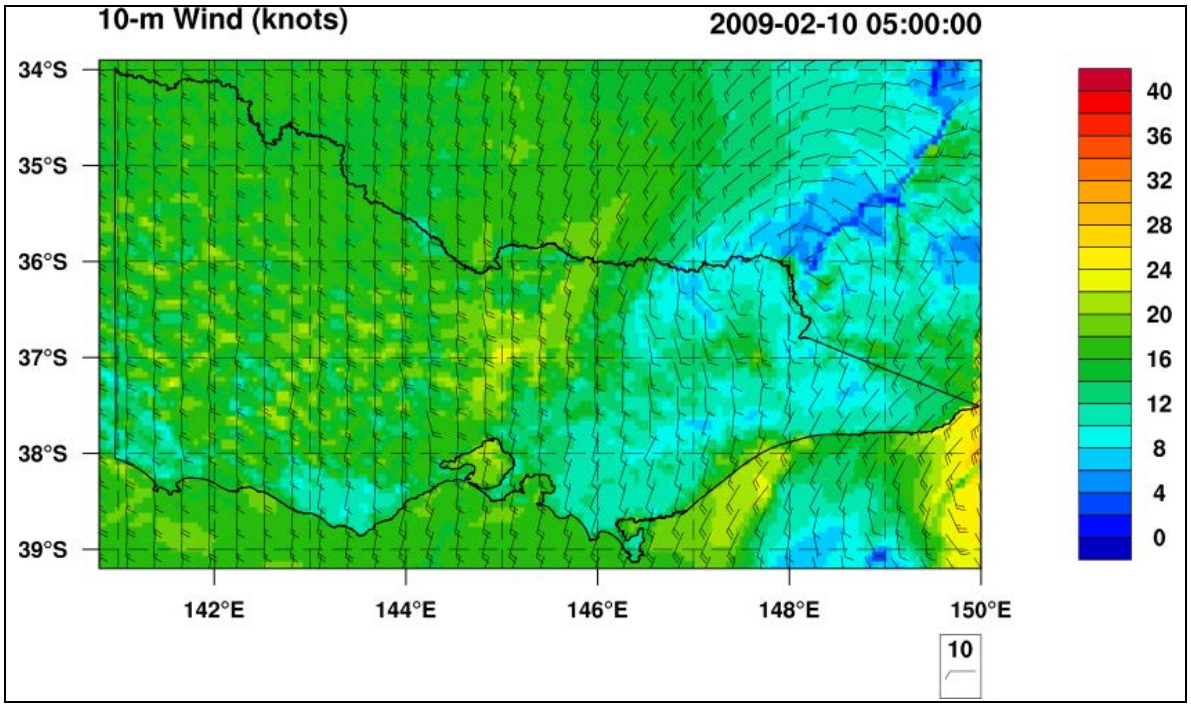

Figure C12. WRF 10-m wind field for 0500 UTC 10 February 2009.

Figure C13 shows the MODIS satellite imagery for the afternoon of 10 February, and considerable cellular convective cloud is seen over western Victoria. Such cloud patterns are often associated with Rayleigh-Benard convective cells in the planetary boundary layer, and in such circumstances increases in wind speed at the surface are expected below the downward branches of these cells, and decreases in surface wind speed below the upward branches. The cells are expected to propagate with the mean wind in the boundary layer.

The smoke from the Black Saturday bushfires can be seen in the right-hand panel of Fig. C13.

Figure C14 shows time-series of wind speed for two AWS in western Victoria – Horsham and Westmere. The arrows on these time series indicate the times between which the variable wind speed patterning could be discerned in the WRF wind fields, and these match reasonably well the times of marked wind speed variation in these observation time-series.

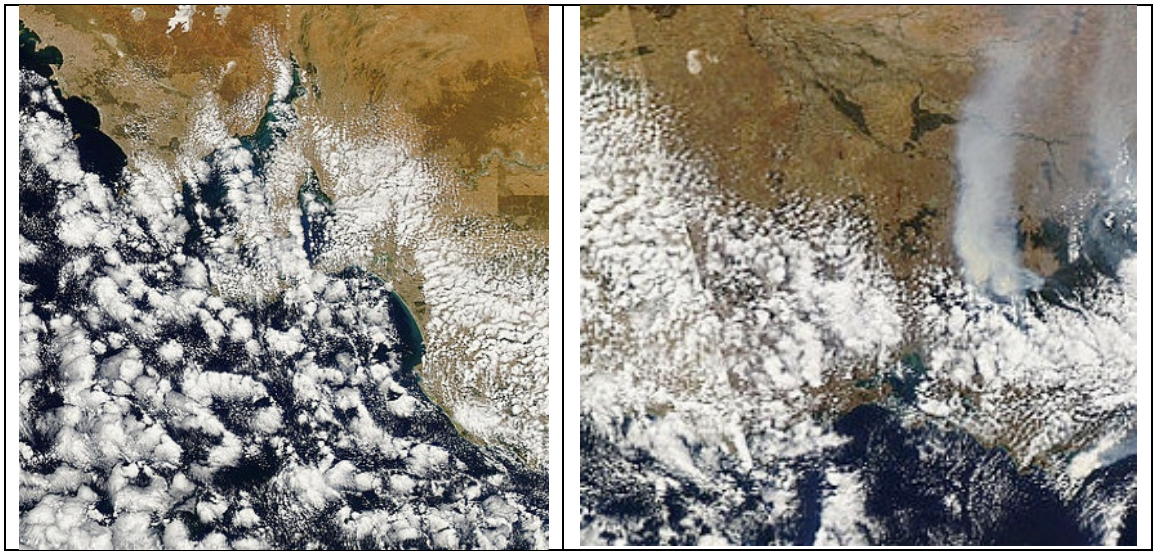

Figure C13. Aqua-MODIS Australia6 and Australia5 subsets (cropped) for the afternoon of 10 February 2009.

While it is perhaps near the limit of the ability of this configuration of the WRF model (4-km grid) to resolve these structures precisely in all cases, it is gratifying that in a case such as this, with relatively large-scale convective cells present, that the model appears able to at least indicate their presence.

AWS stations:
079100, HORSHAM AERODROME ,-36.6697, 142.1731
089112, WESTMERE ,-37.7067, 142.9378

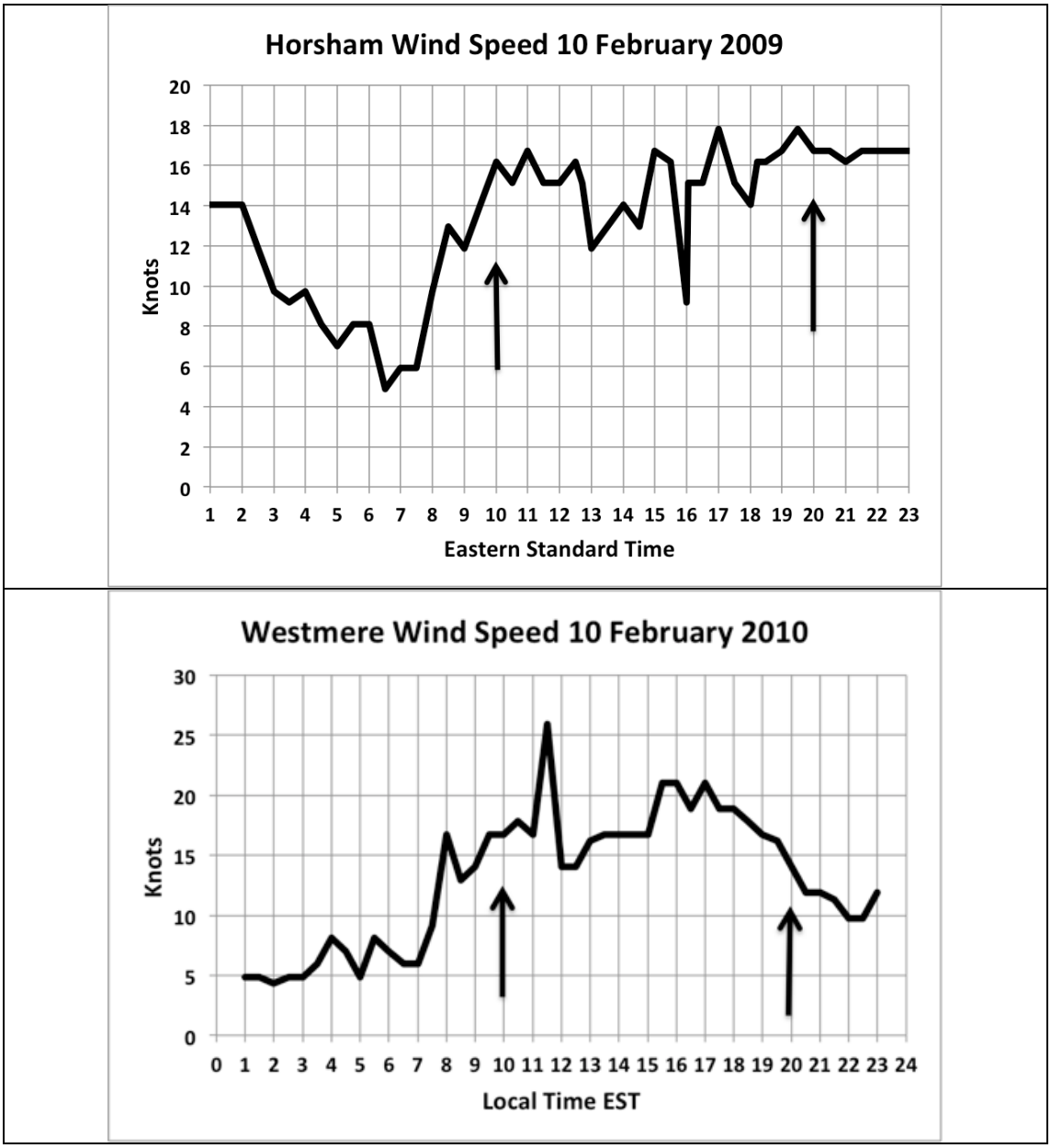

Figure C14. Time series of wind speed from the Horsham (top) and Westmere (bottom) AWS on 10 February 2009. The arrows mark the times of onset and cessation of discernable variable wind structure in the WRF wind fields.

Kilmore Gap wind surges

A very common feature observed in the assessment of the WRF wind fields was, in post-frontal southerly winds, the presence of a small wind maximum through the Kilmore Gap, north of Melbourne. Such a pattern is seen in Fig. C15 as the pale-yellow area near 37S, 145E (there is another example in Fig. C12). Such a maximum is physically reasonable, as with a post-frontal temperature inversion winds would be expected to be funneled through gaps in the ranges.

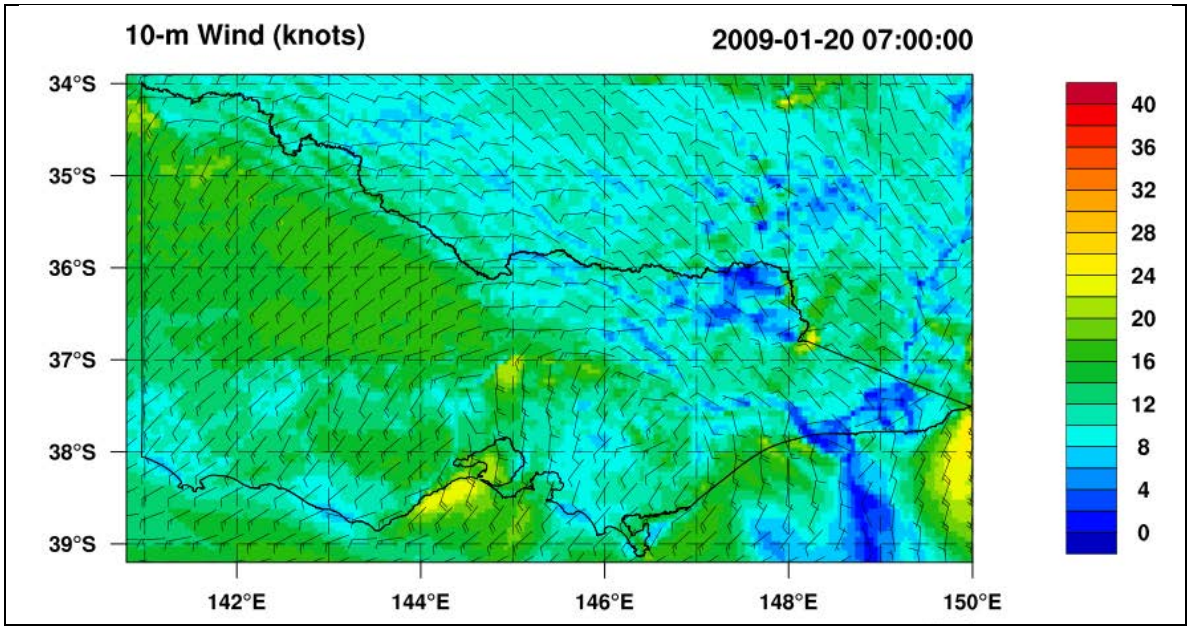

Figure C15. WRF 10-m wind field at 0700 UTC 20 January 2009.

Mesoscale circulations

A very large number of complex patterns apparently forced by topography of by land-sea heating contrast have been noted. Two examples are presented in Figs. C17 - C19.

Figures C17 and C18 show a relatively benign weather pattern with yet interesting detail. Weak sea-breeze flows from the Gippsland and Melbourne basin coastlines moving inland produce convergence lines with the inland weak to moderate northwesterly winds (Fig. C17). The net result is a band of higher temperature and lower relative humidity on the southern slopes of the Great Dividing Range just inland of the sea-breeze convergence zones (Fig. C18).

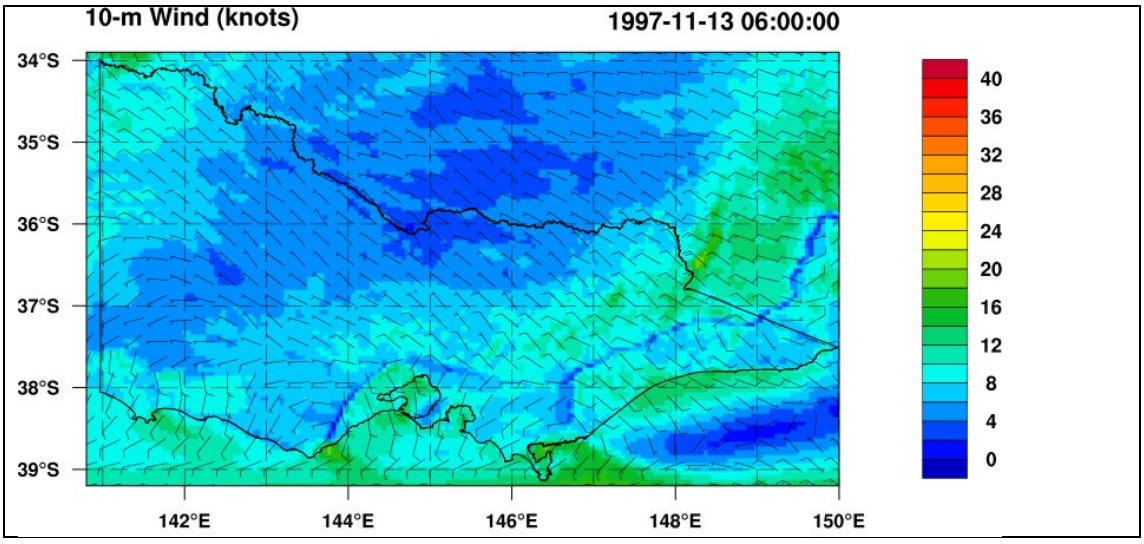

Figure C17. WRF 10-m wind field at 0600 UTC 13 November 1997.

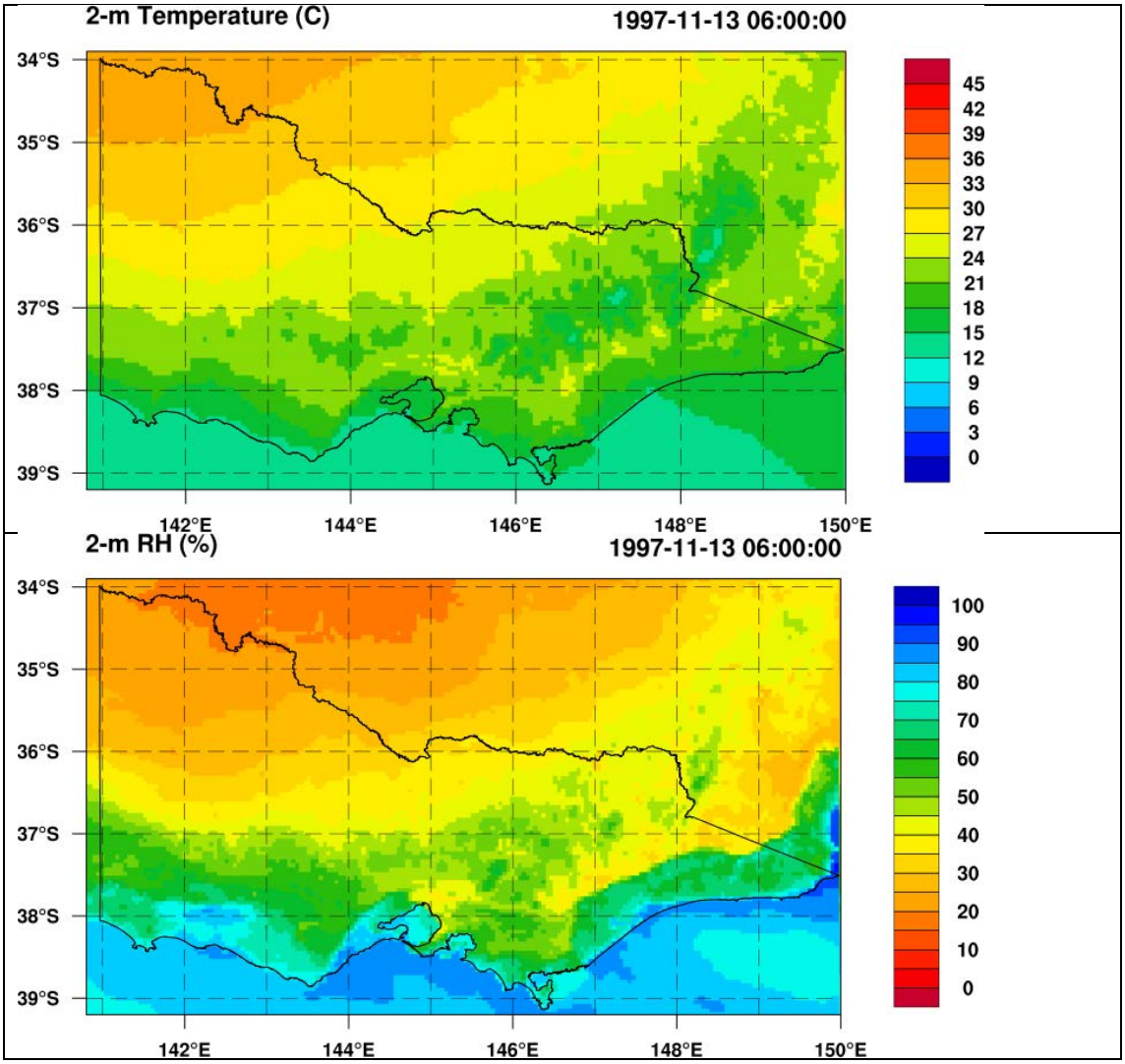

Figure C18. WRF 2-m temperature (top) and relative humidity (bottom) fields at 0600 UTC 13 November 1997.

Figure C19 shows a rather more active situation, yet with similar strong convergence lines. In this case strong southerly wind surges are moving northwards from the Melbourne basin and through the Goldfields, with sharp wind changes associated with these, and observations from Melbourne Airport and from Bendigo AWS are consistent with these patterns.

At the same time, there are strong easterly winds over the Gippsland coastline, with a southwesterly to southeasterly convergence line between the Melbourne basin and west Gippsland, and a convergence between southeasterly and inland northwesterly winds along the southern slopes of the Great Dividing Range.

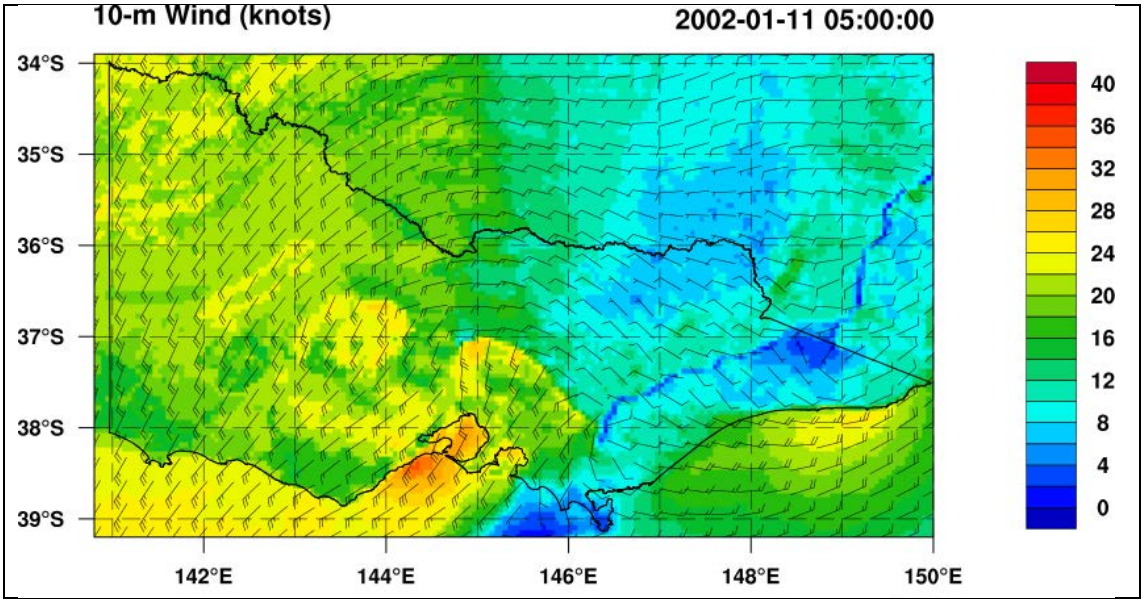

Figure C19. WRF 10-m wind field at 0500 UTC 11 January 2002.

REFERENCES

Mills, G.A., and E. Morgan, 2006. The Winchelsea Convergence – using radar and mesoscale NWP to diagnose cool change structure. *Aust. Meteor. Mag*., **55**, 47-58

Sharples, J.J., McRae, R.H.D., Mills, G.A., and Weber, R.O., 2010. Foehn-like winds and elevated fire danger conditions in southeastern Australia. *J. Appl. Met. and Climat.*, **9**, 1067-1095.

APPENDIX D – LIST OF VARIABLES AVAILABLE IN THE VICTORIA FIRE WEATHER CLIMATOLOGY DATASET

```
variables:
        char Times(Time, DateStrLen) ;
        float XLAT(Time, south_north, west_east) ;
                XLAT:FieldType = 104 ;
                XLAT:MemoryOrder = "XY " ;
                XLAT:description = "LATITUDE, SOUTH IS NEGATIVE" ;
                XLAT:units = "degree_north" ;
                XLAT:stagger = "" ;
        float XLONG(Time, south_north, west_east) ;
                XLONG:FieldType = 104 ;
                XLONG:MemoryOrder = "XY " ;
                XLONG:description = "LONGITUDE, WEST IS NEGATIVE" ;
                XLONG:units = "degree_east" ;
                XLONG:stagger = "" ;
        float LU_INDEX(Time, south_north, west_east) ;
                LU_INDEX:FieldType = 104 ;
                LU_INDEX:MemoryOrder = "XY " ;
                LU_INDEX:description = "LAND USE CATEGORY" ;
                LU_INDEX:units = "" ;
                LU_INDEX:stagger = "" ;
                LU_INDEX:coordinates = "XLONG XLAT" ;
        float ZNU(Time, bottom_top) ;
                ZNU:FieldType = 104 ;
                ZNU:MemoryOrder = "Z  " ;
                ZNU:description = "eta values on half (mass) levels" ;
                ZNU:units = "" ;
                ZNU:stagger = "" ;
        float ZNW(Time, bottom_top_stag) ;
                ZNW:FieldType = 104 ;
                ZNW:MemoryOrder = "Z  " ;
                ZNW:description = "eta values on full (w) levels" ;
                ZNW:units = "" ;
                ZNW:stagger = "Z" ;
        float ZS(Time, soil_layers_stag) ;
                ZS:FieldType = 104 ;
                ZS:MemoryOrder = "Z  " ;
                ZS:description = "DEPTHS OF CENTERS OF SOIL LAYERS" ;
                ZS:units = "m" ;
                ZS:stagger = "Z" ;
        float DZS(Time, soil_layers_stag) ;
                DZS:FieldType = 104 ;
                DZS:MemoryOrder = "Z  " ;
                DZS:description = "THICKNESSES OF SOIL LAYERS" ;
                DZS:units = "m" ;
```

```
        DZS:stagger = "Z" ;
float VAR_SSO(Time, south_north, west_east) ;
        VAR_SSO:FieldType = 104 ;
        VAR_SSO:MemoryOrder = "XY " ;
        VAR_SSO:description = "variance of subgrid-scale orography" ;
        VAR_SSO:units = "m2" ;
        VAR_SSO:stagger = "" ;
        VAR_SSO:coordinates = "XLONG XLAT" ;
float LAP_HGT(Time, south_north, west_east) ;
        LAP_HGT:FieldType = 104 ;
        LAP_HGT:MemoryOrder = "XY " ;
        LAP_HGT:description = "Laplacian of orography" ;
        LAP_HGT:units = "m" ;
        LAP_HGT:stagger = "" ;
        LAP_HGT:coordinates = "XLONG XLAT" ;
float U(Time, bottom_top, south_north, west_east_stag) ;
        U:FieldType = 104 ;
        U:MemoryOrder = "XYZ" ;
        U:description = "x-wind component" ;
        U:units = "m s-1" ;
        U:stagger = "X" ;
        U:coordinates = "XLONG_U XLAT_U" ;
float V(Time, bottom_top, south_north_stag, west_east) ;
        V:FieldType = 104 ;
        V:MemoryOrder = "XYZ" ;
        V:description = "y-wind component" ;
        V:units = "m s-1" ;
        V:stagger = "Y" ;
        V:coordinates = "XLONG_V XLAT_V" ;
float W(Time, bottom_top_stag, south_north, west_east) ;
        W:FieldType = 104 ;
        W:MemoryOrder = "XYZ" ;
        W:description = "z-wind component" ;
        W:units = "m s-1" ;
        W:stagger = "Z" ;
        W:coordinates = "XLONG XLAT" ;
float PH(Time, bottom_top_stag, south_north, west_east) ;
        PH:FieldType = 104 ;
        PH:MemoryOrder = "XYZ" ;
        PH:description = "perturbation geopotential" ;
        PH:units = "m2 s-2" ;
        PH:stagger = "Z" ;
        PH:coordinates = "XLONG XLAT" ;
float PHB(Time, bottom_top_stag, south_north, west_east) ;
        PHB:FieldType = 104 ;
        PHB:MemoryOrder = "XYZ" ;
        PHB:description = "base-state geopotential" ;
```

```
                PHB:units = "m2 s-2" ;
                PHB:stagger = "Z" ;
                PHB:coordinates = "XLONG XLAT" ;
        float T(Time, bottom_top, south_north, west_east) ;
                T:FieldType = 104 ;
                T:MemoryOrder = "XYZ" ;
                T:description = "perturbation potential temperature (theta-t0)" ;
                T:units = "K" ;
                T:stagger = "" ;
                T:coordinates = "XLONG XLAT" ;
        float HFX_FORCE(Time) ;
                HFX_FORCE:FieldType = 104 ;
                HFX_FORCE:MemoryOrder = "0  " ;
                HFX_FORCE:description = "SCM ideal surface sensible heat flux" ;
                HFX_FORCE:units = "W m-2" ;
                HFX_FORCE:stagger = "" ;
        float LH_FORCE(Time) ;
                LH_FORCE:FieldType = 104 ;
                LH_FORCE:MemoryOrder = "0  " ;
                LH_FORCE:description = "SCM ideal surface latent heat flux" ;
                LH_FORCE:units = "W m-2" ;
                LH_FORCE:stagger = "" ;
        float TSK_FORCE(Time) ;
                TSK_FORCE:FieldType = 104 ;
                TSK_FORCE:MemoryOrder = "0  " ;
                TSK_FORCE:description = "SCM ideal surface skin temperature" ;
                TSK_FORCE:units = "W m-2" ;
                TSK_FORCE:stagger = "" ;
        float HFX_FORCE_TEND(Time) ;
                HFX_FORCE_TEND:FieldType = 104 ;
                HFX_FORCE_TEND:MemoryOrder = "0  " ;
                HFX_FORCE_TEND:description = "SCM ideal surface sensible heat flux
tendenc
y" ;
                HFX_FORCE_TEND:units = "W m-2 s-1" ;
                HFX_FORCE_TEND:stagger = "" ;
        float LH_FORCE_TEND(Time) ;
                LH_FORCE_TEND:FieldType = 104 ;
                LH_FORCE_TEND:MemoryOrder = "0  " ;
                LH_FORCE_TEND:description = "SCM ideal surface latent heat flux tendency"
;
                LH_FORCE_TEND:units = "W m-2 s-1" ;
                LH_FORCE_TEND:stagger = "" ;
        float TSK_FORCE_TEND(Time) ;
                TSK_FORCE_TEND:FieldType = 104 ;
                TSK_FORCE_TEND:MemoryOrder = "0  " ;
```

TSK_FORCE_TEND:description = "SCM ideal surface skin temperature tendency"
;
TSK_FORCE_TEND:units = "W m-2 s-1" ;
TSK_FORCE_TEND:stagger = "" ;
float MU(Time, south_north, west_east) ;
MU:FieldType = 104 ;
MU:MemoryOrder = "XY " ;
MU:description = "perturbation dry air mass in column" ;
MU:units = "Pa" ;
MU:stagger = "" ;
MU:coordinates = "XLONG XLAT" ;
float MUB(Time, south_north, west_east) ;
MUB:FieldType = 104 ;
MUB:MemoryOrder = "XY " ;
MUB:description = "base state dry air mass in column" ;
MUB:units = "Pa" ;
MUB:stagger = "" ;
MUB:coordinates = "XLONG XLAT" ;
float NEST_POS(Time, south_north, west_east) ;
NEST_POS:FieldType = 104 ;
NEST_POS:MemoryOrder = "XY " ;
NEST_POS:description = "-" ;
NEST_POS:units = "-" ;
NEST_POS:stagger = "" ;
NEST_POS:coordinates = "XLONG XLAT" ;
float P(Time, bottom_top, south_north, west_east) ;
P:FieldType = 104 ;
P:MemoryOrder = "XYZ" ;
P:description = "perturbation pressure" ;
P:units = "Pa" ;
P:stagger = "" ;
P:coordinates = "XLONG XLAT" ;
float PB(Time, bottom_top, south_north, west_east) ;
PB:FieldType = 104 ;
PB:MemoryOrder = "XYZ" ;
PB:description = "BASE STATE PRESSURE" ;
PB:units = "Pa" ;
PB:stagger = "" ;
PB:coordinates = "XLONG XLAT" ;
float FNM(Time, bottom_top) ;
FNM:FieldType = 104 ;
FNM:MemoryOrder = "Z " ;
FNM:description = "upper weight for vertical stretching" ;
FNM:units = "" ;
FNM:stagger = "" ;
float FNP(Time, bottom_top) ;

```
        FNP:FieldType = 104 ;
        FNP:MemoryOrder = "Z  " ;
        FNP:description = "lower weight for vertical stretching" ;
        FNP:units = "" ;
        FNP:stagger = "" ;
float RDNW(Time, bottom_top) ;
        RDNW:FieldType = 104 ;
        RDNW:MemoryOrder = "Z  " ;
        RDNW:description = "inverse d(eta) values between full (w) levels" ;
        RDNW:units = "" ;
        RDNW:stagger = "" ;
float RDN(Time, bottom_top) ;
        RDN:FieldType = 104 ;
        RDN:MemoryOrder = "Z  " ;
        RDN:description = "inverse d(eta) values between half (mass) levels" ;
        RDN:units = "" ;
        RDN:stagger = "" ;
float DNW(Time, bottom_top) ;
        DNW:FieldType = 104 ;
        DNW:MemoryOrder = "Z  " ;
        DNW:description = "d(eta) values between full (w) levels" ;
        DNW:units = "" ;
        DNW:stagger = "" ;
float DN(Time, bottom_top) ;
        DN:FieldType = 104 ;
        DN:MemoryOrder = "Z  " ;
        DN:description = "d(eta) values between half (mass) levels" ;
        DN:units = "" ;
        DN:stagger = "" ;
float CFN(Time) ;
        CFN:FieldType = 104 ;
        CFN:MemoryOrder = "0  " ;
        CFN:description = "extrapolation constant" ;
        CFN:units = "" ;
        CFN:stagger = "" ;
float CFN1(Time) ;
        CFN1:FieldType = 104 ;
        CFN1:MemoryOrder = "0  " ;
        CFN1:description = "extrapolation constant" ;
        CFN1:units = "" ;
        CFN1:stagger = "" ;
float P_HYD(Time, bottom_top, south_north, west_east) ;
        P_HYD:FieldType = 104 ;
        P_HYD:MemoryOrder = "XYZ" ;
        P_HYD:description = "hydrostatic pressure" ;
        P_HYD:units = "Pa" ;
        P_HYD:stagger = "" ;
```

P_HYD:coordinates = "XLONG XLAT" ;
float Q2(Time, south_north, west_east) ;
Q2:FieldType = 104 ;
Q2:MemoryOrder = "XY " ;
Q2:description = "QV at 2 M" ;
Q2:units = "kg kg-1" ;
Q2:stagger = "" ;
Q2:coordinates = "XLONG XLAT" ;
float T2(Time, south_north, west_east) ;
T2:FieldType = 104 ;
T2:MemoryOrder = "XY " ;
T2:description = "TEMP at 2 M" ;
T2:units = "K" ;
T2:stagger = "" ;
T2:coordinates = "XLONG XLAT" ;
float TH2(Time, south_north, west_east) ;
TH2:FieldType = 104 ;
TH2:MemoryOrder = "XY " ;
TH2:description = "POT TEMP at 2 M" ;
TH2:units = "K" ;
TH2:stagger = "" ;
TH2:coordinates = "XLONG XLAT" ;
float PSFC(Time, south_north, west_east) ;
PSFC:FieldType = 104 ;
PSFC:MemoryOrder = "XY " ;
PSFC:description = "SFC PRESSURE" ;
PSFC:units = "Pa" ;
PSFC:stagger = "" ;
PSFC:coordinates = "XLONG XLAT" ;
float U10(Time, south_north, west_east) ;
U10:FieldType = 104 ;
U10:MemoryOrder = "XY " ;
U10:description = "U at 10 M" ;
U10:units = "m s-1" ;
U10:stagger = "" ;
U10:coordinates = "XLONG XLAT" ;
float V10(Time, south_north, west_east) ;
V10:FieldType = 104 ;
V10:MemoryOrder = "XY " ;
V10:description = "V at 10 M" ;
V10:units = "m s-1" ;
V10:stagger = "" ;
V10:coordinates = "XLONG XLAT" ;
float RDX(Time) ;
RDX:FieldType = 104 ;
RDX:MemoryOrder = "0 " ;
RDX:description = "INVERSE X GRID LENGTH" ;

```
        RDX:units = "" ;
        RDX:stagger = "" ;
float RDY(Time) ;
        RDY:FieldType = 104 ;
        RDY:MemoryOrder = "0  " ;
        RDY:description = "INVERSE Y GRID LENGTH" ;
        RDY:units = "" ;
        RDY:stagger = "" ;
float RESM(Time) ;
        RESM:FieldType = 104 ;
        RESM:MemoryOrder = "0  " ;
        RESM:description = "TIME WEIGHT CONSTANT FOR SMALL STEPS" ;
        RESM:units = "" ;
        RESM:stagger = "" ;
float ZETATOP(Time) ;
        ZETATOP:FieldType = 104 ;
        ZETATOP:MemoryOrder = "0  " ;
        ZETATOP:description = "ZETA AT MODEL TOP" ;
        ZETATOP:units = "" ;
        ZETATOP:stagger = "" ;
float CF1(Time) ;
        CF1:FieldType = 104 ;
        CF1:MemoryOrder = "0  " ;
        CF1:description = "2nd order extrapolation constant" ;
        CF1:units = "" ;
        CF1:stagger = "" ;
float CF2(Time) ;
        CF2:FieldType = 104 ;
        CF2:MemoryOrder = "0  " ;
        CF2:description = "2nd order extrapolation constant" ;
        CF2:units = "" ;
        CF2:stagger = "" ;
float CF3(Time) ;
        CF3:FieldType = 104 ;
        CF3:MemoryOrder = "0  " ;
        CF3:description = "2nd order extrapolation constant" ;
        CF3:units = "" ;
        CF3:stagger = "" ;
int ITIMESTEP(Time) ;
        ITIMESTEP:FieldType = 106 ;
        ITIMESTEP:MemoryOrder = "0  " ;
        ITIMESTEP:description = "" ;
        ITIMESTEP:units = "" ;
        ITIMESTEP:stagger = "" ;
float XTIME(Time) ;
        XTIME:FieldType = 104 ;
        XTIME:MemoryOrder = "0  " ;
```

```
        XTIME:description = "minutes since simulation start" ;
        XTIME:units = "" ;
        XTIME:stagger = "" ;
float QVAPOR(Time, bottom_top, south_north, west_east) ;
        QVAPOR:FieldType = 104 ;
        QVAPOR:MemoryOrder = "XYZ" ;
        QVAPOR:description = "Water vapor mixing ratio" ;
        QVAPOR:units = "kg kg-1" ;
        QVAPOR:stagger = "" ;
        QVAPOR:coordinates = "XLONG XLAT" ;
float QCLOUD(Time, bottom_top, south_north, west_east) ;
        QCLOUD:FieldType = 104 ;
        QCLOUD:MemoryOrder = "XYZ" ;
        QCLOUD:description = "Cloud water mixing ratio" ;
        QCLOUD:units = "kg kg-1" ;
        QCLOUD:stagger = "" ;
        QCLOUD:coordinates = "XLONG XLAT" ;
float QRAIN(Time, bottom_top, south_north, west_east) ;
        QRAIN:FieldType = 104 ;
        QRAIN:MemoryOrder = "XYZ" ;
        QRAIN:description = "Rain water mixing ratio" ;
        QRAIN:units = "kg kg-1" ;
        QRAIN:stagger = "" ;
        QRAIN:coordinates = "XLONG XLAT" ;
float QICE(Time, bottom_top, south_north, west_east) ;
        QICE:FieldType = 104 ;
        QICE:MemoryOrder = "XYZ" ;
        QICE:description = "Ice mixing ratio" ;
        QICE:units = "kg kg-1" ;
        QICE:stagger = "" ;
        QICE:coordinates = "XLONG XLAT" ;
float QSNOW(Time, bottom_top, south_north, west_east) ;
        QSNOW:FieldType = 104 ;
        QSNOW:MemoryOrder = "XYZ" ;
        QSNOW:description = "Snow mixing ratio" ;
        QSNOW:units = "kg kg-1" ;
        QSNOW:stagger = "" ;
        QSNOW:coordinates = "XLONG XLAT" ;
float QGRAUP(Time, bottom_top, south_north, west_east) ;
        QGRAUP:FieldType = 104 ;
        QGRAUP:MemoryOrder = "XYZ" ;
        QGRAUP:description = "Graupel mixing ratio" ;
        QGRAUP:units = "kg kg-1" ;
        QGRAUP:stagger = "" ;
        QGRAUP:coordinates = "XLONG XLAT" ;
float QNICE(Time, bottom_top, south_north, west_east) ;
        QNICE:FieldType = 104 ;
```

QNICE:MemoryOrder = "XYZ" ;
QNICE:description = "Ice Number concentration" ;
QNICE:units = " kg-1" ;
QNICE:stagger = "" ;
QNICE:coordinates = "XLONG XLAT" ;
float QNRAIN(Time, bottom_top, south_north, west_east) ;
QNRAIN:FieldType = 104 ;
QNRAIN:MemoryOrder = "XYZ" ;
QNRAIN:description = "Rain Number concentration" ;
QNRAIN:units = " kg(-1)" ;
QNRAIN:stagger = "" ;
QNRAIN:coordinates = "XLONG XLAT" ;
float SHDMAX(Time, south_north, west_east) ;
SHDMAX:FieldType = 104 ;
SHDMAX:MemoryOrder = "XY " ;
SHDMAX:description = "ANNUAL MAX VEG FRACTION" ;
SHDMAX:units = "" ;
SHDMAX:stagger = "" ;
SHDMAX:coordinates = "XLONG XLAT" ;
float SHDMIN(Time, south_north, west_east) ;
SHDMIN:FieldType = 104 ;
SHDMIN:MemoryOrder = "XY " ;
SHDMIN:description = "ANNUAL MIN VEG FRACTION" ;
SHDMIN:units = "" ;
SHDMIN:stagger = "" ;
SHDMIN:coordinates = "XLONG XLAT" ;
float SNOALB(Time, south_north, west_east) ;
SNOALB:FieldType = 104 ;
SNOALB:MemoryOrder = "XY " ;
SNOALB:description = "ANNUAL MAX SNOW ALBEDO IN FRACTION" ;
SNOALB:units = "" ;
SNOALB:stagger = "" ;
SNOALB:coordinates = "XLONG XLAT" ;
float TSLB(Time, soil_layers_stag, south_north, west_east) ;
TSLB:FieldType = 104 ;
TSLB:MemoryOrder = "XYZ" ;
TSLB:description = "SOIL TEMPERATURE" ;
TSLB:units = "K" ;
TSLB:stagger = "Z" ;
TSLB:coordinates = "XLONG XLAT" ;
float SMOIS(Time, soil_layers_stag, south_north, west_east) ;
SMOIS:FieldType = 104 ;
SMOIS:MemoryOrder = "XYZ" ;
SMOIS:description = "SOIL MOISTURE" ;
SMOIS:units = "m3 m-3" ;
SMOIS:stagger = "Z" ;
SMOIS:coordinates = "XLONG XLAT" ;

```
float SH2O(Time, soil_layers_stag, south_north, west_east) ;
        SH2O:FieldType = 104 ;
        SH2O:MemoryOrder = "XYZ" ;
        SH2O:description = "SOIL LIQUID WATER" ;
        SH2O:units = "m3 m-3" ;
        SH2O:stagger = "Z" ;
        SH2O:coordinates = "XLONG XLAT" ;
float SMCREL(Time, soil_layers_stag, south_north, west_east) ;
        SMCREL:FieldType = 104 ;
        SMCREL:MemoryOrder = "XYZ" ;
        SMCREL:description = "RELATIVE SOIL MOISTURE" ;
        SMCREL:units = "" ;
        SMCREL:stagger = "Z" ;
        SMCREL:coordinates = "XLONG XLAT" ;
float SEAICE(Time, south_north, west_east) ;
        SEAICE:FieldType = 104 ;
        SEAICE:MemoryOrder = "XY " ;
        SEAICE:description = "SEA ICE FLAG" ;
        SEAICE:units = "" ;
        SEAICE:stagger = "" ;
        SEAICE:coordinates = "XLONG XLAT" ;
float XICEM(Time, south_north, west_east) ;
        XICEM:FieldType = 104 ;
        XICEM:MemoryOrder = "XY " ;
        XICEM:description = "SEA ICE FLAG (PREVIOUS STEP)" ;
        XICEM:units = "" ;
        XICEM:stagger = "" ;
        XICEM:coordinates = "XLONG XLAT" ;
float SFROFF(Time, south_north, west_east) ;
        SFROFF:FieldType = 104 ;
        SFROFF:MemoryOrder = "XY " ;
        SFROFF:description = "SURFACE RUNOFF" ;
        SFROFF:units = "mm" ;
        SFROFF:stagger = "" ;
        SFROFF:coordinates = "XLONG XLAT" ;
float UDROFF(Time, south_north, west_east) ;
        UDROFF:FieldType = 104 ;
        UDROFF:MemoryOrder = "XY " ;
        UDROFF:description = "UNDERGROUND RUNOFF" ;
        UDROFF:units = "mm" ;
        UDROFF:stagger = "" ;
        UDROFF:coordinates = "XLONG XLAT" ;
int IVGTYP(Time, south_north, west_east) ;
        IVGTYP:FieldType = 106 ;
        IVGTYP:MemoryOrder = "XY " ;
        IVGTYP:description = "DOMINANT VEGETATION CATEGORY" ;
        IVGTYP:units = "" ;
```

IVGTYP:stagger = "" ;
IVGTYP:coordinates = "XLONG XLAT" ;
int ISLTYP(Time, south_north, west_east) ;
ISLTYP:FieldType = 106 ;
ISLTYP:MemoryOrder = "XY " ;
ISLTYP:description = "DOMINANT SOIL CATEGORY" ;
ISLTYP:units = "" ;
ISLTYP:stagger = "" ;
ISLTYP:coordinates = "XLONG XLAT" ;
float VEGFRA(Time, south_north, west_east) ;
VEGFRA:FieldType = 104 ;
VEGFRA:MemoryOrder = "XY " ;
VEGFRA:description = "VEGETATION FRACTION" ;
VEGFRA:units = "" ;
VEGFRA:stagger = "" ;
VEGFRA:coordinates = "XLONG XLAT" ;
float GRDFLX(Time, south_north, west_east) ;
GRDFLX:FieldType = 104 ;
GRDFLX:MemoryOrder = "XY " ;
GRDFLX:description = "GROUND HEAT FLUX" ;
GRDFLX:units = "W m-2" ;
GRDFLX:stagger = "" ;
GRDFLX:coordinates = "XLONG XLAT" ;
float ACGRDFLX(Time, south_north, west_east) ;
ACGRDFLX:FieldType = 104 ;
ACGRDFLX:MemoryOrder = "XY " ;
ACGRDFLX:description = "ACCUMULATED GROUND HEAT FLUX" ;
ACGRDFLX:units = "J m-2" ;
ACGRDFLX:stagger = "" ;
ACGRDFLX:coordinates = "XLONG XLAT" ;
float ACSNOM(Time, south_north, west_east) ;
ACSNOM:FieldType = 104 ;
ACSNOM:MemoryOrder = "XY " ;
ACSNOM:description = "ACCUMULATED MELTED SNOW" ;
ACSNOM:units = "kg m-2" ;
ACSNOM:stagger = "" ;
ACSNOM:coordinates = "XLONG XLAT" ;
float SNOW(Time, south_north, west_east) ;
SNOW:FieldType = 104 ;
SNOW:MemoryOrder = "XY " ;
SNOW:description = "SNOW WATER EQUIVALENT" ;
SNOW:units = "kg m-2" ;
SNOW:stagger = "" ;
SNOW:coordinates = "XLONG XLAT" ;
float SNOWH(Time, south_north, west_east) ;
SNOWH:FieldType = 104 ;
SNOWH:MemoryOrder = "XY " ;

SNOWH:description = "PHYSICAL SNOW DEPTH" ;
SNOWH:units = "m" ;
SNOWH:stagger = "" ;
SNOWH:coordinates = "XLONG XLAT" ;
float CANWAT(Time, south_north, west_east) ;
CANWAT:FieldType = 104 ;
CANWAT:MemoryOrder = "XY " ;
CANWAT:description = "CANOPY WATER" ;
CANWAT:units = "kg m-2" ;
CANWAT:stagger = "" ;
CANWAT:coordinates = "XLONG XLAT" ;
float SSTSK(Time, south_north, west_east) ;
SSTSK:FieldType = 104 ;
SSTSK:MemoryOrder = "XY " ;
SSTSK:description = "SKIN SEA SURFACE TEMPERATURE" ;
SSTSK:units = "K" ;
SSTSK:stagger = "" ;
SSTSK:coordinates = "XLONG XLAT" ;
float COSZEN(Time, south_north, west_east) ;
COSZEN:FieldType = 104 ;
COSZEN:MemoryOrder = "XY " ;
COSZEN:description = "COS of SOLAR ZENITH ANGLE" ;
COSZEN:units = "dimensionless" ;
COSZEN:stagger = "" ;
COSZEN:coordinates = "XLONG XLAT" ;
float LAI(Time, south_north, west_east) ;
LAI:FieldType = 104 ;
LAI:MemoryOrder = "XY " ;
LAI:description = "Leaf area index" ;
LAI:units = "area/area" ;
LAI:stagger = "" ;
LAI:coordinates = "XLONG XLAT" ;
float VAR(Time, south_north, west_east) ;
VAR:FieldType = 104 ;
VAR:MemoryOrder = "XY " ;
VAR:description = "OROGRAPHIC VARIANCE" ;
VAR:units = "" ;
VAR:stagger = "" ;
VAR:coordinates = "XLONG XLAT" ;
float MAPFAC_M(Time, south_north, west_east) ;
MAPFAC_M:FieldType = 104 ;
MAPFAC_M:MemoryOrder = "XY " ;
MAPFAC_M:description = "Map scale factor on mass grid" ;
MAPFAC_M:units = "" ;
MAPFAC_M:stagger = "" ;
MAPFAC_M:coordinates = "XLONG XLAT" ;
float MAPFAC_U(Time, south_north, west_east_stag) ;

MAPFAC_U:FieldType = 104 ;
MAPFAC_U:MemoryOrder = "XY " ;
MAPFAC_U:description = "Map scale factor on u-grid" ;
MAPFAC_U:units = "" ;
MAPFAC_U:stagger = "X" ;
MAPFAC_U:coordinates = "XLONG_U XLAT_U" ;
float MAPFAC_V(Time, south_north_stag, west_east) ;
MAPFAC_V:FieldType = 104 ;
MAPFAC_V:MemoryOrder = "XY " ;
MAPFAC_V:description = "Map scale factor on v-grid" ;
MAPFAC_V:units = "" ;
MAPFAC_V:stagger = "Y" ;
MAPFAC_V:coordinates = "XLONG_V XLAT_V" ;
float MAPFAC_MX(Time, south_north, west_east) ;
MAPFAC_MX:FieldType = 104 ;
MAPFAC_MX:MemoryOrder = "XY " ;
MAPFAC_MX:description = "Map scale factor on mass grid, x direction" ;
MAPFAC_MX:units = "" ;
MAPFAC_MX:stagger = "" ;
MAPFAC_MX:coordinates = "XLONG XLAT" ;
float MAPFAC_MY(Time, south_north, west_east) ;
MAPFAC_MY:FieldType = 104 ;
MAPFAC_MY:MemoryOrder = "XY " ;
MAPFAC_MY:description = "Map scale factor on mass grid, y direction" ;
MAPFAC_MY:units = "" ;
MAPFAC_MY:stagger = "" ;
MAPFAC_MY:coordinates = "XLONG XLAT" ;
float MAPFAC_UX(Time, south_north, west_east_stag) ;
MAPFAC_UX:FieldType = 104 ;
MAPFAC_UX:MemoryOrder = "XY " ;
MAPFAC_UX:description = "Map scale factor on u-grid, x direction" ;
MAPFAC_UX:units = "" ;
MAPFAC_UX:stagger = "X" ;
MAPFAC_UX:coordinates = "XLONG_U XLAT_U" ;
float MAPFAC_UY(Time, south_north, west_east_stag) ;
MAPFAC_UY:FieldType = 104 ;
MAPFAC_UY:MemoryOrder = "XY " ;
MAPFAC_UY:description = "Map scale factor on u-grid, y direction" ;
MAPFAC_UY:units = "" ;
MAPFAC_UY:stagger = "X" ;
MAPFAC_UY:coordinates = "XLONG_U XLAT_U" ;
float MAPFAC_VX(Time, south_north_stag, west_east) ;
MAPFAC_VX:FieldType = 104 ;
MAPFAC_VX:MemoryOrder = "XY " ;
MAPFAC_VX:description = "Map scale factor on v-grid, x direction" ;
MAPFAC_VX:units = "" ;
MAPFAC_VX:stagger = "Y" ;

```
                MAPFAC_VX:coordinates = "XLONG_V XLAT_V" ;
        float MF_VX_INV(Time, south_north_stag, west_east) ;
                MF_VX_INV:FieldType = 104 ;
                MF_VX_INV:MemoryOrder = "XY " ;
                MF_VX_INV:description = "Inverse map scale factor on v-grid, x direction"
;
                MF_VX_INV:units = "" ;
                MF_VX_INV:stagger = "Y" ;
                MF_VX_INV:coordinates = "XLONG_V XLAT_V" ;
        float MAPFAC_VY(Time, south_north_stag, west_east) ;
                MAPFAC_VY:FieldType = 104 ;
                MAPFAC_VY:MemoryOrder = "XY " ;
                MAPFAC_VY:description = "Map scale factor on v-grid, y direction" ;
                MAPFAC_VY:units = "" ;
                MAPFAC_VY:stagger = "Y" ;
                MAPFAC_VY:coordinates = "XLONG_V XLAT_V" ;
        float F(Time, south_north, west_east) ;
                F:FieldType = 104 ;
                F:MemoryOrder = "XY " ;
                F:description = "Coriolis sine latitude term" ;
                F:units = "s-1" ;
                F:stagger = "" ;
                F:coordinates = "XLONG XLAT" ;
        float E(Time, south_north, west_east) ;
                E:FieldType = 104 ;
                E:MemoryOrder = "XY " ;
                E:description = "Coriolis cosine latitude term" ;
                E:units = "s-1" ;
                E:stagger = "" ;
                E:coordinates = "XLONG XLAT" ;
        float SINALPHA(Time, south_north, west_east) ;
                SINALPHA:FieldType = 104 ;
                SINALPHA:MemoryOrder = "XY " ;
                SINALPHA:description = "Local sine of map rotation" ;
                SINALPHA:units = "" ;
                SINALPHA:stagger = "" ;
                SINALPHA:coordinates = "XLONG XLAT" ;
        float COSALPHA(Time, south_north, west_east) ;
                COSALPHA:FieldType = 104 ;
                COSALPHA:MemoryOrder = "XY " ;
                COSALPHA:description = "Local cosine of map rotation" ;
                COSALPHA:units = "" ;
                COSALPHA:stagger = "" ;
                COSALPHA:coordinates = "XLONG XLAT" ;
        float HGT(Time, south_north, west_east) ;
                HGT:FieldType = 104 ;
                HGT:MemoryOrder = "XY " ;
```

HGT:description = "Terrain Height" ;
HGT:units = "m" ;
HGT:stagger = "" ;
HGT:coordinates = "XLONG XLAT" ;
float TSK(Time, south_north, west_east) ;
TSK:FieldType = 104 ;
TSK:MemoryOrder = "XY " ;
TSK:description = "SURFACE SKIN TEMPERATURE" ;
TSK:units = "K" ;
TSK:stagger = "" ;
TSK:coordinates = "XLONG XLAT" ;
float P_TOP(Time) ;
P_TOP:FieldType = 104 ;
P_TOP:MemoryOrder = "0 " ;
P_TOP:description = "PRESSURE TOP OF THE MODEL" ;
P_TOP:units = "Pa" ;
P_TOP:stagger = "" ;
float T00(Time) ;
T00:FieldType = 104 ;
T00:MemoryOrder = "0 " ;
T00:description = "BASE STATE TEMPERATURE" ;
T00:units = "K" ;
T00:stagger = "" ;
float P00(Time) ;
P00:FieldType = 104 ;
P00:MemoryOrder = "0 " ;
P00:description = "BASE STATE PRESURE" ;
P00:units = "Pa" ;
P00:stagger = "" ;
float TLP(Time) ;
TLP:FieldType = 104 ;
TLP:MemoryOrder = "0 " ;
TLP:description = "BASE STATE LAPSE RATE" ;
TLP:units = "" ;
TLP:stagger = "" ;
float TISO(Time) ;
TISO:FieldType = 104 ;
TISO:MemoryOrder = "0 " ;
TISO:description = "TEMP AT WHICH THE BASE T TURNS CONST" ;
TISO:units = "K" ;
TISO:stagger = "" ;
float MAX_MSTFX(Time) ;
MAX_MSTFX:FieldType = 104 ;
MAX_MSTFX:MemoryOrder = "0 " ;
MAX_MSTFX:description = "Max map factor in domain" ;
MAX_MSTFX:units = "" ;
MAX_MSTFX:stagger = "" ;

```
        float MAX_MSTFY(Time) ;
                MAX_MSTFY:FieldType = 104 ;
                MAX_MSTFY:MemoryOrder = "0  " ;
                MAX_MSTFY:description = "Max map factor in domain" ;
                MAX_MSTFY:units = "" ;
                MAX_MSTFY:stagger = "" ;
        float RAINC(Time, south_north, west_east) ;
                RAINC:FieldType = 104 ;
                RAINC:MemoryOrder = "XY " ;
                RAINC:description = "ACCUMULATED TOTAL CUMULUS PRECIPITATION" ;
                RAINC:units = "mm" ;
                RAINC:stagger = "" ;
                RAINC:coordinates = "XLONG XLAT" ;
        float RAINSH(Time, south_north, west_east) ;
                RAINSH:FieldType = 104 ;
                RAINSH:MemoryOrder = "XY " ;
                RAINSH:description = "ACCUMULATED SHALLOW CUMULUS PRECIPITATION"
;
                RAINSH:units = "mm" ;
                RAINSH:stagger = "" ;
                RAINSH:coordinates = "XLONG XLAT" ;
        float RAINNC(Time, south_north, west_east) ;
                RAINNC:FieldType = 104 ;
                RAINNC:MemoryOrder = "XY " ;
                RAINNC:description = "ACCUMULATED TOTAL GRID SCALE PRECIPITATION" ;
                RAINNC:units = "mm" ;
                RAINNC:stagger = "" ;
                RAINNC:coordinates = "XLONG XLAT" ;
        float SNOWNC(Time, south_north, west_east) ;
                SNOWNC:FieldType = 104 ;
                SNOWNC:MemoryOrder = "XY " ;
                SNOWNC:description = "ACCUMULATED TOTAL GRID SCALE SNOW AND ICE" ;
                SNOWNC:units = "mm" ;
                SNOWNC:stagger = "" ;
                SNOWNC:coordinates = "XLONG XLAT" ;
        float GRAUPELNC(Time, south_north, west_east) ;
                GRAUPELNC:FieldType = 104 ;
                GRAUPELNC:MemoryOrder = "XY " ;
                GRAUPELNC:description = "ACCUMULATED TOTAL GRID SCALE GRAUPEL" ;
                GRAUPELNC:units = "mm" ;
                GRAUPELNC:stagger = "" ;
                GRAUPELNC:coordinates = "XLONG XLAT" ;
        float HAILNC(Time, south_north, west_east) ;
                HAILNC:FieldType = 104 ;
                HAILNC:MemoryOrder = "XY " ;
                HAILNC:description = "ACCUMULATED TOTAL GRID SCALE HAIL" ;
                HAILNC:units = "mm" ;
```

HAILNC:stagger = "" ;
HAILNC:coordinates = "XLONG XLAT" ;
float REFL_10CM(Time, bottom_top, south_north, west_east) ;
REFL_10CM:FieldType = 104 ;
REFL_10CM:MemoryOrder = "XYZ" ;
REFL_10CM:description = "Radar reflectivity (lamda = 10 cm)" ;
REFL_10CM:units = "dBZ" ;
REFL_10CM:stagger = "" ;
REFL_10CM:coordinates = "XLONG XLAT" ;
float CLDFRA(Time, bottom_top, south_north, west_east) ;
CLDFRA:FieldType = 104 ;
CLDFRA:MemoryOrder = "XYZ" ;
CLDFRA:description = "CLOUD FRACTION" ;
CLDFRA:units = "" ;
CLDFRA:stagger = "" ;
CLDFRA:coordinates = "XLONG XLAT" ;
float SWDOWN(Time, south_north, west_east) ;
SWDOWN:FieldType = 104 ;
SWDOWN:MemoryOrder = "XY " ;
SWDOWN:description = "DOWNWARD SHORT WAVE FLUX AT GROUND SURFACE" ;
SWDOWN:units = "W m-2" ;
SWDOWN:stagger = "" ;
SWDOWN:coordinates = "XLONG XLAT" ;
float GLW(Time, south_north, west_east) ;
GLW:FieldType = 104 ;
GLW:MemoryOrder = "XY " ;
GLW:description = "DOWNWARD LONG WAVE FLUX AT GROUND SURFACE" ;
GLW:units = "W m-2" ;
GLW:stagger = "" ;
GLW:coordinates = "XLONG XLAT" ;
float SWNORM(Time, south_north, west_east) ;
SWNORM:FieldType = 104 ;
SWNORM:MemoryOrder = "XY " ;
SWNORM:description = "NORMAL SHORT WAVE FLUX AT GROUND SURFACE (SLOPE-DEPE
NDENT)" ;
SWNORM:units = "W m-2" ;
SWNORM:stagger = "" ;
SWNORM:coordinates = "XLONG XLAT" ;
float SWDDIR(Time, south_north, west_east) ;
SWDDIR:FieldType = 104 ;
SWDDIR:MemoryOrder = "XY " ;
SWDDIR:description = "Shortwave surface downward direct irradiance" ;
SWDDIR:units = "W/m^2" ;
SWDDIR:stagger = "" ;
SWDDIR:coordinates = "XLONG XLAT" ;

```
        float SWDDNI(Time, south_north, west_east) ;
                SWDDNI:FieldType = 104 ;
                SWDDNI:MemoryOrder = "XY " ;
                SWDDNI:description = "Shortwave surface downward direct normal
irradiance"
;
                SWDDNI:units = "W/m^2" ;
                SWDDNI:stagger = "" ;
                SWDDNI:coordinates = "XLONG XLAT" ;
        float SWDDIF(Time, south_north, west_east) ;
                SWDDIF:FieldType = 104 ;
                SWDDIF:MemoryOrder = "XY " ;
                SWDDIF:description = "Shortwave surface downward diffuse irradiance" ;
                SWDDIF:units = "W/m^2" ;
                SWDDIF:stagger = "" ;
                SWDDIF:coordinates = "XLONG XLAT" ;
        float OLR(Time, south_north, west_east) ;
                OLR:FieldType = 104 ;
                OLR:MemoryOrder = "XY " ;
                OLR:description = "TOA OUTGOING LONG WAVE" ;
                OLR:units = "W m-2" ;
                OLR:stagger = "" ;
                OLR:coordinates = "XLONG XLAT" ;
        float XLAT_U(Time, south_north, west_east_stag) ;
                XLAT_U:FieldType = 104 ;
                XLAT_U:MemoryOrder = "XY " ;
                XLAT_U:description = "LATITUDE, SOUTH IS NEGATIVE" ;
                XLAT_U:units = "degree_north" ;
                XLAT_U:stagger = "X" ;
                XLAT_U:coordinates = "XLONG_U XLAT_U" ;
        float XLONG_U(Time, south_north, west_east_stag) ;
                XLONG_U:FieldType = 104 ;
                XLONG_U:MemoryOrder = "XY " ;
                XLONG_U:description = "LONGITUDE, WEST IS NEGATIVE" ;
                XLONG_U:units = "degree_east" ;
                XLONG_U:stagger = "X" ;
                XLONG_U:coordinates = "XLONG_U XLAT_U" ;
        float XLAT_V(Time, south_north_stag, west_east) ;
                XLAT_V:FieldType = 104 ;
                XLAT_V:MemoryOrder = "XY " ;
                XLAT_V:description = "LATITUDE, SOUTH IS NEGATIVE" ;
                XLAT_V:units = "degree_north" ;
                XLAT_V:stagger = "Y" ;
                XLAT_V:coordinates = "XLONG_V XLAT_V" ;
        float XLONG_V(Time, south_north_stag, west_east) ;
                XLONG_V:FieldType = 104 ;
                XLONG_V:MemoryOrder = "XY " ;
```

```
                XLONG_V:description = "LONGITUDE, WEST IS NEGATIVE" ;
                XLONG_V:units = "degree_east" ;
                XLONG_V:stagger = "Y" ;
                XLONG_V:coordinates = "XLONG_V XLAT_V" ;
        float ALBEDO(Time, south_north, west_east) ;
                ALBEDO:FieldType = 104 ;
                ALBEDO:MemoryOrder = "XY " ;
                ALBEDO:description = "ALBEDO" ;
                ALBEDO:units = "-" ;
                ALBEDO:stagger = "" ;
                ALBEDO:coordinates = "XLONG XLAT" ;
        float CLAT(Time, south_north, west_east) ;
                CLAT:FieldType = 104 ;
                CLAT:MemoryOrder = "XY " ;
                CLAT:description = "COMPUTATIONAL GRID LATITUDE, SOUTH IS NEGATIVE" ;
                CLAT:units = "degree_north" ;
                CLAT:stagger = "" ;
                CLAT:coordinates = "XLONG XLAT" ;
        float ALBBCK(Time, south_north, west_east) ;
                ALBBCK:FieldType = 104 ;
                ALBBCK:MemoryOrder = "XY " ;
                ALBBCK:description = "BACKGROUND ALBEDO" ;
                ALBBCK:units = "" ;
                ALBBCK:stagger = "" ;
                ALBBCK:coordinates = "XLONG XLAT" ;
        float EMISS(Time, south_north, west_east) ;
                EMISS:FieldType = 104 ;
                EMISS:MemoryOrder = "XY " ;
                EMISS:description = "SURFACE EMISSIVITY" ;
                EMISS:units = "" ;
                EMISS:stagger = "" ;
                EMISS:coordinates = "XLONG XLAT" ;
        float NOAHRES(Time, south_north, west_east) ;
                NOAHRES:FieldType = 104 ;
                NOAHRES:MemoryOrder = "XY " ;
                NOAHRES:description = "RESIDUAL OF THE NOAH SURFACE ENERGY BUDGET"
;
                NOAHRES:units = "W m{-2}" ;
                NOAHRES:stagger = "" ;
                NOAHRES:coordinates = "XLONG XLAT" ;
        float FLX4(Time, south_north, west_east) ;
                FLX4:FieldType = 104 ;
                FLX4:MemoryOrder = "XY " ;
                FLX4:description = "sensible heat from canopy" ;
                FLX4:units = "W m{-2}" ;
                FLX4:stagger = "" ;
                FLX4:coordinates = "XLONG XLAT" ;
```

```
float FVB(Time, south_north, west_east) ;
        FVB:FieldType = 104 ;
        FVB:MemoryOrder = "XY " ;
        FVB:description = "fraction of vegetation with snow below" ;
        FVB:units = "" ;
        FVB:stagger = "" ;
        FVB:coordinates = "XLONG XLAT" ;
float FBUR(Time, south_north, west_east) ;
        FBUR:FieldType = 104 ;
        FBUR:MemoryOrder = "XY " ;
        FBUR:description = "fraction of vegetation covered by snow" ;
        FBUR:units = "" ;
        FBUR:stagger = "" ;
        FBUR:coordinates = "XLONG XLAT" ;
float FGSN(Time, south_north, west_east) ;
        FGSN:FieldType = 104 ;
        FGSN:MemoryOrder = "XY " ;
        FGSN:description = "fraction of ground covered by snow" ;
        FGSN:units = "" ;
        FGSN:stagger = "" ;
        FGSN:coordinates = "XLONG XLAT" ;
float TMN(Time, south_north, west_east) ;
        TMN:FieldType = 104 ;
        TMN:MemoryOrder = "XY " ;
        TMN:description = "SOIL TEMPERATURE AT LOWER BOUNDARY" ;
        TMN:units = "K" ;
        TMN:stagger = "" ;
        TMN:coordinates = "XLONG XLAT" ;
float XLAND(Time, south_north, west_east) ;
        XLAND:FieldType = 104 ;
        XLAND:MemoryOrder = "XY " ;
        XLAND:description = "LAND MASK (1 FOR LAND, 2 FOR WATER)" ;
        XLAND:units = "" ;
        XLAND:stagger = "" ;
        XLAND:coordinates = "XLONG XLAT" ;
float UST(Time, south_north, west_east) ;
        UST:FieldType = 104 ;
        UST:MemoryOrder = "XY " ;
        UST:description = "U* IN SIMILARITY THEORY" ;
        UST:units = "m s-1" ;
        UST:stagger = "" ;
        UST:coordinates = "XLONG XLAT" ;
float PBLH(Time, south_north, west_east) ;
        PBLH:FieldType = 104 ;
        PBLH:MemoryOrder = "XY " ;
        PBLH:description = "PBL HEIGHT" ;
        PBLH:units = "m" ;
```

PBLH:stagger = "" ;
PBLH:coordinates = "XLONG XLAT" ;
float HFX(Time, south_north, west_east) ;
HFX:FieldType = 104 ;
HFX:MemoryOrder = "XY " ;
HFX:description = "UPWARD HEAT FLUX AT THE SURFACE" ;
HFX:units = "W m-2" ;
HFX:stagger = "" ;
HFX:coordinates = "XLONG XLAT" ;
float QFX(Time, south_north, west_east) ;
QFX:FieldType = 104 ;
QFX:MemoryOrder = "XY " ;
QFX:description = "UPWARD MOISTURE FLUX AT THE SURFACE" ;
QFX:units = "kg m-2 s-1" ;
QFX:stagger = "" ;
QFX:coordinates = "XLONG XLAT" ;
float LH(Time, south_north, west_east) ;
LH:FieldType = 104 ;
LH:MemoryOrder = "XY " ;
LH:description = "LATENT HEAT FLUX AT THE SURFACE" ;
LH:units = "W m-2" ;
LH:stagger = "" ;
LH:coordinates = "XLONG XLAT" ;
float ACHFX(Time, south_north, west_east) ;
ACHFX:FieldType = 104 ;
ACHFX:MemoryOrder = "XY " ;
ACHFX:description = "ACCUMULATED UPWARD HEAT FLUX AT THE SURFACE"
;
ACHFX:units = "J m-2" ;
ACHFX:stagger = "" ;
ACHFX:coordinates = "XLONG XLAT" ;
float ACLHF(Time, south_north, west_east) ;
ACLHF:FieldType = 104 ;
ACLHF:MemoryOrder = "XY " ;
ACLHF:description = "ACCUMULATED UPWARD LATENT HEAT FLUX AT THE
SURFACE" ;
ACLHF:units = "J m-2" ;
ACLHF:stagger = "" ;
ACLHF:coordinates = "XLONG XLAT" ;
float SNOWC(Time, south_north, west_east) ;
SNOWC:FieldType = 104 ;
SNOWC:MemoryOrder = "XY " ;
SNOWC:description = "FLAG INDICATING SNOW COVERAGE (1 FOR SNOW
COVER)" ;
SNOWC:units = "" ;
SNOWC:stagger = "" ;
SNOWC:coordinates = "XLONG XLAT" ;

```
        float SR(Time, south_north, west_east) ;
                SR:FieldType = 104 ;
                SR:MemoryOrder = "XY " ;
                SR:description = "fraction of frozen precipitation" ;
                SR:units = "-" ;
                SR:stagger = "" ;
                SR:coordinates = "XLONG XLAT" ;
        int SAVE_TOPO_FROM_REAL(Time) ;
                SAVE_TOPO_FROM_REAL:FieldType = 106 ;
                SAVE_TOPO_FROM_REAL:MemoryOrder = "0  " ;
                SAVE_TOPO_FROM_REAL:description = "1=original topo from real/0=topo
modifi
ed by WRF" ;
                SAVE_TOPO_FROM_REAL:units = "flag" ;
                SAVE_TOPO_FROM_REAL:stagger = "" ;
        int SEED1(Time) ;
                SEED1:FieldType = 106 ;
                SEED1:MemoryOrder = "0  " ;
                SEED1:description = "RANDOM SEED NUMBER 1" ;
                SEED1:units = "" ;
                SEED1:stagger = "" ;
        int SEED2(Time) ;
                SEED2:FieldType = 106 ;
                SEED2:MemoryOrder = "0  " ;
                SEED2:description = "RANDOM SEED NUMBER 2" ;
                SEED2:units = "" ;
                SEED2:stagger = "" ;
        float LANDMASK(Time, south_north, west_east) ;
                LANDMASK:FieldType = 104 ;
                LANDMASK:MemoryOrder = "XY " ;
                LANDMASK:description = "LAND MASK (1 FOR LAND, 0 FOR WATER)" ;
                LANDMASK:units = "" ;
                LANDMASK:stagger = "" ;
                LANDMASK:coordinates = "XLONG XLAT" ;
        float SST(Time, south_north, west_east) ;
                SST:FieldType = 104 ;
                SST:MemoryOrder = "XY " ;
                SST:description = "SEA SURFACE TEMPERATURE" ;
                SST:units = "K" ;
                SST:stagger = "" ;
                SST:coordinates = "XLONG XLAT” ;
```